DEVELOPMENT AND APPLICATION OF THETA TIPS AS A NOVEL NESI-MS ION SOURCE AND PROTEIN IDENTIFICATION USING LIMITED TRYPSIN DIGESTION AND MASS SPECTROMETRY

by

Feifei Zhao

A Dissertation

Submitted to the Faculty of Purdue University

In Partial Fulfillment of the Requirements for the degree of

Doctor of Philosophy
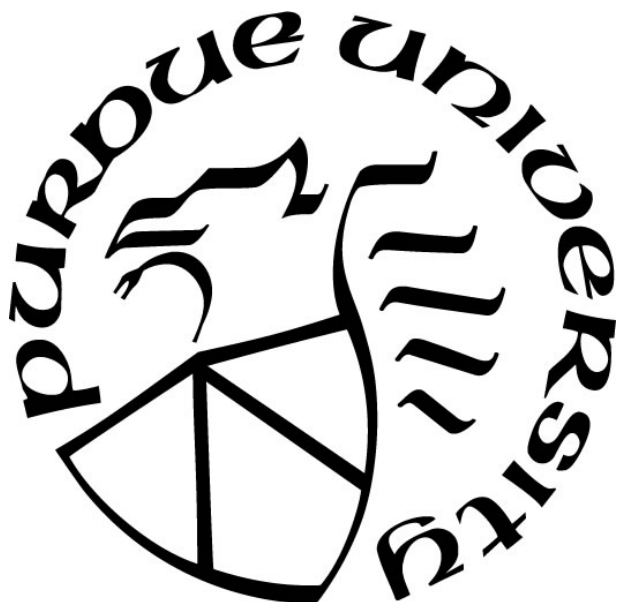
Department of Chemistry

West Lafayette, Indiana

May 2019

THE PURDUE UNIVERSITY GRADUATE SCHOOL
STATEMENT OF COMMITTEE APPROVAL

Dr. Scott A. McLuckey, Chair
> Department of Chemistry

Dr. Peter T. Kissinger
> Department of Chemistry

Dr. Mingji Dai
> Department of Chemistry

Dr. Hilkka I. Kenttämaa
> Department of Chemistry

Approved by:
> Dr. Christine Hrycyna
>> Head of the Graduate Program

For everyone who has helped me throughout the whole journey:

Thank you for all your love, help, support and encouragement!

ACKNOWLEDGMENTS

I would start with my deepest acknowledgement to my supervisor Professor Scott McLuckey. Thank you for giving me the opportunity to join this group and dig into the world of mass spectrometry as well as analytical chemistry. Thank you for your encouragement and guidance throughout the whole journey. Thank you for allowing me to research into new ideas when I am curious about some interesting phenomenon. You make me find that science is so fun after the five years of PhD study and make me want to pursue my career along the scientific track and solve new problems. I always remember that you said "The reason I come back to academia is that I want to help more students", and I saw how you have been devoting into your mission. Because of your model, I desire to help others as you do in my future life and career. Thank you for giving us so many opportunities to develop ourselves, including attending and presenting in conferences, collaboration with others and developing leadership in student organizations. These experiences help us grow as better scientists. Thank you!

I also thank the whole McLuckey group, which is a fantastic group. I was initially attracted by the close relationship and nice group culture from the beginning and I have been enjoying living and working with the group throughout my PhD. I thank the senior students before me, who served as great mentors, colleagues and friends. I thank Dr. Christine Fisher, who has always been nice and patient to teach me all the tricks and theories in the theta tip project. You are a very nice person to talk to. Dr. Alice Pilo, thank you very much for your encouragement and help, and thank you for your model as a positive and passionate scientist. Dr. Jiexun Bu and Dr. Zhou Peng, thank you for your help in providing scientific ideas, thank you for your model as curious scientists and also thank you for your encouragement. Dr. Stella Betancourt, thank you for being my officemate and friend. Thank you for your great friendship. Dr. Eric Dziekonski and Dr. Josh Gilbert, it's nice to

be overlapping with you and thank you for helping with all your ideas in subgroup and also helping fixing the QStar. I also thank my peers Nan Wang and Mack Shih. You are great friends and thank you very much for your teaching, helping and sharing. Thank you all the younger colleagues for creating the nice group culture and we support each other as a group to move forward together.

I thank my whole family. Thank you for raising me up as a good person and always supporting and encouraging me to pursue the right things. I know you will always be there whenever I need you and you are willing to share my happiness and sorrows. I know you will love me always. I am so lucky to be born in such a lovely family. I love you all!

TABLE OF CONTENTS

LIST OF TABLES

LIST OF FIGURES

LIST OF ABBREVIATIONS

MS	Mass Spectrometry
EI	Electron Ionization
CI	Chemical Ionization
MALDI	Matrix Assisted Laser Desorption Ionization
ESI	Electrospray Ionization
nESI	nano-Electrospray Ionization
TOF	Time of Flight
CRM	Charge Residue Mechanism
IEM	Ion Evaporation Mechanism
CEM	Chain Ejection Mechanism
EO	electroosmosis
Mb	myoglobin
aMb	apo-myoglobin
hMb	holo-myoglobin
CA	carbonic anhydrase
aCA	apo-carbonic anhydrase
hCA	holo-carbonic anhydrase
Cyt *c*	cytochrome *c*
eCyt *c*	equine cytochrome *c*
bCyt *c*	bovine cytochrome *c*
Ubi	ubiquitin
AA	ammonium acetate
aa	acetic acid
AF	ammonium formate
PTM	Post-Translational Modification
CD	Circular Dichroism

ABSTRACT

Author: Zhao, Feifei. PhD
Institution: Purdue University
Degree Received: May 2019
Title: Development and Application of Theta Tips as a Novel nESI-MS Ion Source and Protein Identification Using Limited Trypsin Digestion and Mass Spectrometry
Committee Chair: Scott A. McLuckey

Mass spectrometry is a widely used tool for efficient chemical characterization and identification. The development of electrospray ionization as a soft ionization method enables mass spectrometry for large biomolecule investigation. Protein is one of the most important classes of biomolecules, and its structural changes including folding, unfolding, aggregation, degradation and post-translational modification all influence protein bioactivity. Therefore, characterization and identification of proteins are important to understand protein functional mechanism, and eventually may contribute to disease treatment development. Protein conformational changes are normally very fast, and the initial stages, which significantly influence the conformation changing pathway, normally occur in milliseconds or shorter time scale. Such a fast structural change is hard to be monitored using traditional bulk solution manipulations, and fast sample preparation methods are required.

In this thesis project, theta tips were applied as a microreactor and nESI-MS emitter to perform fast protein manipulation immediately before MS analysis. Theta tips were operated in two modes. The first mode was for submillisecond time scale reactions. Proteins and reagents were loaded into different channels and sprayed out simultaneously. Proteins and reagents mixed and reacted in the Taylor cone and subsequent droplets for submillisecond time scale. Through this method, pH induced protein folding was investigated and protein folding intermediates were captured. The second mode was for milliseconds or longer reactions. Differential voltages were

applied to each channel before ionization and spray. The electric field between the two channels induced in-tip electroosmosis, which led to an in-tip mixing and reaction. In this mode, the reaction time was not limited by the droplet lifetime as in the first mode, but was controlled by electroosmosis time. By changing the electroosmosis square wave frequency and cycles, the mixing time was elongated to milliseconds or longer, which was suitable for slower reaction study.

Joule heating was discovered during theta tip electroosmosis when samples were dissolved in buffer. The Joule heating effect was high enough to heat up the aqueous solution to at least 75 ^{o}C based on Raman thermometry measurement, while the actual peak temperature could be higher. The Joule heating effect in theta tip electroosmosis was easily controlled by electroosmosis voltage, time, buffer concentration etc.. Proteins were thermally denatured by the Joule heating effect, and the denaturation extent was correlated with Joule heating parameters.

With this results in hand, we developed a protein melting temperature measurement method using theta tip Joule heating effect and mass spectrometry. This new melting temperature measurement method measured changes in protein mass and charge state distributions. Therefore, it could sensitively detect ligand loss and protein tertiary structural changes, which is an important compensation to current protein melting temperature measurement techniques like CD or DSC. Since the heating time is short and protein concentration for MS is low, protein aggregation and thermal fragmentation were highly avoided so a complete protein thermal unfolding process was monitored. Through theta tip electroosmosis denaturation of proteins and data processing using Gaussian fitting and sigmoidal fitting, protein melting voltages were identified, which could be converted to melting temperature with a calibrated temperature-voltage curve. The curve calibration still needs some further study to find a proper way to obtain standard protein melting temperature based on MS.

Besides single protein folding and unfolding, protein identification and post-translational modification are important for proteomics study. The traditional bottom-up, top-down and middle-down methods are not able to both preserve intact protein mass and efficiently generate fragment peaks without performing gas phase dissociation. In this thesis, we also developed a new way to identify proteins combining limited trypsin digestion and mass spectrometry. Intact protein mass was preserved for protein size and PTM identification. Enough tryptic peptides were also generated for protein identification through database search.

CHAPTER 1. INTRODUCTION

In 1912, Sir J. J. Thomson collected the first parabola mass spectrum [1, 2] , since when mass spectrometry has been quickly developed. Nowadays, mass spectrometry has become an irreplaceable analytical tool widely used in various areas like clinical [4], pharmaceutical [5], academic [6] , forensic [7] and geochronological [8] fields. Mass spectrometry measures chemical mass to charge ratio to identify ion mass. In combination with various dissociation methods, chemicals can be fragmented and generate certain fragmentation pattern. Based on the dissociation pathway and fragmentation patter, analyte structural information can be deduced. [3] Mass spectrometry is now a widely used chemical identification and characterization tool, taking advantage of its high accuracy, resolution, analytical speed and sensitivity.

1.1   Mass spectrometry

Mass spectrometry analysis involves multiple steps, from ionization, analyzation to detection. Through ionization, analyte molecules get charged and are able to be transferred to the analyzer and detector under electric fields. In the analyzer, analytes are isolated, dissociated or transformed through gas phase reaction for characterization. In the detector, the mass to charge ratio of the analytes is measured. Instrument schemes of the mass spectrometers used in this research are shown in Figure 1. 1.

1.1.1   Ionization

Ionization is the initial step for mass spectrometry analysis, where analytes lose or capture charged particles like electron, proton, Na^+ etc.to get ionized. [21] Based on energy level, ionization is normally categorized as "hard" ionization and "soft" ionization. [9] Electric ionization

(EI) is the most common hard ionization method. [10-12] Analyte molecules interact with high energy electron beam to get ionized, activated and fragmented. With the high energy interaction, a large amount of fragment information can be generated, which make it easy to establish an EI fragment database for quick chemical identification.

However, hard ionization method dissociates the majority of molecular ions, which make it difficult to preserve analyte molecular weight information. Chemical ionization (CI) as an alternative ionization method charges analyte molecules using charged chemicals. [13-15] Comparing to high energy electrons used in EI, charged chemical ions like CH_5^+ and NH_4^+ are milder, which will not fully break analyte molecules during ion-molecule reactions. Through this way, more molecular ions are generated for molecular mass identification. However, both EI and CI are mainly applied for small molecule analysis. Large biomolecule ionization has been a big challenge prior to 1980s.

In 1980s, the development of soft ionization techniques electrospray ionization (ESI) [16, 20] and matrix assisted laser desorption ionization (MALDI) [18, 19], promoted a big progress in bio-mass spectrometry development. With these techniques, large molecules with a molecular weight higher than 1000 Da can be very efficiently ionized and transferred and there's no obvious mass limit. [48] Through depositing a low energy onto analyte molecules, the thermal unstable biomolecules can survive from fragmentation during MALDI and ESI. ESI can even multiply charge biomolecules, which can reduce the mass to charge range of large molecules and make it possible to measure high molecular weight analytes on an instrument with low mass range limit. A more detailed mechanism analysis will be discussed in Section 1.2.

1.1.2   Ion manipulation and ion-ion reaction

In the analysis step, ions are transferred into the mass spectrometer and get isolated, fragmented or transformed. [22] In a quadrupole analyzer, by applying a certain combination of AC/DC voltages to generate a specific electric field, ions can be selectively ejected or preserved in the ion path. The ion stability relationship with quadrupolar electric field is described on a Mathew stability diagram. [129]

Ion-ion reaction is a gas phase reaction performed in an ion trap, which is used to efficiently manipulate analyte charge or manipulate chemical structure. [23] Through ionization of reagent molecules using opposite ionization voltages, reagent molecules will get opposite charges. Ions of opposite charges are sprayed into mass spectrometer separately and stored in the trap simultaneously for reaction. Reaction efficiency can be controlled by adjusting reagent ratio and mutual storage time. Various analyte modification has been performed including proton transfer,[24, 27, 28] covalent modification,[29, 32] complex formation, [30] oxidation [31, 33, 34] etc. Comparing to solution phase reactions and ion-molecule reactions, gas phase ion-ion reactions are kinetically and thermodynamically favored. [23] Ion-ion reactions are normally very exothermic and the transition state energy barriers are low. These properties increased ion-ion reaction efficiency.

Proton transfer reaction as shown in the scheme below is one of the most common gas phase ion-ion reactions, which is driven by gas phase proton affinity (PA) of reagents. [23]

$$[M+n\text{H}]^{n+} + \text{B}^- \rightarrow [M+(n\text{-}1)\text{H}]^{(n-1)+} + \text{HB} \quad (1)$$
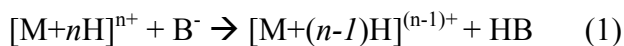
$$\Delta H_{rxn} = PA[M+(n\text{-}1)\text{H}]^{(n-1)+} - PA(\text{B}^-) \quad (2)$$

Proton transfer reactions are normally performed to reduce or even reverse charges of an analyte. [25, 26, 27] Biomolecules are multiply charged during ESI process, which increases the complexity of mass spectra. By reducing the charges of analytes through proton transfer, peaks are

better separated and the amount of peaks are reduced. [24, 27] This is especially useful in large biomolecules or mixture ESI-MS analysis. As proton transfer is physically reducing the charge state of analyte, it is less ambiguous comparing to software data processing like deconvolution operation.

1.2   Electrospray ionization (ESI)

In 1989, John Fenn et al. applied ESI to ionize protein molecules and successfully obtained multiply charged intact protein ions, which opened a new door for biomolecule analysis. [16, 17] In recognition of his contribution in large biomolecule analysis using mass spectrometry, John Fenn shared the 2002 Nobel prize in chemistry with Koichi Tanaka and Kurt Wüthrich.

1.2.1   Ionization process

The ESI process involves electric field induced charge uneven distribution, formation of Taylor cone, generation of charged droplets, releasing naked charged ions and transferring charged ions from ambient environment to vacuum. [35, 36, 49]

ESI ion source is normally a capillary and samples were loaded into the capillary through syringe pump. For ionization, a kilovolts voltage is applied to the sample and generate an electric field between the sample solution and the mass spectrometer counter electrode. The electric field leads to solvent polarization and forms a cone structure at the outlet of the tip pointing to the downfield of electric field. The cone structure is referred as Taylor cone. [37, 38] The electric force also drives the movement of positively charged ions along the downfield of electric field, while negative ions move in the opposite direction. This counter direction movement leads to charge uneven distribution in solution, and more positive ions accumulate in the Taylor cone. If the electric field is high enough and surpasses the surface tension of the Taylor cone, the Taylor cone

will rupture and form a jet emerging from the tip. Since the jet is highly occupied by positive ions, the high Coulomb repulsion on the jet surface will break the jet into small droplets. [39, 40]

Upon solvent evaporation, droplets will shrink and surface area is reduced. Therefore, droplet surface charge concentrates and the Coulomb repulsion significantly increase. When Coulomb repulsion surpasses the surface tension again, the droplet will encounter instability and rupture to smaller daughter droplets. The fission limit is normally referred as Rayleigh limit, which describes the stability of a charged droplet. The charge and radius of a droplet at the fission limit has a relationship of

$$q^2 = 64\pi^2\varepsilon_0\gamma a^3,$$

where q is charge, a is droplet radius, ε_0 is the vacuum permittivity, γ is the surface tension of the droplet. The fission process continues until naked ions are released.

1.2.2   Ionization mechanism

The way that naked ions get released from droplets are ionization mechanism. There are mainly three mechanisms for electrospray ionization, which are charge residue mechanism (CRM), ion evaporation mechanism (IEM) and chain ejection mechanism (CEM). (Figure 1. 2)

1.2.2.1   Charge residue mechanism (CRM)

Charge residue mechanism is most applicable to large molecule ionization. When the droplets get emitted from Taylor cone, they rapidly shrink through solvent evaporation and the charge concentrates in the droplets. Further droplet fission occurs when droplet charge and surface tension reaches Rayleigh limit. The repeated solvent evaporation and droplet fission eventually lead to the generation of small droplets containing only one analyte molecule in a droplet, along with some charged ions like protons and sodium cations. The charged ions will deposit onto naked molecules

upon final solvent evaporation and ionize the analyte molecules. Since CRM is based on charge deposition, biomolecule ions generated from CRM are normally highly adducted. [49, 50]

1.2.2.2   Ion evaporation mechanism (IEM)

Small molecule electrospray ionization is normally through ion evaporation mechanism. Different from charge residue mechanism that relies on full evaporation of solvent to deposit ions onto analyte, in ion evaporation model, charged small analyte directly escape from the droplets before droplet drying up. In this model, since most salt ions will be left in the droplets instead of sticking onto the evaporated ions, ions generated through evaporation mechanism are normally less adducted. Upon the evaporated ion-solvent cluster colliding with the curtain gas, solvent will be completely stripped off and naked ions can be transmitted to the mass spectrometer for further analysis. [51-54]

1.2.2.3   Chain ejection mechanism (CEM)

For large biomolecules, besides the commonly applied charge residue ionization mechanism, chain ejection mechanism is an alternative ionization pathway. The chain ejection mechanism was brought up by Lars Konermann et al. in 2013, which describes the ionization process for unfolded proteins. [55, 56] Different from charge residue mechanism, which is depositing ions onto compact protein molecules, chain ejection mechanism is protruding of unfolded protein ions directly from charged droplet through a process similar to ion evaporation. When droplet charge concentrated, part of the charged unfolded protein chain may escape from the droplet to reduce the Coulomb repulsion on the droplets. The Coulomb force between the droplet surface and the protruding portion of charged protein chain keeps interacting and drives the chain to eject out of the droplet to form a charged protein ion. This chain ejection model is proved by simulation, and it is also

supported by the phenomenon that high charge state protein peaks are normally less adducted comparing to low charge state protein peaks.

1.2.3 nano-Electrospray ionization (nESI)

In 1996, Wilm and Mann miniaturized the traditional ESI source to nESI, intending to reduce the amount of sample required. [43] Since then, nESI has been quickly developed and especially widely applied in bioanalytical field. [44, 45] Comparing to normal ESI, the biggest difference for miniaturized nESI ion source is the reduced capillary size. Conventional ESI ion source emitter diameter is about 100 μm and solution movement is driven by a syringe pump. The flow rate is normally in the range of μL/min, and the initial droplet diameter is of about 1-2 μm. [36, 43] However, nESI normally uses a pulled capillary as emitter and the tip size is less than10 μm. The solution flow is directly driven by electric field, and the flow rate is about tens or several nL/min, which is 100-1000 times lower than conventional ESI. [43, 46] These differences result in several advantages for nESI. (1) nESI requires smaller amount of sample. This is especially important for bioanalysis since biomolecules like proteins are normally precious and sample amount is limited. [36] (2) nESI has higher ionization efficiency. The initial droplet size formed from nESI is smaller, so solvent evaporation and ion formation efficiency is increased. (3) nESI has higher salt tolerance. Since the droplet is smaller, there is only about one molecule in a droplet, so the salt content is lower. This reduces the salt and contaminant signal suppression effect and results in cleaner spectra. [46, 43] (4) nESI emitter is usually a capillary, which is good for off-line operation. It is also disposable and reduces cross contamination between experiments. [43]

1.3   Protein structure

Protein is one of the most important classes of large biomolecules, which significantly influences physiological function. Protein bioactivity is directly related to its structure, which is categorized as primary, secondary, tertiary and quaternary structures. [47, 57]

1.3.1   Primary structures

Protein primary structure is the sequence of amino acids connected through peptide bonds from N-terminus to C-terminus. Primary structure analysis and amino acid sequence identification normally requires peptide bond dissociation, which is done either through solution phase digestion/degradation or gas phase dissociation. [60, 63, 64] The covalent bonding property determines the high stability of protein primary structure. To break peptide bonds in gas phase without the assistance of enzyme or catalyst, a high energy need to be deposited onto the protein sample. In mass spectrometry analysis, the energy can be deposited during the ionization step (eg. EI), transition step or dissociation step (eg. collision induced dissociation, electron capture dissociation). [58-62]

1.3.2   Secondary structures

The linear primary structure is normally not the most common structure for proteins. Instead, amino acid peptide bond and side chains will interact with each other and form secondary structures like alpha helices, beta sheets, beta turns, beta hairpins, random coils etc. [47] Since some secondary structures have an ordered folding pattern, they could selectively absorb certain light wavelength. Therefore, spectroscopic analysis like circular dichroism (CD) can be readily applied to investigate the secondary structural changes. [65-68]

1.3.3   Tertiary and quaternary structures

To fulfill a protein biofunction, it normally needs to form a certain tertiary or quaternary structure. Tertiary structure is formed by further folding of the primary and secondary structure to form more delicate and complex three dimensional domains. The high order structure is stabilized by various forces including disulfide covalent bond linkage, [69-72] hydrogen bonding, [73] hydrophobic interaction [74, 75] and ligand-protein chelation [76]. Intermolecular interactions among different protein molecules resulted in the formation of protein complex, which is refereed as quaternary structure. [77] Formation of tertiary or quaternary structure significantly changes the globular size and surface property of proteins. Since the higher order structures are mainly stabilized by noncovalent interactions besides disulfide bond linkage, these structures are not as stable, which cannot stand high energy analysis methods. X-ray crystallization analysis could give very accurate crystal high order structure of proteins, while it is not suitable for solution phase conformation analysis. [78] Spectroscopic methods like fluorescence spectroscopy is able to provide some conformation information, but it mainly probes limited amount of chromophores. [79]

Mass spectrometry coupling with soft ionization methods like ESI provided an alternative way to investigate protein high order structures. [80-87] As mentioned before, proteins are normally multiply charged during ESI process and the charge state distribution is related to protein conformation. It is widely accepted that high charge state distribution corresponds to more unfolded conformation while low charge state distribution corresponds to more folded conformation. [84] (Figure 1. 3) Protein quaternary structure dissociation can also be easily detected by measuring the mass loss of the complex. [88, 89]

Protein three-dimensional structure is referred to as protein conformation. Each protein has a well-defined unique low entropy structure, which is normally called the native state. Upon

treatment of different denaturation conditions, protein three dimensional structure will be destructed and form structures with different random configurations. The final fully destructed structure is the unfolded conformation or denatured state. [90]

1.4 Protein conformation manipulation methods

Protein conformation can be changed by various factors including pH, temperature, surface tension, ionic strength, salt interaction etc. [92-95] To study protein conformation, these environmental conditions need to be well considered and controlled. Protein folding and unfolding are normally a stepwise process, and the time scale for each folding process is different. Protein equilibrium states also vary at different conditions. Here I will categorize protein manipulation methods into three categories: bulk solution reaction, droplet reaction and gas phase ion-ion reaction.

1.4.1 Bulk solution reaction

The traditional method to manipulate protein conformation is performed in bulk solution. [103-105] The bulk solution provides protein an environmental condition, under which proteins exist in specific steady states. By changing the bulk solution environment like pH and temperature, protein conformation can be altered. The bulk solution environmental condition can be adjusted by adding acid/base, increasing/decreasing temperature and changing solvent composition. Bulk solution reactions are very suitable for thermodynamic studies. The operation time is long so it's easy for proteins to reach equilibrium states.

1.4.2 Droplet reaction

As mentioned before, protein folding and unfolding are stepwise through multiple folding intermediates. [106-109] The folding intermediates determines the folding pathway and

mechanism. Intermediates can misfold or aggregate and eventually cause some diseases like Alzehimer's disease and Parkinson's disease. [110, 111] Since the time scale to form the intermediates is normally within milliseconds or even submillisecond and most of the folding intermediates are very short lived, they cannot be preserved in bulk solution manipulation. [112-114] Therefore, fast manipulation and sampling methods are required.

The commercialized fast reaction method is performed in a stopped flow device, in which the reaction time is limited by the mixing cell size. [115-118] The mixing time is in milliseconds time scale, although some newer modification can reduce the reaction time to microseconds. Comparing to stopped flow, droplet reaction is simpler and normally doesn't require very special equipment. Several droplet reaction methods have been developed, include multiple spray[128], vapor leak-in [119-121] and theta tip mixing [98-101, 122-127]. For all droplet interactions, the reaction time is easily shortened to microseconds or even nanoseconds, which enables the capture of short-lived intermediates.

1.4.2.1   Multiple spray

Multiple spray is using multiple emitters to spray protein solution and reagents separately from different capillaries. [128] By adjusting the angle and position of the emitters, the droplets are able to mix before drying up so proteins are able be modified by the reagent in droplets. The reaction time is limited by droplet lifetime, which is normally several microseconds. To achieve good droplet reaction using the multiple spray technique, tip lining direction and position are essential. More advanced setup is to manufacture a multispray chip or a multiple spray stage to facilitate the position adjusting steps.

1.4.2.2   Vapor leak-in

Besides droplet-droplet interaction, droplets are able to interact with reagent vapor to fulfill fast reactions. [119-121] Vapor leak-in method was developed by McLuckey group to investigate pH induced protein unfolding. By spraying protein solution from a nESI tip and leak-in acid vapor into the curtain gas, protein reacted with volatile reagent for microseconds and unfolded. Protein unfolding intermediates were successfully captured. Leaking-in organic vapor was also applied to reduce salt adduction in protein ions. Vapor leak-in is a very convenient and efficient reaction technique, but it requires the reagent to be volatile, which becomes a limitation to this technique.

1.4.2.3   Theta tip

Theta tips were pulled from dual channel theta capillaries, which contain a septum passing along the whole capillary to divide a capillary into two parallel channels. Since theta tips have two channels, different solutions can be loaded into each channel, and mix in the common Taylor cone and subsequent droplet upon application of spray voltages. Theta tips were first developed by Mark, et al to study vancomycin interaction with a small peptide. [122] Since the success of the first fast reaction performed in theta tips, several groups including McLuckey group, Williams group, Zare group etc. have been devoting into the development of this novel nESI-MS emitter and micromixer and apply it to perform all kinds of fast droplet reactions. [98-101, 122-127]. Currently, there are mainly two ways to operate theta tips (Figure 1. 4): one is to apply spray voltages to one or two channels directly and spray the solutions out simultaneously. Reagents in the two channels could react in the Taylor cone and droplets. [98, 101] In this case, the reaction time is limited by droplet lifetime, which is several microseconds or even shorter. The droplet lifetime is related to tip size. Within this short reaction time scale, protein-reagent interaction is very immediate so multiple folding intermediates were captured. HDX were also performed in theta tips. [123] A second

operation mode is inducing electroosmosis by applying differential voltages between the two channels before spray. [127] In this case, reaction time is controlled by electroosmosis time, which can be milliseconds or longer. This allows the study of relatively slower reactions and the reaction time is more controllable.

1.5   Conclusions

Mass spectrometry is a very useful tool to analyze chemical structure, taking advantage of its high sensitivity, accuracy, analytical speed and low sample amount requirement. The development of soft ionization methods promoted mass spectrometry application in biomolecule analysis. Electrospray ionization as an important soft ionization technique especially contributed to the protein high order structure analysis using mass spectrometry. One important advantage for ESI-MS protein analysis is that proteins get multiply charged through ESI and the charge state distributions reflect protein conformations.

Biomolecule high order structural change like protein folding and unfolding directly influence their function, so understanding folding process and mechanism is essential. However, the folding/unfolding is fast and the folding intermediates are short-lived. Droplet interaction provides a fast sampling method, which can couple to mass spectrometry to investigate the short lived folding intermediates and help understand protein folding or misfolding mechanisms. Theta-tip is one of the useful tools to manipulate protein conformation during submillisecond to milliseconds or longer time based on the operation modes. The combination of theta tips with mass spectrometry could establish a fast reaction performing and monitoring platform, which can be applied to study fast protein conformational changes.

1.6   References

1. Thomson, J. J. XXVI. Rays of positive electricity. Philos. Mag. Series 6, 1911, 21, 225-249.

2. Thomson, J. J. XIX. Further experiments on positive rays. Philos. Mag. Series 6, 1912, 24, 209-253.

3. Glish, G. L.; Vachet, R. W. The basics of mass spectrometry in the twenty first century. Nat. Rev. Drug Discov. 2003, 2, 140-150.

4. Roux, A.; Lison, D.; Junot, C.; Heilier, J. Applications of liquid chromatography coupled to mass spectrometry-based metabolomics in clinical chemistry and toxicology: A review. Clin. Biochem. 2011, 44, 119-135.

5. Lee, M. S.; Kerns, E. H. LC/MS applications in drug development. Mass Spectrom. Rev. 1999, 18, 187-279.

6. Bantscheff, M.; Schirle, M.; Sweetman, G.; Rich, J.; Kuster, B. Quantitative mass spectrometry in proteomics: a critical review. Anal. Bioanal. Chem. 2007, 389, 1017-1031.

7. Benson, S.; Lennard, C.; Maynard, P.; Roux, C. Forensic applications of isotope ratio mass spectrometry-A review. Forensic Sci. Int. 157, 2006, 1-22.

8. Jackson, S. E.; Pearson, N. J.; Griffin, W. L.; Belousova, E. A. The application of laser ablation-inductively coupled plasma-mass spectrometry to in situ U-Pb zircon geochronology. Chem. Geol. 211, 2004, 47-69.

9. Wang, Y.; Sun, J.; Qiao, J.; Ouyang, J.; Na, N. A "soft" and "hard" ionization method for comprehensive studies of molecules. Anal. Chem. 2018, 90, 14095-4099.

10. Aiken, A. C.; DeCarlo, P. F.; Jimenez, J. L. Elemental analysis of organic species with electron ionization high-resolution mass spectrometry. Anal. Chem. 2007, 79, 8350-8358.

11. Luffer, D. R.; Schram, K. H. Electron ionization mass spectrometry of synthetic C_{60}. Rapid Commun. Mass Spectrom. 1990, 4, 552-556.

12. Regert, M.; Rolando, C. Identification of archaeological adhesives using direct inlet electron ionization mass spectrometry. Anal. Chem. 2002, 74, 965-975.

13. Harrison, A. G. Chemical Ionization Mass Spectrometry, 2nd Edition. CRC Press: New York ,1992.

14. Munsun, M. S. B.; Field, F. H. Chemical ionization mass spectrometry. J. Am. Chem. Soc. 1966, 88, 2621-2630.

15. Hunt, D. F.; Stafford Jr., G. C.; Crow, F. W.; Russel, J. W. Pulsed positive negative ion chemical ionization mass spectrometry. Anal. Chem. 1976, 48, 2098-2104.

16. Fenn, J. B.; Mann, M.; Meng, C. K.; Wong, S. F.; Whitehouse, C. M. Electrospray ionization for mass spectrometry of large biomolecules. Science 1989, 246, 64-71.

17. Yamashita, M.; Fenn, J. B. Electrospray ion source. another variation of the free-jet theme. J. Phys. Chem. 1984, 88, 4451-4459.

18. Karas, M.; Bachmann, D.; Bahr, U.; Hillenkamp, F. Matrix-assisted ultraviolet laser desorption of non-volatile compounds. Int. J. Mass Spectrom. Ion Proc. 1987, 78, 53-68.

19. Mädler S.; Erba E.B.; Zenobi, R. MALDI-TOF mass spectrometry for studying noncovalent complexes of biomolecules. In: Cai Z., Liu S. (eds) Applications of MALDI-TOF Spectroscopy. Topics in Current Chemistry. Springer: Berlin, Heidelberg, 2012.

20. Banerjee, S.; Mazumdar, S. Electrospray ionization mass spectrometry: A technique to access the information beyond the molecular weight of the analyte. Int. J. Anal. Chem. 2012. Article ID 282574.

21. Siuzdak, G. An introduction to mass spectrometry ionization: an excerpt from the expanding role of mass spectrometry in biotechnology, 2nd Edition. MCC Press: San Diego, 2005.

22. March, R. E. An introduction to quadrupole ion trap mass spectrometry. J. Mass Spectrom. 1997, 32, 351-369.

23. McLuckey, S. A.; Stephenson Jr., J. L. Ion/ion chemistry of high-mass multiply charged ions. Mass Spectrom. Rev. 1998, 17, 369-407.

24. Stephenson, J. L.; McLuckey, S. A. Ion/ion proton transfer reactions for protein mixture analysis. Anal. Chem. 1996, 68, 4026-4032.

25. Randolph, C. E.; Foreman, D. J.; Betancourt, S. K.; Blanksby, S. J.; McLuckey, S. A. Gas-phase ion/ion reactions involving tris-phenanthroline alkaline earth metal complexes as charge inversion reagents for the identification of fatty acids. Anal. Chem. 2018, 90, 12861-12869.

26. Loo, R. R. O.; Udseth, H. R.; Smith, R. D. Evidence of charge inversion in the reaction of singly charged anions with multiply charged macroions. J. Phys. Chem., 1991, 95, 6412-6415.

27. Betancourt, S. K.; Pilo, A. L.; Bu, J.; McLuckey, S. A. Simplification of electrospray mass spectra of polysorbate 80 via cation transfer to carborane anions. J. Mass Spectrom. 2016, 51, 453-458.

28. Scalf, M.; Westphall, M. S.; Smith, L. M. Charge reduction electrospray mass spectrometry. Anal. Chem., 2000, 72, 52-60.

29. Mentinova, M.; McLuckey, S. A. Intra- and inter-molecular cross-linking of peptide ions in the gas-phase: Reagents and conditions. J. Am. Soc. Mass Spectrom. 2011, 22, 912-921.

30. Foreman, D. J.; Betancourt, S. K.; Pilo, A. L.; McLuckey, S. A. Novel peptide ion chemistry associated with gold (I) cationization: Preferential cleavage at lysine residues. Int. J. Mass Spectrom. 2018, 42, 114-122.

31. Pilo, A. L.; Bu, J.; McLuckey, S. A. Gas-phase oxidation of neutral basic residues in polypeptide cations by periodate. J. Am. Soc. Mass Spectrom. 2016, 27, 1979-1988.

32. Bu, J.; Pilo, A. L.; McLuckey, S. A. Gas phase click chemistry via ion/ion reactions. Int. J. Mass Spectrom., 2015, 390, 118-123.

33. Pilo, A. L.; McLuckey, S. A. Selective gas-phase ion/ion reactions: enabling disulfide mapping via oxidation and cleavage of disulfide bonds in intermolecularly-linked polypeptide ions. Anal. Chem. 2016, 88, 8972-8979.

34. Pilo, A. L.; Zhao, F.; McLuckey, S. A. Selective gas-phase oxidation and localization of alkylated cysteine residues in polypeptide ions via ion/ion chemistry. J. Proteome. Res. 2016, 15, 3139-3146.

35. Bruins, A. P. Mechanistic aspects of electrospray ionization. J. Chromatogr. A 1998, 794, 345-357.

36. Kebarle, P.; Verkerk, U. H. Electrospray: From ions in solution to ions in the gas phase, what we know now. Mass Spectrom. Rev. 2009, 28, 898-917.

37. Taylor, G. I.; McEwan, A. D. The stability of a horizontal fluid interface in a vertical electric field. J. Fluid Mech. 1965, 22, 1-15.

38. Fernandez de la Mora, J. The fluid dynamics of Taylor cones. J. Annu. Rev. Fluid. Mech. 2007, 39, 217-243.

39. Cloupeau, M. Recipes for use of EHD spraying in cone-jet mode and notes on corona discharge effects. J. Aerosol. Sci. 1994, 25, 1143-1157.

40. Cloupeau, M.; Prunet-Foch, B. Electrohydrodynamic spraying functioning modes: A critical review. J. Aerosol. Sci. 1994, 25, 1021-1036.

41. Wilm, M.; Mann, M. Electrospray and Taylor-Cone theory, Dole's beam of macromolecules at last? Int. J. Mass Spectrom. Ion Proc. 1994, 136, 167-180.

42. Juraschek, R.; Dulks, T.; Karas, M. Nanoelectrospray-More than just a minimized-flow electrospray ion source. J. Am. Soc. Mass Spectrom., 1999, 10, 300-308.

43. Wilm, M.; Mann, M. Analytical properties of the nanoelectrospray ion source. Anal. Chem. 1996, 68, 1-8.

44. Pan, P.; Guawardena, H. P.; Xia, Y.; McLuckey, S. A. Nanoelectrospray ionization of protein mixtures: solution pH and protein pI. Anal. Chem. 2004, 76, 1165-1174.

45. Chen, S. Rapid protein identification using direct infusion nanoelectrospray ionization mass spectrometry. Proteomics 2006, 6, 16-25.

46. Schmidt, A.; Karas, M.; Dülcks, T. Effect of different solution flow rates on analyte ion signals in nano-ESI MS, or: When does ESI turn into nano-ESI? J. Am. Soc. Mass Spectrom. 2003, 14, 492-500.

47. Boye, J. I.; Ma, C. Y.; Harwalkar, V. R. Thermal denaturation and coagulation of proteins. In: Damodaran, S.; Paraf, A. (eds) Food Proteins and Their Applications. CRC Press: Marcel Dekker, Inc. 1997.

48. Wilm, M. Principles of electrospray ionization. Mol. Cell Proteomics 2011, 10, M111.009407.

49. Kebarle, P.; Peschke, M. On the mechanisms by which the charged droplets produced by electrospray lead to gas phase ions. Anal. Chim. Acta. 2000, 406, 11-35.

50. Cole, R. B. Some tenets pertaining to electrospray ionization mass spectrometry. J. Mass Spectrom. 2000, 35, 763-772.

51. Iribarne, J. V.; Thomson, B. A. On the evaporation of small ions from charged droplets. J. Chem. Phys. 1976, 64, 2287-2294.

52. Znamenskiy, V.; Marginean, I.; Vertes, A. Solvated ion evaporation from charged water nanodroplets. J. Phys. Chem. A 2003, 107, 7406-7412.

53. Loscertales, I. G.; Fernández de la Mora, J. Experiments on the kinetics of field evaporation of small ions from droplets. J. Chem. Phys. 1995, 103, 5041-5060.

54. Labowskya, M.; Fenn, J. B.; Fernandez de la Mora, J. A continuum model for ion evaporation from a drop: effect of curvature and charge on ion solvation energy. Anal. Chim. Acta. 2000, 406, 105-118.

55. Konermann, L.; Ahadi, E.; Rodriguez, A. D.; Vahidi, S. Unraveling the mechanism of electrospray ionization. Anal. Chem., 2013, 85, 2-9.

56. Konermann, L.; Rodriguez, A. D.; Liu, J. Unraveling the mechanism of electrospray ionization. Anal. Chem. 2012, 84, 6798-6804.

57. Andersen, N. H. Protein Structure, Stability and Folding. Methods in Molecular Biology. Humana Press: Totowa, NJ, 2001.

58. Fung, Y. M. E.; Adams, C. M.; Zubarev, R. A. Electron ionization dissociation of singly and multiply charged peptides. J. Am. Chem. Soc. 2009, 131, 9977-9985.

59. Syka, J. E. P.; Coon, J. J.; Schroeder, M. J.; Shabanowitz, J.; Hunt, D. F. Peptide and protein sequence analysis by electron transfer dissociation mass spectrometry. Proc. Natl. Acad. Sci. U.S.A. 2004, 101, 9528-9533.

60. Brodbelt, J. S. Ion activation methods for peptides and proteins. Anal. Chem. 2016, 88, 30-51.

61. Zhurov, K. O.; Fornelli, L.; Wodrich, M. D.; Laskay, Ü, A.; Tsybin, Y. O. Principles of electron capture and transfer dissociation mass spectrometry applied to peptide and protein structure analysis. Chem. Soc. Rev. 2013, 42, 5014-5030.

62. Wells, J. M.; McLuckey, S. A. Collision-induced dissociation (CID) of peptides and proteins. Methods Enzymol. 2005, 402, 148-185.

63. Klemm, P. Manual Edman degradation of proteins and peptides. Methods Mol. Biol. 1984, 1, 243-254.

64. Williams, K. R.; Stone, K. L. Enzymatic cleavage and HPLC peptide mapping of proteins. Mol. Biotechnol. 1997, 8, 155-167.

65. Greenfield, N. J. Using circular dichroism spectra to estimate protein secondary structure. Nat. Protoc. 2006, 1, 2876-2890.

66. Johnson Jr., W. C. Protein secondary structure and circular dichroism: A practical guide. Proteins: Structure, Stability and Genetics 1990, 7, 205-214.

67. Whitmore, L.; Wallace, B. A. Protein secondary structure analyses from circular dichroism spectroscopy: Methods and reference databases. Biopolymers 2008, 89, 392-400.

68. Sreerama, N.; Woody, R. W. A self-consistent method for the analysis of protein secondary structure from circular dichroism. Anal. Biochem. 1993, 209, 32-44.

69. Anfinsen, C. B. Principles that govern the folding of protein chains. Science 1973, 181, 223-230.

70. Wedemeyer, W. J.; Welker, E.; Narayan, M.; Scheraga, H. A. Disulfide bonds and protein folding. Biochemistry 2000, 39, 4207-4216.

71. Shimaoka, M.; Lu, C.; Palframan, R. T.; von Andrian, U. H.; McCormack, A.; Takagi, J.; Springer, T. A. Reversibly locking a protein fold in an active conformation with a disulfide bond: Integrin αL I domains with high affinity and antagonist activity in vivo. Proc. Natl. Acad. Sci. U.S.A. 2001, 98, 6009-6014.

72. Pace, C. N. Conformational stability of globular proteins. Cell Press: Trends in Biochemical Sciences 1990, 15, 14-17.

73. Pace, C. N.; Fu, H.; Fryar, K. L.; Landua, J.; Trevino, S. R.; Schell, D.; Thurlkill, R. L.; Imura, S.; Scholtz, J. M.; Gajiwala, K.; Sevcik, J.; Urbanikova, L.; Myers, J. K.; Takano, K.; Hebert, E. J.; Shirley, B. A.; Grimsley, G. R. Contribution of hydrogen bonds to protein stability. Protein Sci. 2014, 23, 652-661.

74. Tanford, C. Contribution of hydrophobic interactions to the stability of the globular conformation of proteins. 1962, 84, 4240-4247.

75. Creighton, T. E. Proteins: Structures and Molecular Properties. W. H. Freeman and Company: New York, NY, 1993.

76. Ikura, M. Calcium binding and conformational response in EF-hand proteins. Trends Biochem Sci. 1996, 21, 14-17.

77. Janin, J.; Bahadur, R. P.; Chakrabarti, P. Protein-protein interaction and quaternary structure. Q. Rev. Biophys. 2008, 41, 133-180.

78. Svergun, D. I.; Petoukhov, M. V.; Koch, M. H. J. Determination of domain structure of proteins from X-ray solution scattering. Biophys. J. 2001, 80, 2946-2953.

79. Eftink, M. R. Fluorescence techniques for studying protein structure. Methods Biochem. Anal. Protein Struct. Determ. 2006, 35, 127-205.

80. Fenn, J. B.; Mann, M.; Meng, C. K.; Wong, S. F.; Whitehouse, C. M. Electrospray ionization for mass spectrometry of large biomolecules. Science 1989, 246, 64-71.

81. Wilm, M.; Mann, M. Analytical properties of the nanoelectrospray ion source. Anal. Chem. 1996, 68, 1-8.

82. Pan, P.; Guawardena, H. P.; Xia, Y.; McLuckey, S. A. Nanoelectrospray ionization of protein mixtures: solution pH and protein pI. Anal. Chem. 2004, 76, 1165-1174.

83. Chen, S. Rapid protein identification using direct infusion nanoelectrospray ionization mass spectrometry. Proteomics 2006, 6, 16-25.

84. Chowdhury, S. K.; Katta, V.; Chait, B. T. Probing conformational changes in proteins by mass spectrometry. J. Am. Chem. Soc. 1990, 112, 9012-9013.

85. Kaltashov, I. A.; Eyles, S. J. Studies of biomolecular conformations and conformational dynamics by mass spectrometry. Mass Spectrom. Rev. 2002, 21, 37-71.

86. Fenn, J. B. Ion formation from charged droplets: Roles of geometry, energy, and time. J. Am. Soc. Mass Spectrom. 1993, 4, 524-535.

87. Loo, J. A.; Loo, R. R.; Udseth, H. R.; Edmonds, C. G.; Smith, R. D. Solvent-induced conformational changes of polypeptides probed by electrospray-ionization mass spectrometry. Rapid Commun. Mass Spectrom. 1991, 5, 101-105.

88. Light-Wahl, K. J.; Schwartz, B. L.; Smith, R. D. Observation of the noncovalent quaternary associations of proteins by electrospray ionization mass spectrometry. J. Am. Chem. Soc. 1994, 116, 5271-5278.

89. Back, J. W.; Hartog, F.; Dekker, H. L.; Muijsers, A. O.; de Koning, L. J.; de Jong, L. A new crosslinker for mass spectrometric analysis of the quaternary structure of protein complexes. J. Am. Soc. Mass Spectrom. 2001, 12, 222-227.

90. Mirsky, A. E.; Pauling, L. On the structure of native, denatured, and coagulated proteins. Proc. Natl. Acad. Sci. U.S.A. 1936, 22, 439-447.

91. Iavarone, A. T.; Jurchen, J. C.; Williams, E. R. Effects of solvent on the maximum charge state and charge state distribution of protein ions produced by electrospray ionization. J. Am. Soc. Mass Spectrom. 2000, 11, 976-985.

92. Le Blanc, J. C. Y.; Wang, J.; Guevremont, R.; Siu, K. W. M. Electrospray mass spectra of protein cations formed in basic solutions. Org. Mass Spectrom. 1994, 29, 587-593.

93. Iavarone, A. T.; Jurchen, J. C.; Williams, E. R. Supercharged protein and peptide ions formed by electrospray ionization. Anal. Chem. 2001, 73, 1455-1460.

94. Ueki, N.; Chow, C.; Ochiai, Y. Characterization of bullet tuna myoglobin with reference to the thermostability-structure relationship. J. Agric. Food Chem. 2005, 53, 4968-4975.

95. Ibarra-Molero, B.; Loladze, V. V.; Makhatadze, G. I.; Sanchez-Ruiz, J. M. Thermal versus guanidine-induced unfolding of ubiquitin. an analysis in terms of the contributions from charge-charge interactions to protein stability. Biochemistry 1999, 38, 8138-8149.

96. Bushmarina, N. A.; Kuznetsova, I. M.; Biktashev, A. G.; Turoverov, K. T.; Uversky, V. N. Partially folded conformations in the folding pathway of bovine carbonic anhydrase II: a fluorescence spectroscopic analysis. Chembiochem 2001, 2, 813-821.

97. Semisotnov, G. V.; Rodionova, N. A.; Kutyshenko, V. P.; Ebert, B.; Blanck, J.; Ptitsyn, O. B. Sequential mechanism of refolding of carbonic anhydrase B. FEBS Lett. 1987, 224, 9-13.

98. Fisher, C. M.; Kharlamova, A.; McLuckey, S. A. Affecting protein charge state distributions in nano-electrospray ionization via in-spray solution mixing using theta capillaries. Anal. Chem. 2014, 86, 4581-4588.

99. Mortensen, D. N.; Williams, E. R. Theta-glass capillaries in electrospray ionization: rapid mixing and short droplet lifetimes. Anal. Chem. 2014, 86, 9315-9321.

100. Mortensen, D. N.; Williams, E. R. Investigating protein folding and unfolding in electrospray nanodrops upon rapid mixing using theta-glass emitters. Anal. Chem. 2015, 87, 1281-1287.

101. Mortensen, D. N.; Williams, E. R. Ultrafast (1 µs) mixing and fast protein folding in nanodrops monitored by mass spectrometry. J. Am. Chem. Soc. 2016, 138, 3453-3460.

102. Urban, P. L.; Chen, Y.; Wang, Y. Applications of time-resolved mass spectrometry in the studies of protein structure dynamics. In: Time-Resolved Mass Spectrometry: From Concept to Applications. John Wiley & Sons, Ltd: West Sussex, 2016.

103. Monahan, F. J.; German, J. B.; Kinsella, J. E. Effect of pH and temperature on protein unfolding and thiol/disulfide interchange reactions during heat-induced gelation of whey proteins. J. Agric. Food Chem. 1995, 43, 46-52.

104. Otzen, D. E. Protein unfolding in detergents: Effect of micelle structure, ionic strength, pH, and temperature. Biophys. J. 2002, 83, 2219-2230.

105. Sahin, E.; Grillo, A. O.; Perkins, M. D.; Roberts, C. J. Comparative effects of pH and ionic strength on protein-protein interactions, unfolding, and aggregation for IgG1 antibodies. J. Pharm. Sci. 2010, 99, 4830-4848.

106. Baldwin, R. L. The nature of protein folding pathways: The classical versus the new view. J. Biomol. NMR. 1995, 5, 103-109.

107. Evans, P. A.; Radford, S. E. Probing the structure of folding intermediates. Curr. Opin. Struc. Biol. 1994, 4, 100-106.

108. Balbach, J.; Forge, V.; van Nuland, N. A. J.; Winder, S. L.; Hore, P. J.; Dobson, C. M. Following protein folding in real time using NMR spectroscopy. Nature Struct. Biol. 1995, 2, 865-870.

109. Dill, K. A.; Stigter, D. Modeling protein stability as hetero polymer collapse. Advan. Protein Chem. 1995, 46, 59-104.

110. Selkoe, D. J. Alzheimer's disease: genes, proteins, and therapy. Physiol. Rev. 2001, 81, 741-766.

111. Bucciantini, M.; Giannoni, E.; Chiti, F.; Baroni, F.; Formigli, L.; Zurdo, J.; Taddei, N.; Ramponi, G.; Dobson, C. M.; Stefani, M. Inherent toxicity of aggregates implies a common mechanism for protein misfolding diseases. Nature 2002, 416, 507-511.

112. Jackson, S. E.; Fersht, A. R. Folding of chymotrypsin inhibitor 2. Evidence for a two-state transition. Biochemistry 1991, 30, 10428-10435.

113. Otzen, D. E.; Itzhaki, L. S.; ElMasry, N. F.; Jackson, S. E.; Fersht, A. R. Structure of the transition state for the folding/unfolding of the barley chymotrypsin inhibitor 2 and its implication for mechanisms of protein folding. Proc. Natl. Acad. Sci. U.S.A. 1994, 91, 10422-10425.

114. Alexander, P.; Fahnestock, S.; Lee, T.; Orban, J.; Bryan, P. Thermodynamic analysis of the folding of the streptococcal protein G IgG-binding domains B1 and B2: why small proteins tend to have high denaturation temperatures. Biochemistry 1992, 31, 3597-3603.

115. Groves, J. T.; Lee, J.; Marla, S. S. Detection and characterization of an oxomanganese(V) porphyrin complex by rapid-mixing stopped-flow spectrophotometry. J. Am. Chem. Soc. 1997, 119, 6269-6273.

116. Kuwajima, K.; Yamaya, H.; Miwa, S.; Sugai, S.; Nagamura, T. Rapid formation of secondary structure framework in protein folding studied by stopped-flow circular dichroism. FEBS Lett. 1987, 31, 115-118.

117. Bevilacqua, P. C.; Kierzek, R.; Johnson, K. A.; Turner, D. H. Dynamics of ribozyme binding of substrate revealed by fluorescence-detected stopped-flow methods. Science 1992, 258, 1355-1358.

118. Scarpa, A.; Graziotti, P. Mechanisms for intracellular calcium regulation in heart. J. Gen. Physiol. 1973, 62, 756-772.

119. Kharlamova, A.; Prentice, B. M.; Huang, T.; McLuckey, S. A. Electrospray droplet exposure to gaseous acids for the manipulation of protein charge state distributions. Anal. Chem. 2010, 82, 7422-7429.

120. Kharlamova, A.; McLuckey, S. A. Negative electrospray droplet exposure to gaseous bases for the manipulation of protein charge state distributions. Anal. Chem. 2011, 83, 431-439.

121. Kharlamova, A.; DeMuth, J. C.; McLuckey, S. A. Vapor treatment of electrospray droplets: evidence for the folding of initially denatured proteins on the sub-millisecond time-scale. J. Am. Soc. Mass Spectrom. 2011, 23, 88-101.

122. Mark, L. P.; Gill, M. C.; Mahut, M.; Derrick, P. J. Dual nano-electrospray for probing solution interactions and fast reactions of complex biomolecules. Eur. J. Mass Spectrom. 2012, 18, 439-446.

123. Jansson, E. T.; Lai, Y.; Santiago, J. G.; Zare, R. N. Rapid hydrogen-deuterium exchange in liquid droplets. J. Am. Chem. Soc. 2017, 139, 6851-6854.

124. Walker, K. L.; Dornan, L. M.; Zare, R. N.; Waymouth, R. M.; Muldoon, M. J. Mechanism of catalytic oxidation of styrenes with hydrogen peroxide in the presence of cationic palladium(II) complexes. J. Am. Chem. Soc. 2017, 139, 12495-12503.

125. Miller, C. F.; Kulyk, D. S.; Kim, J. W.; Badu-Tawiah, A. K. Re-configurable, multi-mode contained electrospray ionization for protein folding and unfolding on the millisecond time scale. Analyst 2017, 142, 2152-2160.

126. Liu, F.; Lu, W.; Yin, X.; Liu, J. Mechanistic and kinetic study of singlet O_2 oxidation of methionine by on-line electrospray ionization mass spectrometry. J. Am. Soc. Mass Spectrom. 2016, 27, 59-72.

127. Fisher C. M.; Hilger, R. T.; Zhao, F.; McLuckey, S. A. Electroosmotically driven solution mixing in borosilicate theta glass nESI emitters. J. Mass Spectrom. 2015, 50, 1063-1070.

128. Qiu, R.; Zhang, C.; Qin, Z.; Luo, H. A multichannel rotating electrospray ionization mass spectrometry (MRESI): instrumentation and plume interactions. RSC Adv. 2016, 6, 36615-36622.

129. March, R. E.; Londry, F. A. Theory of mass spectrometry. In: Practical Aspects of Ion Trap Mass Spectrometry. March, R. E.; Todd, J. F. J. (eds) CRC Press: New York, NY, 1995.
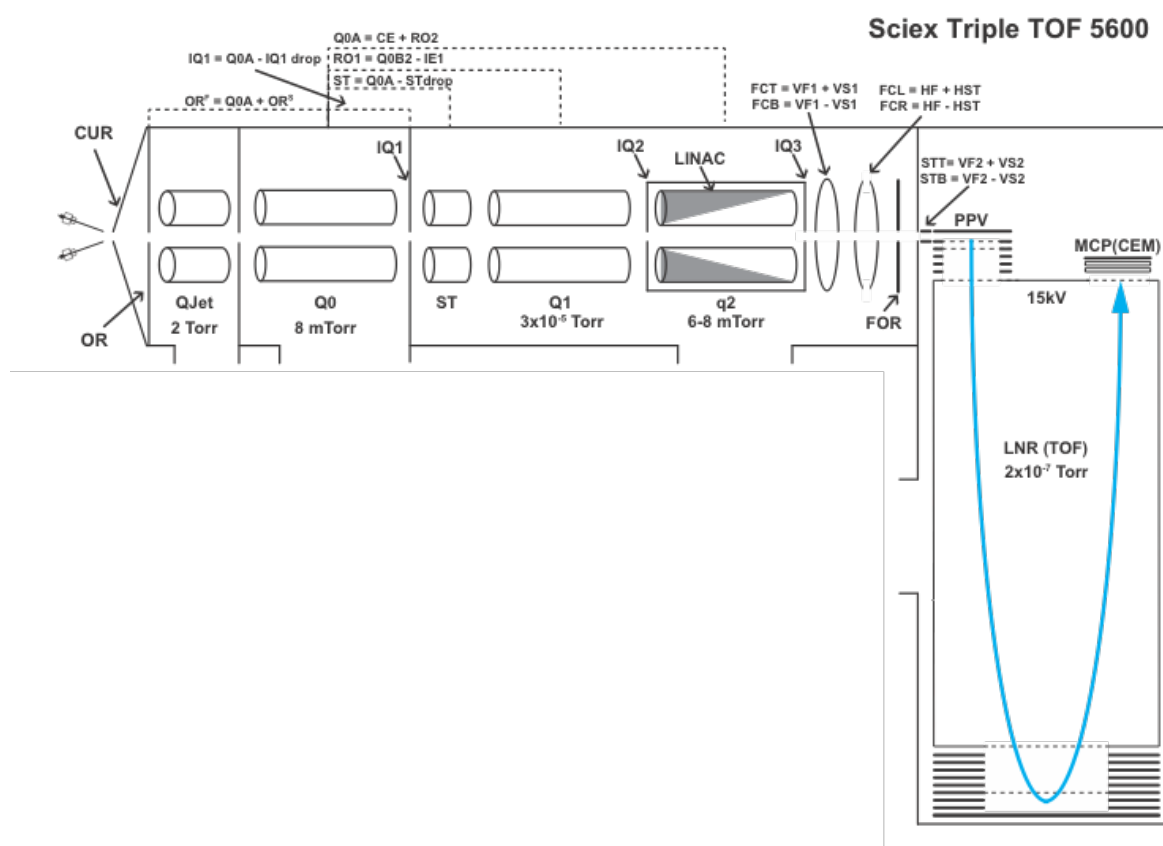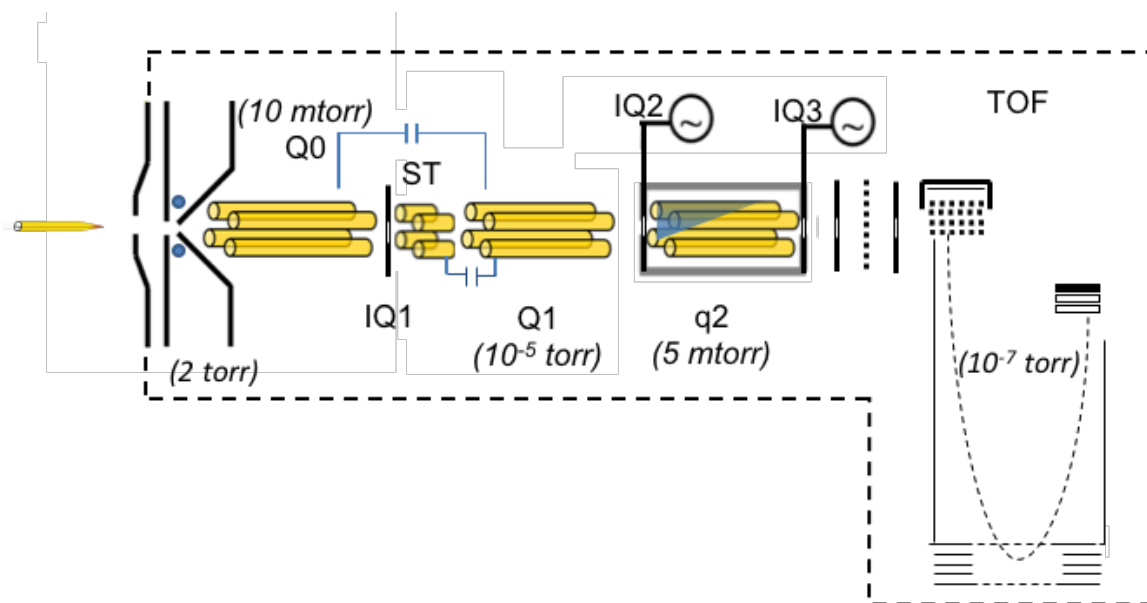
Figure 1. 1. Instrument schematic for Sciex QqToF mass spectrometers modified for ion-ion reactions. Top model Q-Star Pulsar XL; Bottom model: TripleTOF 5600.
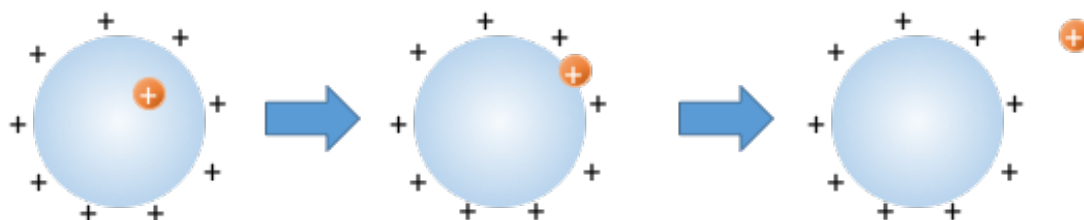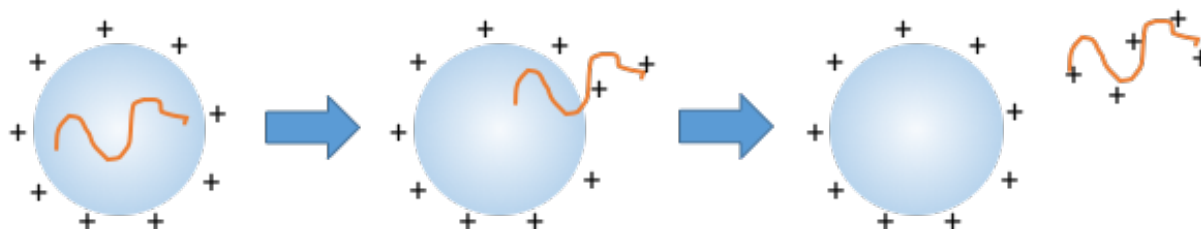
Figure 1. 2. Electrospray ionization (ESI) mechanisms.

(a) Protein charge state distribution with one conformation

Folded

Low CSD

Intermediate

Medium CSD

Unfolded

High CSD

m/z
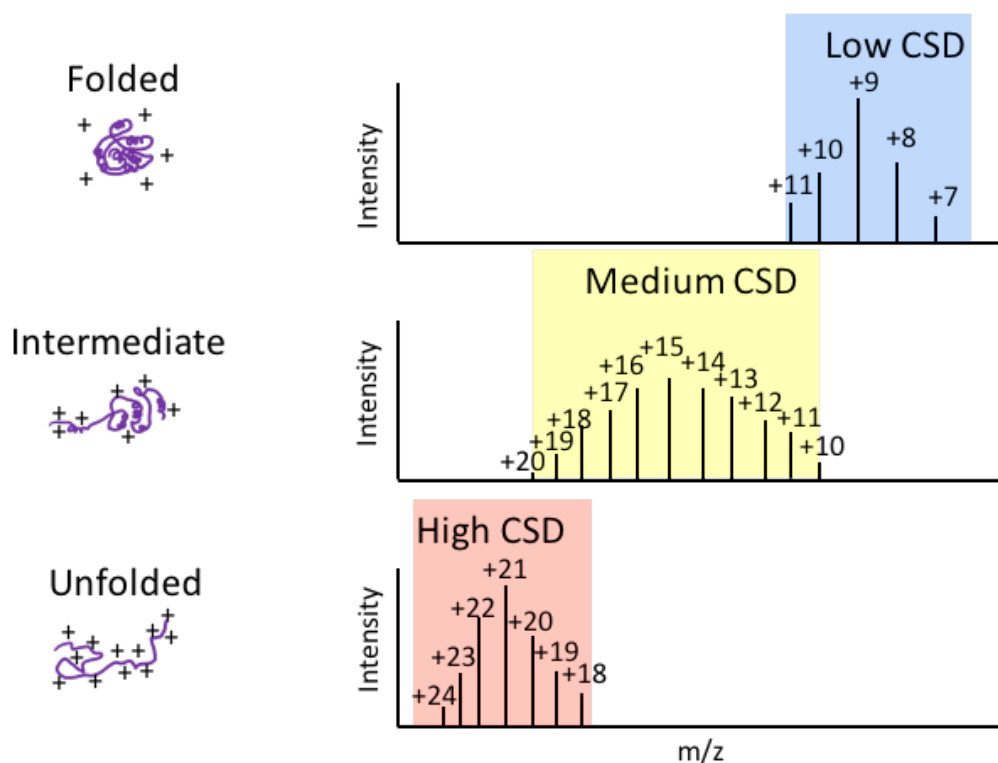
(b) Protein charge state distributions with multiple conformations

High CSD Medium CSD Low CSD

m/z

Unfolded   Intermediate   Folded
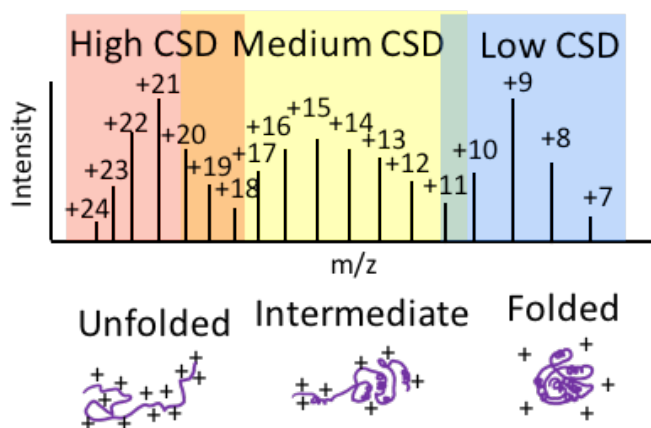
Figure 1. 3. A cartoon showing the relationship between protein charge state distribution and protein conformation. (a) High charge states correspond to more unfolded protein conformation. Low charge states correspond to more folded conformation. (b) A protein sample containing multiple conformations will generate multiple charge state distributions.

Operation Mode I
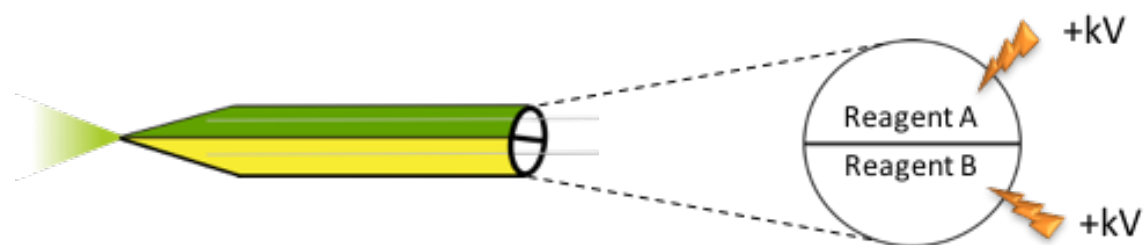
Operation Mode II
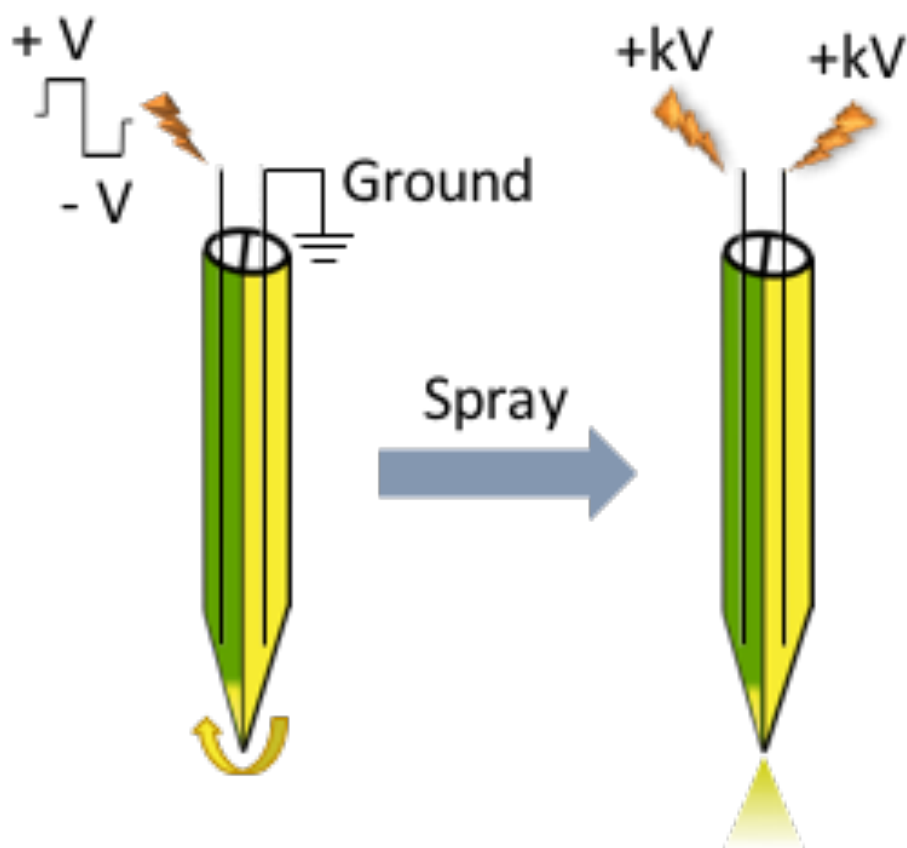
Figure 1. 4. Theta tip and its two operation modes. Operation Mode I: direct spray. Solutions mix in the Taylor cone and subsequent droplets. This mode is good for submillisecond time scale reactions. Operation Mode II: electroosmosis before spray. Solutions mainly mix and react inside of the tip through in-tip electroosmosis induced by differential voltages applied in two channels. This mode is good for reactions of milliseconds or longer time scale.

CHAPTER 2. INVESTIGATION OF PROTEIN FOLDING WITH THETA TIPS AND MASS SPECTROMETRY

2.1 Introduction

Protein is one of the most important classes of biomolecules, which involve in many physiological activities including metabolism, [1, 2] enzymatic catalysis, [3] signal transduction, [4] nutrition transportation, [5, 1] etc. Protein bioactivities directly relate to protein three dimensional conformation or folding state, which derived a hot topic of protein structure-function relationship. [2] The analysis of protein conformation helps understanding protein stability under various environmental conditions including pH and solvent, [28-30], temperature [32, 33], the existence of denaturing agents[29, 34, 35] and supercharging agents [51], etc. In pharmaceutical industry, protein or modified protein products can be directly developed as potent and low toxicity drugs to treat life threatening diseases like cancer and cardio diseases. [5, 6] Protein folding state analysis can also help determining biomedicine stability and developing appropriate drug delivery, packaging and storage conditions.

Most protein folding process proceeds through multiple intermediates. [7, 10-12] Investigation of the folding intermediates is essential to understand the folding sequence and progress. Some folding intermediates could also misfold or aggregate, which may lead to various diseases like the Alzheimer's and Parkinson's diseases. [3, 4] Therefore, a lot of studies have been focusing on catching and investigating the folding intermediates, aiming to understand disease mechanisms and develop treatment methods. [3, 4]. However, protein folding is a very fast process and a lot of proteins could fold to their native states within about tens of milliseconds. The initial folding/unfolding could even occur on a submillisecond to several milliseconds time scale. [9, 10, 13-15] This fast conversion put the intermediate capturing task in a very challenging situation. The

development of fast mixing methods like stopped flow, pulsed hydrogen exchange in combination with CD and fluorescence methods shortened the detection time to several milliseconds and are able to capture some relatively stable intermediates. However, the initial folding stages that finish in less than several milliseconds are still within the deadtime of such analytical methods. [10]

Mass spectrometry is widely used for fast chemical analysis, taking advantage of its high analytical speed, low sample amount requirement, high resolution etc.. [16-20] The advent of electrospray ionization (ESI) enables MS-based methods for protein conformation study, since this soft ionization process deposits a lower energy on protein molecules during ionization and highly preserves protein solution phase structure. [21] The development of nESI-MS further promoted the application of mass spectrometry on biomolecule analysis by reducing the sample amount as well as increasing ionization efficiency and salt tolerance. [22-24] During electrospray ionization, proteins are normally multiply charged and the charge state distribution directly relates to protein conformation. It is generally accepted that high charge states correspond to more unfolded conformation and low charge states indicate more folded conformation. [25-27] With this feature, nESI-MS has been widely applied as a good analytical method to study protein folding and unfolding.

In recent years, several groups have been developing fast mixing/reaction methods coupling with MS to investigate protein folding and unfolding process. [36-43] One successful method is vapor leak-in. [44-46] Volatile reagents, like acetic acid and piperidine, are carried by curtain gas to the interface between curtain plate and the MS inlet. Proteins in solution are sprayed from nESI emitter and react with the reagent vapor in droplets for microseconds time scale and change conformation. With this method, multiple protein folding intermediates were successfully captured. However, vapor leak-in requires volatility of the reagent.

Dual channel theta tips was first developed and reported by Mark et al in 2012 for its application to perform fast vancomycin-diacetyl KAA peptide interaction right prior to MS. [43]. Since the success of this fast reaction, theta tips have been further investigated and developed to study various fast reactions like small molecule interactions, HDX etc.. [36-39, 47-51]. The most common operating mode for theta tip is to load different reagent solutions in different channels and apply a high spray voltage to both channels simultaneously. [36-39, 47] In this case, both solutions will be sprayed out and mix in the common Taylor cone and the subsequent droplets. The mixing and reaction time is limited by droplet lifetime, which is within several microseconds. This time scale is short enough to capture short-lived protein folding intermediates. McLuckey group has further developed theta tip ion source and operated the tip in a second mode, which is inducing in-tip electroosmosis. [51] With differential voltages applied to the two channels prior to spray, electroosmosis flow between channels will be driven by the electric field and mixing/reaction time is elongated to milliseconds or longer. In this case, the reaction time is easily controlled by electroosmosis time and slower reactions of milliseconds or longer can be performed in theta tips.

In both operation mode, theta tips have been successfully applied to investigate protein folding process in combination with mass spectrometry. With the direct spray operation method, protein unfolding has been investigated and short-lived unfolding intermediates were successfully captured. [36] Williams group has demonstrated the concept of applying theta tips to study protein folding by mixing acid denatured protein with volatile ammonium acetate buffer. [37] In this study, we investigated more details into the application of theta tips in protein folding study. We changed the protein folding extent by either changing the reaction rate through manipulating base

concentration or directly increase the reaction time by running electroosmosis. We also investigated the influence of different folding reagents on protein folding using theta tips.

2.2 Experimental

2.2.1 Chemicals

Equine skeletal muscle myoglobin, cytochrome *c* from bovine heart, carbonic anhydrase II from bovine erythrocytes were purchased from Sigma Aldrich (St. Louis, MO). Glacial acetic acid and ammonium hydroxide (28.0%-30.0%) was purchased from Malinckrodt Chemicals (Phillipsburg, NJ). Piperidine was purchased from Aldrich Chemical Company, Inc. (Milwaukee, WI). All solutions were prepared using water purified by a Barnstead Nanopure Infinity ultrapure water system (Thermo Fisher Scientific, Waltham, MA) at 15 MΩ. All proteins and other chemicals were used without further purification. Aqueous stock solutions of protein were diluted to a final concentration of 5-20 μM in water.

2.2.2 Instrumentation

2.2.2.1 Mass spectrometry

All mass spectra were collected using a quadrupole/time-of-flight (QqTOF) tandem mass spectrometer (Q-Star Pulsar XL, Sciex, Concord, ON, Canada), previously modified to allow for ion trap collision-induced dissociation and ion/ion reactions; although, these modifications were not utilized for the experiments described here.

2.2.2.2 Capillaries and tip holder

Dual channel borosilicate theta capillaries (1.5 mm O.D., 1.17mm I.D., 0.165 mm septum thickness, 10 cm length) and single channel thick/standard wall borosilicate capillaries (1.5 mm O.D., 0.86 mm I.D., 10 cm length) were purchased from Sutter Instrument Co. (Novato, CA). The theta capillaries contain a 0.165 mm thick glass septum that runs the length of the capillary which

divides a capillary into two parallel channels. Theta capillaries and standard capillaries were pulled to theta tips (O.D. about 10 μm) and regular tips (O. D. about 5 μm) from a Flaming/Brown micropipette puller (P-87) from Sutter Instrument Co. (Novato, CA).

Protein and reagent solutions were loaded into each channel of a theta tip individually using seque\pro pipette tips from Bio-Rad Laboratories (Hercules, CA). A theta tip holder containing two polytetrafluoroethylene coated silver wire electrodes was purchased from Warner Instruments, LLC (Hamden, CT). (Figure 2. 1) Silver wires were replaced with Teflon coated platinum wires with a 125 μm bare diameter and 200 μm coated diameter (AD Instruments, Colorado Springs, CO) to avoid redox reactions. The Teflon coating was removed from the last 1 mm of the wire to improve its exposed surface area. Each wire was connected to an electrode separately so voltages can be applied to each wire independently.

2.2.3 Electroosmosis experiment

The whole analysis process includes electroosmosis, ionization, dump spray and cool/TOF/Dump steps. In electroosmosis step, one wire was grounded, while the other one was applied a square wave voltage. A transistor-transistor logic (TTL) trigger provided in the instrument software was used to trigger a waveform generator (Agilent 33220A, Santa Clara, CA), which provided a square wave trigger to a DEI pulser (Directed Energy, Inc., PVX-4140, Fort Collins, CO). Two high-voltage ORTEC power supplies were used to provide the positive and negative electroosmosis voltages through the DEI pulser. In the following ionization step, both wires were applied the high ionization and spray voltage from instrument supply (controlled by the Q-Star software). The voltage was switched by a home-built high voltage switch box, which was triggered by another TTL trigger. The ionization step is short relative to electroosmosis step such that ions from mixed volume are sampled. The dump spray step relatively long to spray out

any residue mixed solutions. In this step, low mass cut off in Q1 is very low to prevent ion transmission.

2.3   Results

2.3.1   Protein folding in droplets by fast pH adjustment

2.3.1.1   Ubiquitin refolding

Ubiquitin is a 8560 Da globular protein, which contains 12 basic residues. Ubiquitin folds through an intermediate state which was called "A state". [52] In "A state' N-terminal of ubiquitin is folded while C-terminal still expands. As C-terminal is very dynamic, "A state" can quickly convert to folded or unfolded states. Native ubiquitin has a charge states of +5 and +6. (Figure 2. 2 a)). Addition of 20% acetic acid completely denatured ubiquitin and fully protonate all the basic residues. (Figure 2. 2 b)). Equal volume mixing of acid denatured ubiquitin with 0.25% piperidine in bulk solution completely refolded ubiquitin back to native state, and folding intermediate "A state" was completely missed. (Figure 2. 2 c)) When 20% denatured ubiquitin was sprayed against 0.25% piperidine solutions in theta tips, the two solutions mixed in the common Taylor cone and droplets. Limited by the short droplet lifetime, ubiquitin refolding reaction was effectively stopped after microseconds. Therefore, the majority of ubiquitin remains in its unfolded state, with only a small amount of intermediate state centered in +7 showed up, which corresponds to the "A state". (Figure 2. 2 d)) Since the reaction time was constant, to increase the reaction extent and see a stepwise protein folding, base concentration was adjusted to gradually increase the reaction rate. When 4% piperidine was sprayed against acid denatured ubiquitin, an apparent three state distribution was observed, with a dominant charge state of +9, +7 and +5 separately. (Figure 2. 2 e)). Besides the unfolded and folded states, the intermediate "A state" was significantly accumulated and well captured. Further increase of the piperidine concentration to 15%, reaction

rate was higher. The majority of ubiquitin was completely folded to the native state in microseconds. ((Figure 2. 2 f))

2.3.1.2   Carbonic anhydrase refolding

Comparing to ubiquitin, carbonic anhydrase II (CAII) is a bigger protein with a molecular weight of 29090 Da. Carbonic anhydrase folding proceeds through at least two folding intermediates before reaches the native conformation. [34, 35] The most unfolded random coil first quickly desolvates and folds to a molten globule state. Molten globule keeps folding and forms a more ordered tertiary conformation which is the near native state. From the near native state, protein undergoes slow delicate tertiary structure modifications like proline isomerization to form the final native protein. When carbonic anhydrase is fully denatured using 1% acetic acid, the basic residues were fully charged and CA II has a high charge state distribution centered at +29 (Figure 2. 3 b)). Equal volume mixing of 1% acetic acid denatured CA II with 0.25% piperidine in bulk solution resulted in a complete folding of CAII to its compact conformation with charge state distribution centered in +13 (Figure 2. 3 c)). The charge state distribution of the refolded conformation is very similar to the native conformation (Figure 2. 3 a)). Since the refolding process is very fast, both folding intermediates were lost through the bulk solution pH adjustment. Addition of base increased solution pH and reduced protein ionization efficiency under positive mode. Simultaneously, piperidine gets ionized easily and further suppressed the protein signal. Therefore, protein signal to noise ratio is pretty low in the bulk solution refolding MS spectrum.

Comparing to solution phase refolding, when 1% acetic acid denatured CAII was refolded with the same 0.25% piperidine solution in theta tip, the refolding extent is much lower, with only a slight shift of the charge state to a lower range (Figure 2. 3 d)). Only a small amount of intermediate state with CSD centered in +19 showed up. To accumulate more folding

intermediates, the base concentration was increased to 1% to increase reaction rate. In the same reaction time, a further refolding was observed and an apparent two state distribution centered in +27 and +19 was formed. The shoulder centered in +15 may correspond to another folding intermediate (Figure 2. 3 e)). To confirm the existence of a second intermediate, the base concentration was increased to 2.5% and further refold carbonic anhydrase. Under this condition, the conformation with CSD centered in +16 was well accumulated and four CSDs coexisted in a MS spectrum, which were centered in +28, +21, +16 and +10 separately (Figure 2. 3 f)). These four states could be assigned to "unfold state", "molten globule" "native-like state" and "native state". With this assignment, the native conformation charge state is lower than that from CA II in water. This may result from proton transfer from protein to base molecules. As is reported, conversion from "native-like state" to "native state" requires a proline isomerization. This isomerization is very slow regarding to the microseconds time scale reaction in theta tips, so the native conformation was not highly generated.

2.3.1.3   Cytochrome *c* refolding

Cytochrome *c* has a covalently bound heme ligand in its native state. Unfolding of cytochrome *c* may disrupt the ligand bond between heme and the protein. Therefore, cytochrome *c* refolding proceeds through a complex ligand exchange process. [53] Refolding of cytochrome *c* in bulk solution using piperidine resulted in a complete refolding from the unfolded state to the folded state (Figure 2. 4 a)-c)). When the cytochrome *c* was refolded by piperidine in theta tips, multiple folding intermediates were observed (Figure 2. 4 d)-f)). When the piperidine concentration was gradually increased from 0.5% to 4%, multiple CSD centered in +15, +11, +9 and +6 were generated. Besides the unfold (+15) and fold (+9) states, at least two intermediates were stabilized by piperidine and captured by theta tip reactions.

2.3.2 Base variety influence on protein folding

Besides changing solution pH, base molecules can directly influence protein conformation through salt-protein interaction. When ammonium hydroxide solution (28%-30%) was used to refold cytochrome *c*, different conformation distributions were observed comparing to that generated in piperidine. In bulk solution, mixing 10% acetic acid denatured cytochrome *c* with 2.5% ammonium hydroxide aqueous solution (28%-30%) refolded protein back to its native state with the dominant charge +7. (Figure 2. 5 a)-c)) When the refolding of cytochrome *c* using ammonium hydroxide from 2.5% to 100% was performed in theta tips, only a bimodal distribution was generated. No folding intermediates were observed during this process (Figure 2. 5 d)-f)). Reaction of ammonium hydroxide with acetic acid generated ammonium acetate, which is widely acknowledged for its stabilization effect on protein native conformation. With this stabilization salt formed, a proposed mechanism is that the protein intermediates, if there are any, may quickly convert to native conformation without being captured in microseconds theta tip reaction time.

2.3.3 Control protein folding extent by changing reaction time through electroosmosis

To control reaction extent, besides changing the reaction rate, another way is to control reaction time. In theta tip experiment, direct spray and mixing reagent in droplets controls the reaction time to submillisecond time scale. This method is very suitable for fast reaction monitoring. However, for milliseconds or longer reactions, to manipulate reaction time is difficult, since the reaction time is limited by droplet lifetime. Although by changing tip size and tip-interface distance could manipulate the droplet lifetime, the time is still generally in microseconds scale. [56, 57] To better control reaction time, electroosmosis is performed. By applying a square wave voltage to one channel of a theta tip and ground the other channel, electroosmosis flow is induced and the reaction time can be easily controlled by changing the square wave cycles.

When refolding of carbonic anhydrase II was performed in theta tips by spraying 1% acetic acid denatured CA II against 60 mM NH_4OAc buffer, only a slight shift of charge state to lower range was observed without a lot of folded conformation (Figure 2. 6 a)-b)). This is resulted from a short reaction time in the droplet. When one cycle of a +/- 100 V square wave was applied to induce electroosmosis, the reaction time was elongated from microseconds to 100 ms. With the elongated reaction time, protein was further refolded and a three modal distribution was observed with CSD centers at +19, +16 and +12 (Figure 2. 6 c)). Comparing to the results using different base concentration, these three conformation may be assigned to the two intermediates and a folded native state. All the unfolded random coil was converted during this folding period. This result is also consistent with the relative folding rate for the three folding steps of CAII that the first folding from random coil to molten globule intermediate is fastest, while the following steps get slower step by step.

Similar results were observed with ubiquitin. Normal theta tip spray of 20% acetic acid denatured ubiquitin against 10 mM NH_4OAc buffer partially folded ubiquitin, showing a shoulder conformation with CSD centered at +9, which is corresponding to the "A state". (Figure 2. 6 d) and e)) Using the same buffer to refold ubiquitin, but elongate the reaction time to 100 ms by running one cycle of +/- 100 V electroosmosis in the theta tip resulted in the formation of a large amount of native ubiquitin. (Figure 2. 6 f)) With that, controlling protein refolding extent by increasing reaction time with electroosmosis was demonstrated.

With electroosmosis as the way to control reaction extent, the reaction time can be easily controlled by changing electroosmosis square wave cycles. Myoglobin contains a non-covalently bound heme ligand, and the native complex form of myoglobin was called holo-myoglobin. 1% Acidic acid breaks myoglobin-heme complex and turns it to high charge state apo-myoglobin.

(Figure 2. 7 a)) [54, 55] When 1% acetic acid denatured myoglobin was sprayed against 2.5% ammonium hydroxide solution (28-30% aq.) in theta tips, no folded conformation was generated. (Figure 2. 7 b)). By applying 10 Hz electroosmosis and gradually increasing the time from 100 ms to 400 ms, a bimodol distribution gradually shows up. (Figure 2. 7 c)-e)). The high and low CSDs are corresponding to unfolded and folded apo-myoglobin. 100 μM heme was added to the myoglobin solution to facilitate the incorporation of ligand into the protein. However, ligand incorporation was not accomplished, which may result from short reaction time scale or inappropriate environmental condition. Longer electroosmosis resulted in bubble generation in tip, which may result from Joule heating effect. Bulk solution mixing of 5% acetic acid denatured myoglobin with 5% ammonium hydroxide solution (28-30% aq.) folded myoglobin to compact apo-myoglobin conformation. (Figure 2. 7 f)).

2.4 Conclusions

Theta tips were successfully applied as a micromixer and nESI-MS emitter to study protein refolding process. Protein folding extent was controlled in two ways. One way was through direct theta tip spray and mixing acid denatured proteins with base in the common Taylor cone and subsequent droplets. In this method, the reaction time was controlled constant to microseconds, which was limited by the droplet lifetime. Reaction extent was modified by changing the base concentration, which changed the folding reaction rate. The results showed that protein folding extent increased with base concentration and multiple folding intermediates were observed. The folding process was also influenced by the base variety, which may be due to the different salt-protein interactions. The other way to control protein folding extent in theta tip is by changing the reaction time, which was accomplished by inducing in-tip electroosmosis. With the same reagent, protein folding extent was increased when performing electroosmosis. The refolding can be further

pushed forward by elongating the electroosmosis time through increasing square wave cycles.

2.5 References

1. Kahn, B. B.; Alquier, T.; Carling, D.; Hardie, D. G. AMP-activated protein kinase: Ancient energy gauge provides clues to modern understanding of metabolism. Cell Metab. 2005, 1, 15-25.

2. Brummell, D. A.; Harpster, M. H.; Civello, P. M.; Palys, J. M.; Bennett, A. B.; Dunsmuir, P. Modification of expansin protein abundance in tomato fruit alters softening and cell wall polymer metabolism during ripening. Plant Cell, 1999, 11, 2203-2216.

3. Cooper, G. M. The central role of enzymes as biological catalysts. In: The Cell: A Molecular Approach. 2nd Edition. Sinauer Associates: Sunderland, MA, 2000.

4. Cabrera-Vera, T. M.; Vanhauwe, J.; Thomas, T. O.; Medcova, M.; Preininger, A.; Mazzoni, M. R.; Hamm, H. E. Insights into G-protein structure, function and regulation. Endocr. Rev. 2003, 24, 765-781.

5. de Keyzer, J.; van der Does, C.; Driessen, A. J. M. The bacterial translocase: a dynamic protein channel complex. Cell. Mol. Life Sci. 2003, 60, 2034-2052.

1. Kovacs, F. A.; Cross, T. A. Transmembrane four-helix bundle of influenza A M2 protein channel: structural implications from helix tilt and orientation. Biophys. J. 1997, 73, 2511-2517.

2. Wright, P. E.; Dyson, H. J. Intrinsically unstructured proteins: Re-assessing the protein structure-function paradigm. J. Mol. Biol. 1999, 293, 321-331.

3. Selkoe, D. J. Alzheimer's disease: Genes, proteins, and therapy. Physiol. Rev. 2001, 81, 741-766.

4. Bucciantini, M.; Giannoni, E.; Chiti, F.; Baroni, F.; Formigli, L.; Zurdo, J.; Taddei, N.; Ramponi, G.; Dobson, C. M.; Stefani, M. Inherent toxicity of aggregates implies a common mechanism for protein misfolding diseases. Nature 2002, 416, 507-511.

5. Lagassé, H. A. D.; Alexaki, A.; Simhadri, V. L.; Katagiri, N. H.; Jankowski, W.; Sauna, Z. E.; Kimchi-Sarfaty, C. Recent advances in (therapeutic protein) drug development. F1000Res. 2017, 6, 1-17.

6. Bruno, B. J.; Miller, G. D.; Lim, C. S. Basics and recent advances in peptide and protein drug delivery. Ther. Deliv. 2013, 4, 1443-1467.

7. Baldwin, R. L. The nature of protein folding pathways: The classical versus the new view. J. Bio. NMR. 1995, 5, 103-109.

8. Fersht, A. R. Characterizing transition states in protein folding: An essential step in the puzzle. Curr. Opin. Struc. Biol. 1994, 5, 79-84.

9. Privalov, P. L. Intermediate states in protein folding. J. Mol. Biol. 1996, 258, 707-725.

10. Evans, P. A.; Radford, S. E. Probing the structure of folding intermediates. Curr. Opin. Struc. Biol. 1994, 4, 100-106.

11. Balbach, J.; Forge, V.; van Nuland, N. A. J.; Winder, S. L.; Hore, P. J.; Dobson, C. M. Following protein folding in real time using NMR spectroscopy. Nature Struct. Biol. 1995, 2, 865-870.

12. Dill, K. A.; Stigter, D. Modeling protein stability as hetero polymer collapse. Advan. Protein Chem. 1995, 46, 59-104.

13. Jackson, S. E.; Fersht, A. R. Folding of chymotrypsin inhibitor 2. 1. Evidence for a two-state transition. Biochemistry 1991, 30, 10428-10435.

14. Otzen, D. E.; Itzhaki, L. S.; ElMasry, N. F.; Jackson, S. E.; Fersht, A. R. Structure of the transition state for the folding/unfolding of the barley chymotrypsin inhibitor 2 and its implication for mechanisms of protein folding. Proc. Natl Acad. Sci. U.S.A. 1994, 91, 10422-10425.

15. Alexander, P.; Fahnestock, S.; Lee, T.; Orban, J.; Bryan, P. Thermodynamic analysis of the folding of the streptococcal protein G IgG-binding domains B1 and B2: why small proteins tend to have high denaturation temperatures. Biochemistry 1992, 31, 3597-3603.

16. Glish, G. L.; Vachet, R. W. The basics of mass spectrometry in the twenty first century. Nat. Rev. Drug Discov. 2003, 2, 140-150.

17. Roux, A.; Lison, D.; Junot, C.; Heilier, J. Applications of liquid chromatography coupled to mass spectrometry-based metabolomics in clinical chemistry and toxicology: A review. Clin. Biochem. 2011, 44, 119-135.

18. Bantscheff, M.; Schirle, M.; Sweetman, G.; Rich, J.; Kuster, B. Quantitative mass spectrometry in proteomics: a critical review. Anal. Bioanal. Chem. 2007, 389, 1017-1031.

19. Benson, S.; Lennard, C.; Maynard, P.; Roux, C. Forensic applications of isotope ratio mass spectrometry-A review. Forensic Sci. Int. 157, 2006, 1-22.

20. Jackson, S. E.; Pearson, N. J.; Griffin, W. L.; Belousova, E. A. The application of laser ablation-inductively coupled plasma-mass spectrometry to in situ U-Pb zircon geochronology. Chem. Geol. 211, 2004, 47-69.

21. Fenn, J. B.; Mann, M.; Meng, C. K.; Wong, S. F.; Whitehouse, C. M. Electrospray ionization for mass spectrometry of large biomolecules. Science 1989, 246, 64-71.

22. Wilm, M.; Mann, M. Analytical properties of the nanoelectrospray ion source. Anal. Chem. 1996, 68, 1-8.

23. Pan, P.; Guawardena, H. P.; Xia, Y.; McLuckey, S. A. Nanoelectrospray ionization of protein mixtures: Solution pH and protein pI. Anal. Chem. 2004, 76, 1165-1174.

24. Chen, S. Rapid protein identification using direct infusion nanoelectrospray ionization mass spectrometry. Proteomics 2006, 6, 16-25.

25. Chowdhury, S. K.; Katta, V.; Chait, B. T. Probing conformational changes in proteins by mass spectrometry. J. Am. Chem. Soc. 1990, 112, 9012-9013.

26. Kaltashov, I. A.; Eyles, S. J. Studies of biomolecular conformations and conformational dynamics by mass spectrometry. Mass Spectrom. Rev. 2002, 21, 37-71.

27. Fenn, J. B. Ion formation from charged droplets: Roles of geometry, energy, and time. J. Am. Soc. Mass Spectrom. 1993, 4, 524-535.

28. Loo, J. A.; Loo, R. R.; Udseth, H. R.; Edmonds, C. G.; Smith, R. D. Solvent-induced conformational changes of polypeptides probed by electrospray-ionization mass spectrometry. Rapid Commun. Mass Spectrom. 1991, 5, 101-105.

29. Iavarone, A. T.; Jurchen, J. C.; Williams, E. R. Effects of solvent on the maximum charge state and charge state distribution of protein ions produced by electrospray ionization. J. Am. Soc. Mass Spectrom. 2000, 11, 976-985.

30. Le Blanc, J. C. Y.; Wang, J.; Guevremont, R.; Siu, K. W. M. Electrospray mass spectra of protein cations formed in basic solutions. Org. Mass Spectrom. 1994, 29, 587-593.

31. Iavarone, A. T.; Jurchen, J. C.; Williams, E. R. supercharged protein and peptide ions formed by electrospray ionization. Anal. Chem. 2001, 73, 1455-1460.

32. Ueki, N.; Chow, C.; Ochiai, Y. Characterization of bullet tuna myoglobin with reference to the thermostability-structure relationship. J. Agric. Food Chem. 2005, 53, 4968-4975.

33. Ibarra-Molero, B.; Loladze, V. V.; Makhatadze, G. I.; Sanchez-Ruiz, J. M. Thermal versus guanidine-induced unfolding of ubiquitin. an analysis in terms of the contributions from charge-charge interactions to protein stability. Biochemistry 1999, 38, 8138-8149.

34. Bushmarina, N. A.; Kuznetsova, I. M.; Biktashev, A. G.; Turoverov, K. T.; Uversky, V. N. Partially folded conformations in the folding pathway of bovine carbonic anhydrase II: a fluorescence spectroscopic analysis. Chembiochem 2001, 2, 813-821.

35. Semisotnov, G. V.; Rodionova, N. A.; Kutyshenko, V. P.; Ebert, B.; Blanck, J.; Ptitsyn, O. B. Sequential mechanism of refolding of carbonic anhydrase B. FEBS Lett., 1987, 224, 9-13.

36. Fisher, C. M.; Kharlamova, A.; McLuckey, S. A. Affecting protein charge state distributions in nano-electrospray ionization via in-spray solution mixing using theta capillaries. Anal. Chem. 2014, 86, 4581-4588.

37. Mortensen, D. N.; Williams, E. R. Theta-glass capillaries in electrospray ionization: rapid mixing and short droplet lifetimes. Anal. Chem. 2014, 86, 9315-9321.

38. Mortensen, D. N.; Williams, E. R. Investigating protein folding and unfolding in electrospray nanodrops upon rapid mixing using theta-glass emitters. Anal. Chem. 2015, 87, 1281-1287.

39. Mortensen, D. N.; Williams, E. R. Ultrafast (1 μs) mixing and fast protein folding in nanodrops monitored by mass spectrometry. J. Am. Chem. Soc., 2016, 138, 3453-3460.

40. Urban, P. L.; Chen, Y.; Wang, Y. Applications of time-resolved mass spectrometry in the studies of protein structure dynamics. In: Time-Resolved Mass Spectrometry: From Concept to Applications, 1ˢᵗ Edition. John Wiley & Sons, Ltd: West Sussex, 2016.

41. Lento, C.; Wilson, D. J. Unravelling the mysteries of sub-second biochemical processes using time-resolved mass spectrometry. Analyst 2017, 142, 1640-1653.

42. Li, Y.; Zhang, N.; Zhou, Y.; Wang, J.; Zhang, Y.; Wang, J.; Xiong, C.; Chen, S.; Nie, Z. Induced dual-nanospray: a novel internal calibration method for convenient and accurate mass measurement. J. Am. Soc. Mass Spectrom. 2013, 24, 1446-1449.

43. Mark, L. P.; Gill, M. C.; Mahut, M.; Derrick, P. J. Dual nano-electrospray for probing solution interactions and fast reactions of complex biomolecules. Eur. J. Mass Spectrom. 2012, 18, 439-446

44. Kharlamova, A.; Prentice, B. M.; Huang, T.; McLuckey, S. A. Electrospray droplet exposure to gaseous acids for the manipulation of protein charge state distributions. Anal. Chem. 2010, 82, 7422-7429.

45. Kharlamova, A.; McLuckey, S. A. Negative electrospray droplet exposure to gaseous bases for the manipulation of protein charge state distributions. Anal. Chem. 2011, 83, 431-439.

46. Kharlamova, A.; DeMuth, J. C.; McLuckey, S. A. Vapor treatment of electrospray droplets: evidence for the folding of initially denatured proteins on the sub-millisecond time-scale. J. Am. Soc. Mass Spectrom. 2011, 23, 88-101.

47. Jansson, E. T.; Lai, Y.; Santiago, J. G.; Zare, R. N. Rapid hydrogen-deuterium exchange in liquid droplets. J. Am. Chem. Soc. 2017, 139, 685-6854.

48. Walker, K. L.; Dornan, L. M.; Zare, R. N.; Waymouth, R. M.; Muldoon, M. J. Mechanism of catalytic oxidation of styrenes with hydrogen peroxide in the presence of cationic palladium(II) complexes. J. Am. Chem. Soc. 2017, 139, 12495-12503.

49. Miller, C. F.; Kulyk, D. S.; Kim, J. W.; Badu-Tawiah, A. K. Re-configurable, multi-mode contained electrospray ionization for protein folding and unfolding on the millisecond time scale. Analyst 2017, 142, 2152-2160.

50. Liu, F.; Lu, W.; Yin, X.; Liu, J. Mechanistic and kinetic study of singlet O_2 oxidation of methionine by on-line electrospray ionization mass spectrometry. J. Am. Soc. Mass Spectrom. 2016, 27, 59-72.

51. Fisher C. M.; Hilger, R. T.; Zhao, F.; McLuckey, S. A. Electroosmotically driven solution mixing in borosilicate theta glass nESI emitters. J. Mass Spectrom. 2015, 50, 1063-1070.

52. Hoerner, J. K.; Xiao, H.; Kaltashov, I. A. Structural and dynamic characteristics of a partially folded state of ubiquitin revealed by hydrogen exchange mass spectrometry. Biochemistry 2005, 44, 11286-11294.

53. Yeh, S.; Rousseau, D. L. Folding intermediates in cytochrome *c*. Nature Struct. Mol. Biol. 1998, 5, 222-228.

54. Evans, S. V.; Brayer, G. D. High-resolution study of the three-dimensional structure of horse heart metmyoglobin. J. Mol. Biol. 1990, 23, 885-897.

55. Konermann, L.; Rosell, F. I.; Mauk, A. G.; Douglas, D. J. Acid-induced denaturation of myoglobin studied by time-resolved electrospray ionization mass spectrometry. Biochemistry 1997, 36, 6448-6454.

56. Xia, Z.; Williams, E. R. Effect of droplet lifetime on where ions are formed in electrospray ionization. Analyst 2019, 144, 237-248.

57. Jansson, E. T.; Lai, Y.; Santiago, J. G.; Zare, R. N. Rapid hydrogen-deuterium exchange in liquid droplets. J. Am. Chem. Soc. 2017, 139, 6851-6854.

Figure 2. 1. Theta tip holder
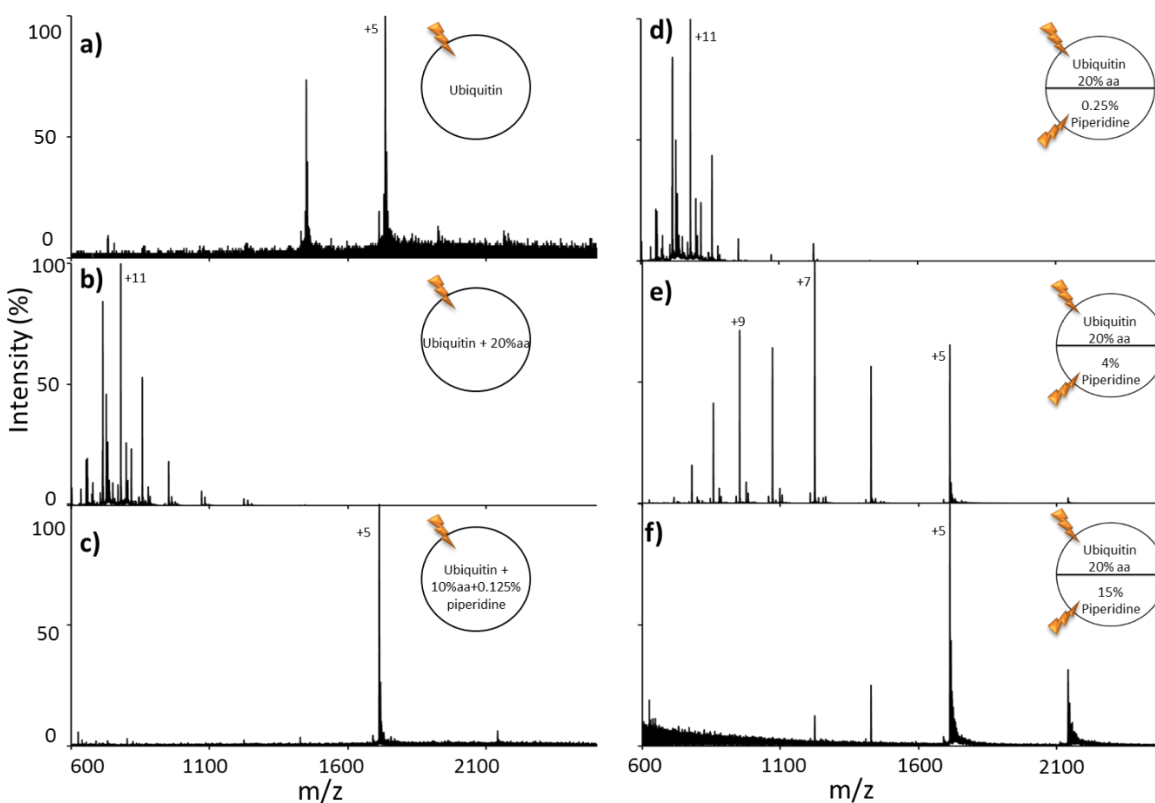
Figure 2. 2. 20% Acetic acid denatured ubiquitin was refolded by piperidine in a theta-tip spray. a) Native ubiquitin was sprayed in a regular tip; b) 20% Acetic acid denatured ubiquitin was sprayed in a regular tip; c) Equal volume of 20% acetic acid denatured carbonic anhydrase II and 0.25% piperidine were mixed and sprayed in a regular tip; 20% Acetic acid denatured ubiquitin was sprayed against d) 0.25%, e) 4% and f) 15% piperidine in theta-tips.
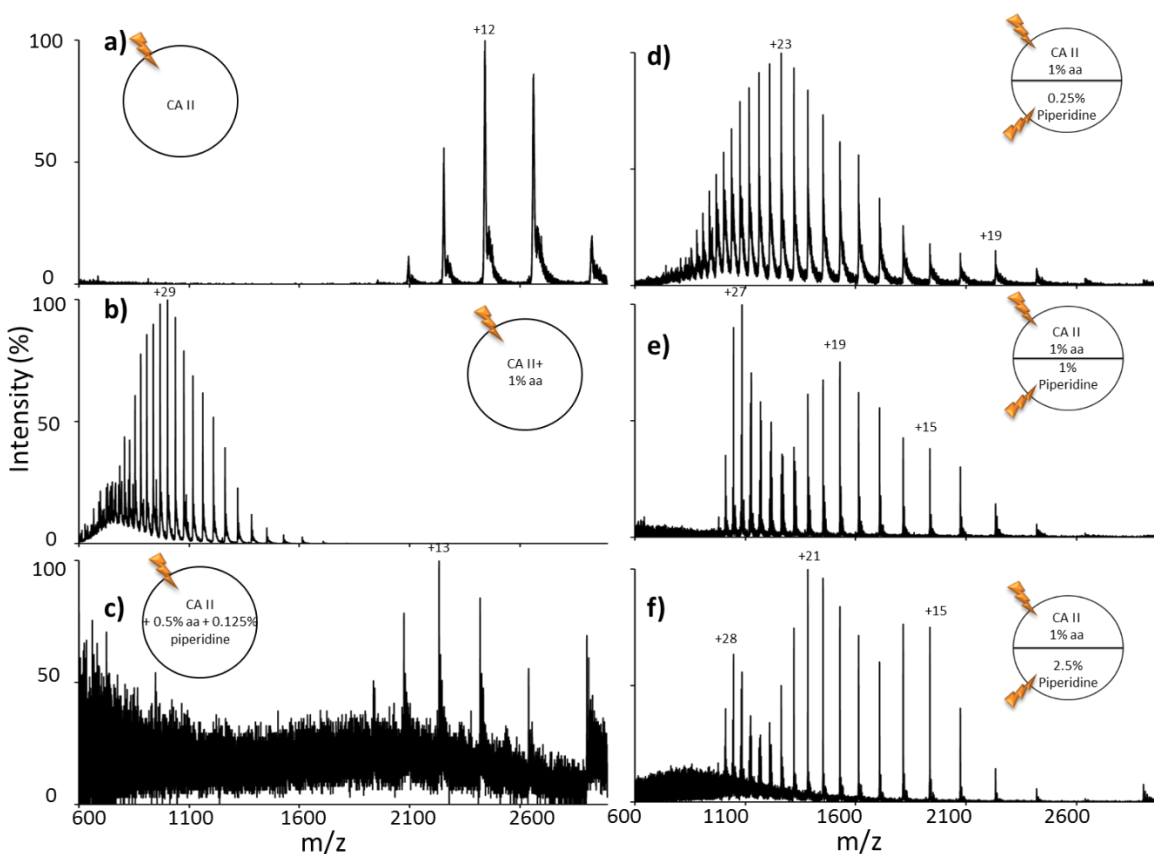
Figure 2. 3. 1% Acetic acid denatured carbonic anhydrase II (CA II) was refolded by piperidine in a theta-tip spray. a) Native carbonic anhydrase II was sprayed in a regular tip; b) 1% Acetic acid denatured carbonic anhydrase II was sprayed in a regular tip; c) Equal volume of 1% acetic acid denatured carbonic anhydrase II and 0.25% piperidine were mixed and sprayed in a regular tip; 1% Acetic acid denatured carbonic anhydrase II was sprayed against d) 0.25%, e) 1% and f) 2.5% piperidine in theta-tips.
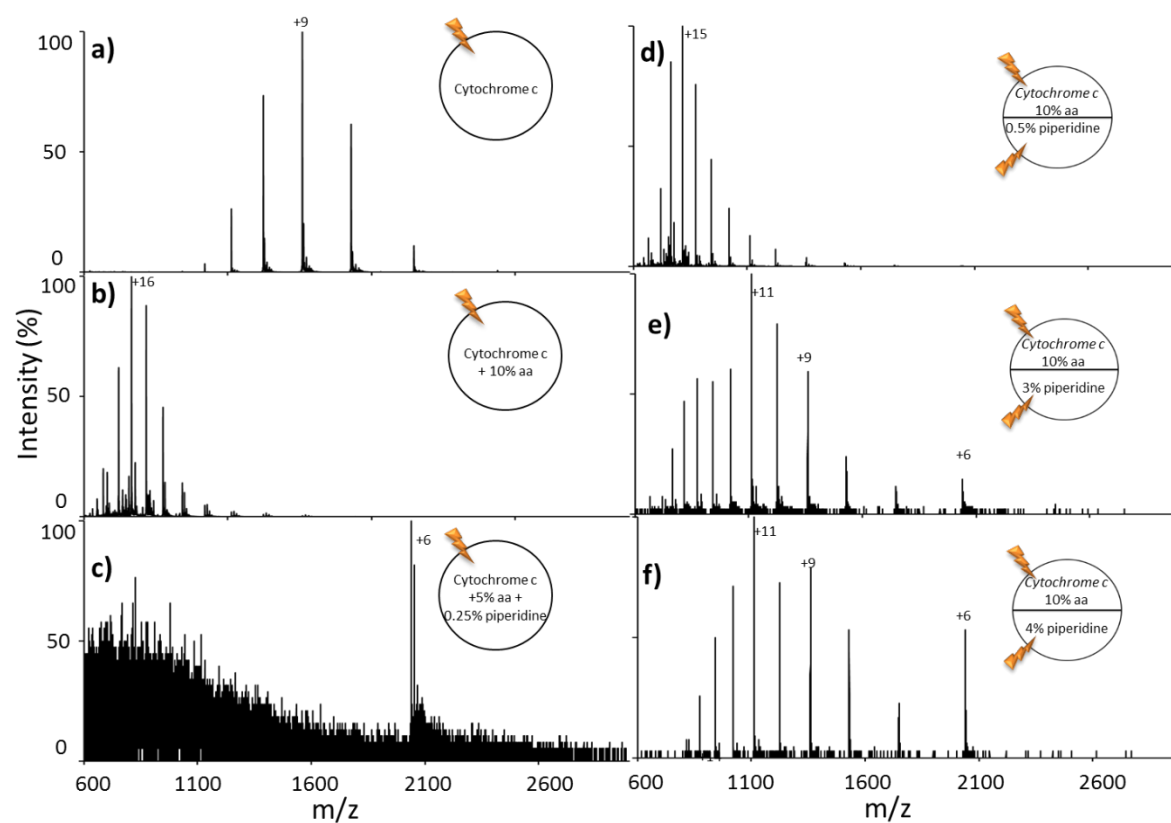
Figure 2. 4. 10% Acetic acid denatured cytochrome *c* was refolded by piperidine in a theta-tip spray. a) Native cytochrome *c* was sprayed in a regular tip; b) 10% Acetic acid denatured cytochrome *c* was sprayed in a regular tip; c) Equal volume of 10% acetic acid denatured cytochrome *c* and 0.5% piperidine were mixed and sprayed in a regular tip; 10% Acetic acid denatured cytochrome *c* was sprayed against d) 0.5%, e) 3% and f) 4% piperidine in theta-tips.
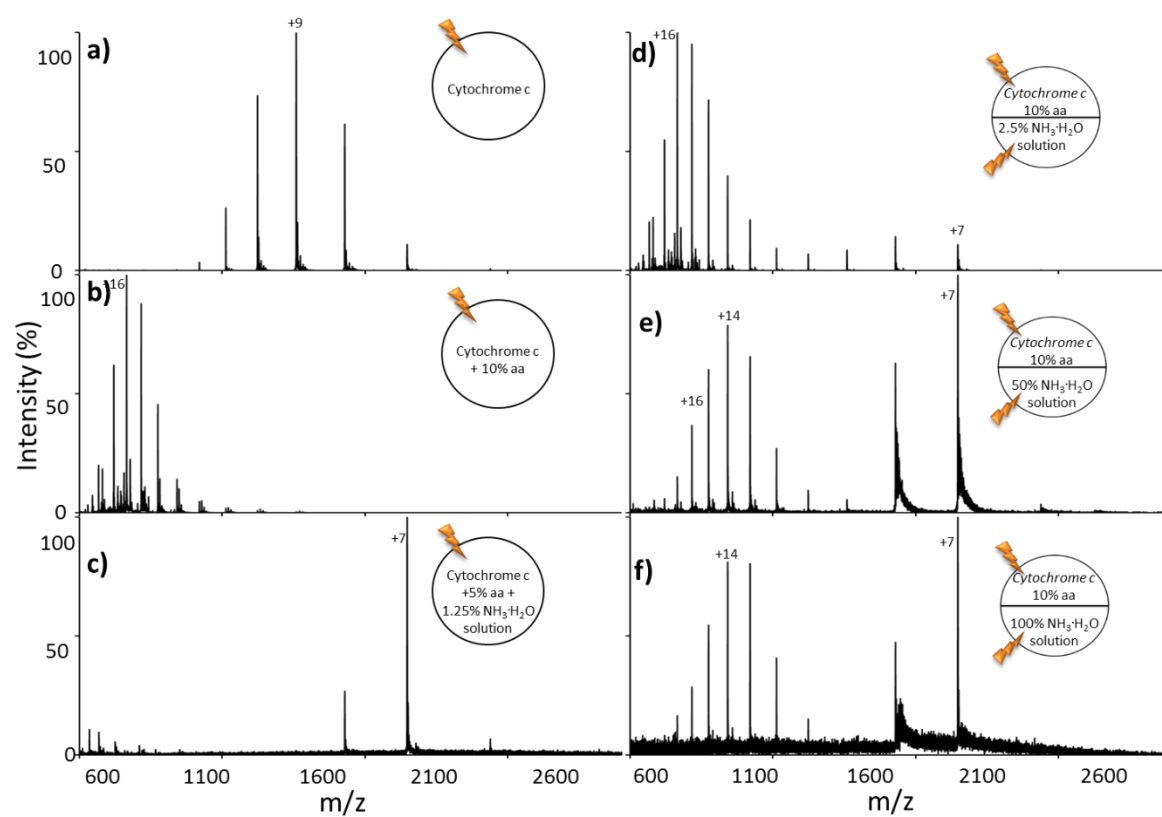
Figure 2. 5. 10% Acetic acid denatured cytochrome *c* was refolded by ammonium hydroxide in a theta-tip spray. a) Native cytochrome *c* was sprayed in a regular tip; b) 10% Acetic acid denatured cytochrome *c* was sprayed in a regular tip; c) Equal volume of 10% acetic acid denatured cytochrome *c* and 2.5% ammonium hydroxide solution were mixed and sprayed in a regular tip; 10% Acetic acid denatured cytochrome *c* was sprayed against d) 2.5%, e) 50% and f) 100% ammonium hydroxide solution in theta-tips.
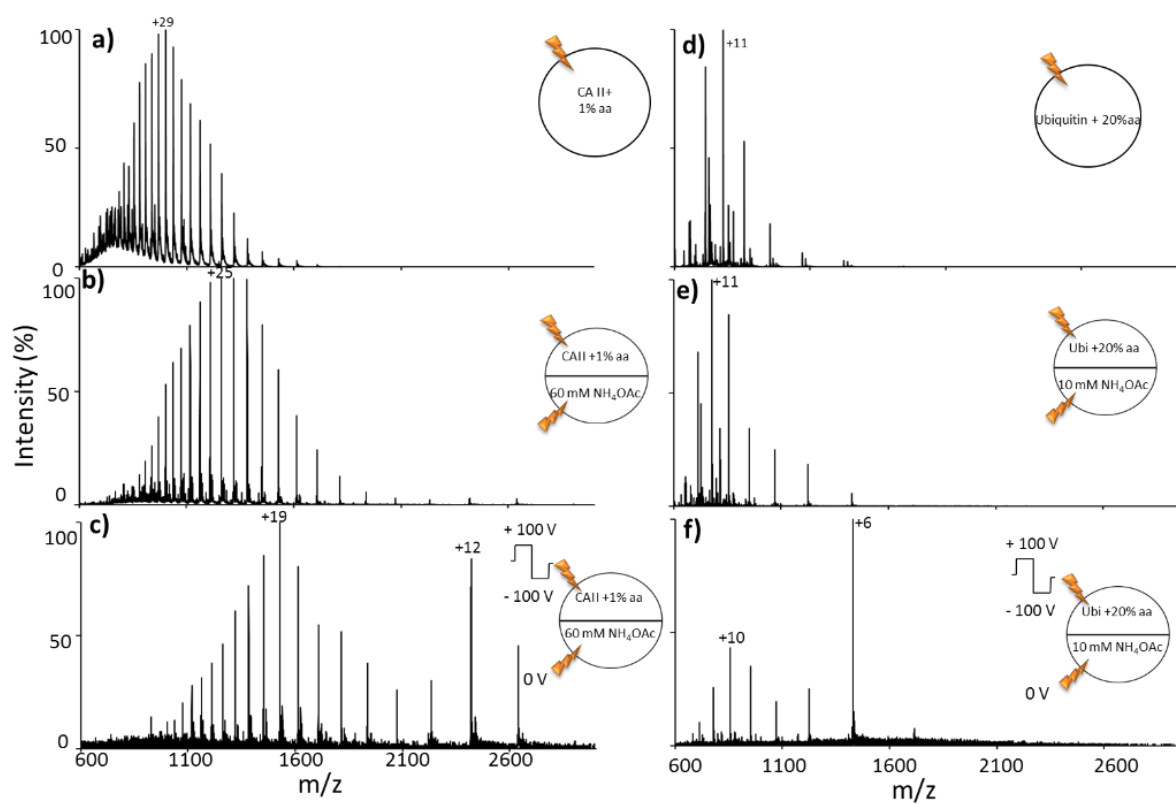
Figure 2. 6. Refolding of ubiquitin and carbonic anhydrase II with NH_4OAc buffer in a theta tip with or without electroosmosis. 20% Acetic acid denatured ubiquitin was sprayed against 10 mM NH_4OAc buffer in a theta-tip a) without or c) with one cycle of +/- 100V electroosmosis. 1% Acetic acid denatured carbonic anhydrase II was sprayed against 60 mM NH_4OAc buffer in a theta-tip b) without or d) with one cycle of +/- 100V electroosmosis.
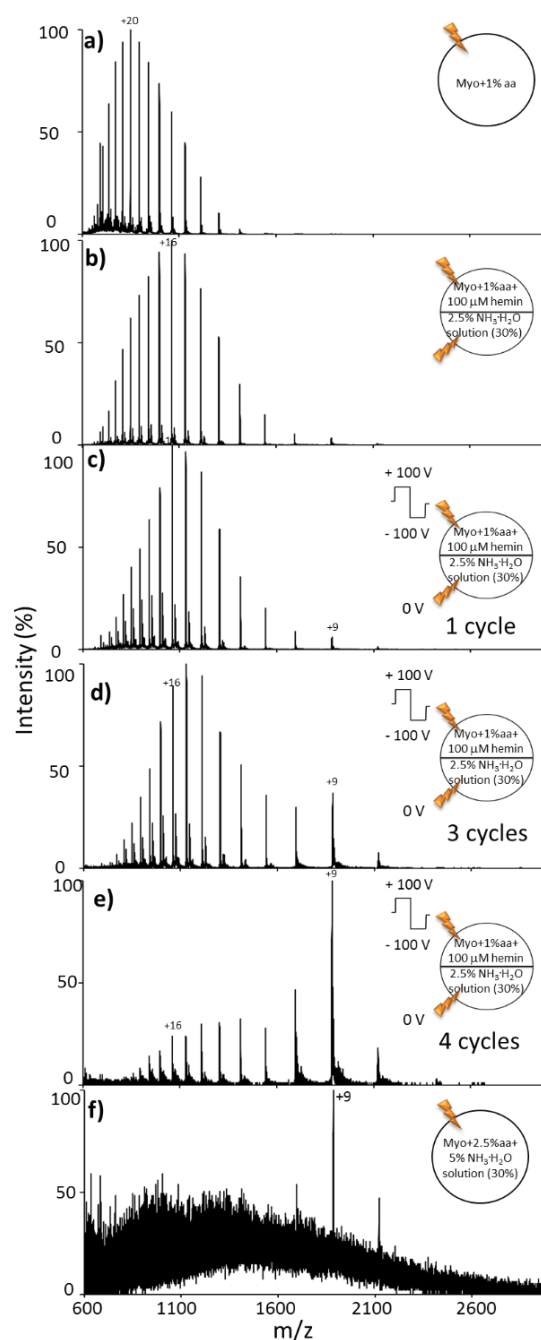
Figure 2. 7. Theta tip spray of myoglobin in 1% acetic acid and 100 uM hemin against 2.5% ammonium hydroxide solution (28-30% aq.) with or without electroosmosis. a) 1% Acetic acid denatured myoglobin was sprayed in a regular tip; b) 1% Acetic acid denatured myoglobin with 100 uM hemin was sprayed against 2.5% ammonium hydroxide solution in a theta-tip. +/- 100 V Square wave voltage was applied to myoglobin side with the ammonium hydroxide side grounded to induce electroosmosis for c) 1 cycle; d) 3 cycles and e) 4 cycles. All the peaks correspond to apo-myoglobin. f) Solution phase equal volume mixing of 5% acetic acid denatured myoglobin with 10% ammonium hydroxide solution (28%-30% aq)

CHAPTER 3. JOULE HEATING AND THERMAL DENATURATION OF PROTEINS IN NANO-ESI THETA TIPS

3.1   Introduction

Nano-electrospray ionization (nESI) is used to generate gaseous ions of biomolecules such as proteins, carbohydrates, lipids, *et cetera*. [1, 2] Proteins normally result in multiply charged ions when subjected to electrospray ionization and charge state distributions are related to protein conformation. It is generally accepted, for example, the magnitude of charges is relatively high for unfolded conformations, which are described as high charge state distributions, while more folded conformations usually display relatively low charge state distributions. [3-5] For this reason, charge state distributions have been used in a biophysical context to monitor protein conformations using mass spectrometry. The magnitude of protein ion charge also has analytical implications. For example, high charge state ions are more efficiently detected by charge sensitive detectors like those used by Fourier transform based mass analyzers. [6] Furthermore, increasing the charge state of a protein ion can lead to improved sequence coverage in top-down analysis, [7-9] especially when electron transfer dissociation (ETD) and electron capture dissociation (ECD) are used as dissociation methods. [10] Therefore, in-source protein denaturation can be desirable for the primary structural characterization of a protein via tandem mass spectrometry.

Tertiary and quaternary protein structures are stabilized by various interactions including salt bridges, hydrogen bonding, hydrophobic interactions and van der Waals interactions. [11, 12] These interactions can be affected by a variety of factors including temperature, [4, 13-15] pH, [16-18] ionic strength, [19] solvent, [20-22] surface effects, [23] as well as instrumental parameters. [24] Most methods intended to change protein conformation involve bulk solution manipulations, such as the addition of acid, base, organic solvent, supercharging reagents [14] or other additives,

as well as heating. These methods can be time consuming and require larger sample volumes. In recent years, fast conformation manipulation methods in conjunction with ESI have been developed, including vapor exposure, [25-27] electrothermal denaturation, [24, 28]and theta tip mixing. [29-32] During vapor exposure, the ESI droplets containing the protein are allowed to interact with acidic or basic vapors added to the nitrogen curtain gas, leading to protein denaturation or refolding on the basis of pH changes. [25, 26] The electrothermal supercharging method manipulates protein conformation by changing the ionization voltage. [24] It has been reasoned that by applying a high spray voltage the droplet size is increased, thereby elongating its lifetime in the hot capillary interface and maximizing the thermal denaturation of the protein in the droplet.

Theta tips are nESI dual channel emitters that also function as micro-mixers prior to the ionization step. [29] They are pulled from theta capillaries made of borosilicate glass that contain a septum in the center dividing a capillary into two separate channels into which different solutions can be loaded. A platinum wire is placed in each channel to apply spraying and mixing voltages. By applying the same ESI voltage to both channels, the solutions are sprayed out simultaneously and subsequently mix in the Taylor cone as well as in the ensuing droplets on a sub-millisecond time scale. [29, 33] This method has been applied to study protein unfolding and folding by mixing protein solutions with acid or ammonium acetate in the theta tip Taylor cone and droplets. [29, 30, 32] Due to the short mixing time, short-lived unfolding intermediates have been observed. [29] A more recent study has shown that electroosmotic flow can be induced between channels of a theta tip when applying differential voltages in the two channels. [31] The duration and extent of mixing can be controlled by tuning the applied voltage and time of electroosmosis. The solution phase mixing overcomes the reagent volatility limitation in the vapor exposure strategy and does not

require a special mass spectrometric interface set up. However, the mixing step can alter the protein solution pH and composition if the two sides are mixed with dissimilar solutions. This is unfavorable for reagent or pH-sensitive studies like covalent modification and HDX. [34] Here we demonstrate thermal denaturation of proteins in theta tips via Joule heating, which can be a useful way to manipulate protein conformation without altering solution composition.

Joule heating, also known as resistive or ohmic heating, arises from an electrical current passing through a conductor or semi-conductor. It is widely used in various research areas including, for example, melting point measurements, [35] controlling thermosensitive polymer behavior, [36] and facilitating chemical reactions. [37] Joule heating in electrophoretic separation has been well-studied as it has been shown to reduce separation efficiency. [38] The magnitude of the temperature change due to Joule heating in a solution is related *inter alia* to voltage, molar conductivity, and concentration via the following relationship: [39]

$$\Delta T \sim V^2\, \Lambda c \qquad\qquad (1)$$

where ΔT is the temperature change (^{o}C), V is the voltage (V), Λ is the molar conductivity ($S \cdot m^2 \cdot mol^{-1}$) of the electrolyte and c is the electrolyte concentration ($mol \cdot L^{-1}$). Other factors that affect the temperature change include geometric considerations, such as the radius at the tip, glass thickness, heat dissipation, etc. Herein, we demonstrate Joule heating in theta tip resulting from electroosmosis and take advantage of the effect to thermally denature proteins. The solution temperature was directly measured by Raman spectroscopy to establish a relationship between voltage and temperature. The influence of voltage and electrolyte concentration on the magnitude of Joule heating were investigated.

3.2 Experimental

3.2.1 Materials

Myoglobin from equine skeletal muscle, cytochrome *c* from bovine heart, cytochrome *c* from equine heart, ubiquitin from bovine erythrocytes, carbonic anhydrase II from bovine erythrocytes, and ammonium acetate were purchased from Sigma Aldrich (St. Louis, MO). HPLC grade water was purchased from Fisher Scientific (Fair Lawn, NJ). All proteins were dissolved in 0, 5 or 10 mM ammonium acetate solution at pH around 6 and the final protein concentration is 5-20 μM unless specifically noted. Proteins and chemical reagents were used without further purification.

3.2.2 Capillaries and tip holders

Dual channel borosilicate theta capillaries (1.5 mm O.D., 1.17 mm I.D., 0.165 mm septum thickness, 10 cm length) were purchased from Sutter Instrument Co. (Novato, CA). Theta capillaries were pulled to theta tips (O.D. 10 μm) using a Flaming/Brown micropipette puller (P-87) from Sutter Instrument Co. (Novato, CA).

Solutions were loaded into both channels of a theta tip, which was held by a theta tip holder from Warner Instruments, LLC (Hamden, CT). The original silver wires in the holder were replaced with Teflon coated platinum wires (A-M Systems, Sequim, WA) to avoid discharge between the wires at the back of the theta capillary when voltages applied to the wires were different. The two wires were inserted into each channel of a theta tip to apply voltage to each side independently.

3.2.3 Mass spectrometry

A quadrupole/time-of-flight (QqTOF) tandem mass spectrometer (QStar Pulsar XL, Sciex, Concord, ON, Canada) was used to perform all mass spectrometric experiments. The experimental procedure consists of four steps: electroosmosis, ionization, dump spray, and mass analysis. In the

electroosmosis step the protein solution was electrically pumped back and forth between the two channels by grounding the wire in one theta tip channel while applying 100 ms of 10 Hz square wave voltage to the wire in the opposite channel. The square wave duty cycle is 50% and the voltage is +/-100 V to +/-500 V, where "+/-" was used to indicate the switch between positive and negative voltages during an electroosmotic cycle. Next, the ionization step was triggered (1500 V on both wires, 80 ms), during which the ions are accumulated in Q2. The dump spray step was then triggered to spray out any residual analyte that had been exposed to the electroosmosis step. For this purpose, a dump spray step of 200 ms was found sufficient to return the mass spectrum to that of the pre-osmosis step. The ion path voltages were set such that no ions were accumulated in Q2 during the dump spray step. Finally, the mass spectrum was recorded during the 150 ms mass analysis step.

3.2.4   Power supplies and triggering system used in electroosmosis experiment on MS

A transistor-transistor logic (TTL) trigger, TTL-1, was generated by the instrument software to trigger a waveform generator (Agilent 33220A, Santa Clara, CA). A 5 V, 10 Hz square wave generated from the waveform generator was then used to trigger a DEI pulser (Directed Energy, Inc., PVX-4150, Fort Collins, CO). Two high-voltage ORTEC DC power supplies were used to provide the positive (+100 V to +500 V) and negative (-500 V to -100 V) heating voltages through the DEI pulser. Switching from heating voltage to ionization voltage was realized through a home-built high voltage switch box, which was triggered by another TTL trigger, TTL-2. In the electroosmosis step, the two switches are in B_1 and B_2 position, while in the ionization step the two switches are in A_1 and A_2 positions. The power supplies and detailed trigger system is summarized in Figure 3. 1.

3.2.5 Power supplies and triggering system used in electroosmosis experiment on Raman

The whole experimental cycle was controlled by waveform generator-1, which triggered both waveform generator-2 and a digital delay generator (Stanford research systems, Inc. DG535, Sunnyvale, CA).

Electroosmotic frequency is controlled by the square wave generated from waveform generator-2, which triggered the DEI pulser. The alternated positive (+100 V to +500 V) and negative (-500 V to -100 V) heating voltages are supplied by two ORTEC high voltage DC power supplies connected to the DEI pulser and feed to channel B_2 on the switch box. A_1 and A_2 on the switch box are connected to another DC power supply, which provides the +1500 V ionization and spray voltage.

In the electroosmosis step, the switch box state is $B_1B_2A_3A_4$; in the spray step, the switch box state change to $A_1A_2A_3A_4$; in the simulated mass analysis step when no voltage is applied to the tip, the switch box state is $A_1A_2B_3B_4$. The time of each step is controlled by the delay generator. The power supplies and detailed trigger system is summarized in Figure 3. 2.

3.2.6 Raman temperature measurement

The temperature of the fluid near the apex of the theta tip was obtained non-invasively using Raman spectroscopy. The micro-Raman spectra were measured using a custom-built instrument which includes a 532 nm laser excitation (Coherent Sapphire SF CDRH 532 nm) and a TE-cooled CCD (Princeton Instruments SP2300). A 100x objective (Olympus LM Plan Fl) with a working distance of 3.4 mm was used to both focus the laser and collect the backscattered Raman signal. Laser power at the sample was set to 24.5 mW. Fine positional control was accomplished with a motorized microscope stage (Prior H101A/C). For the Raman experiments, both channels of the theta tip were filled with 5 mM ammonium acetate. Consecutive spectra with 100 ms exposure

time were acquired while continuously cycling through the process of electroosmosis-spray-simulated mass analysis. To obtain the training spectra for temperature calibration, a Pyrex 9530-3 borosilicate glass capillary (1.5-1.8 mm O.D., 90 mm length) was filled with 18.2 MΩ cm ultrapure water and heated using a Physitemp TS-4MPER thermal stage to temperatures between 20 °C and 90 °C, measured using a needle thermocouple (Physitemp MT-26/4 with an Omega DP701 reader). The temperature training spectra were collected with an integration time of 5 minutes per spectrum.

The shape and intensity of the OH stretching mode of water is highly temperature dependent and has been used in the past for Raman thermometry. For example, D'Arrigo et al. calibrated temperatures based on a ratio of OH stretch areas with respect to measured temperature values from a thermocouple. [40] These areas were based on an approximate isosbestic point near 3400 cm^{-1}, and the calibrated value was the ratio of the OH area to the left and to the right of that point. We employed an alternative hyperspectral procedure using self-modeling curve resolution (SMCR) to decompose the OH stretch into the two primary spectral components such that each spectrum is a linear combination of those two components. Each spectrum was first baseline subtracted in the OH stretch region using a quadratic fit to user-defined points in the baseline on either side of the OH band. Next, using the baseline subtracted training spectra, a quadratic calibration curve relating measured temperature to a parameter representing the fractional spectral weight of the high temperature component in each measured spectrum was generated. Then for each experimental spectrum, a total least squares fit of the measured spectrum to the two SMCR components was used to quantify the fractional weight of the high temperature component, which was in turn converted to temperature using the training calibration curve. Two of these

experimental spectra and their corresponding temperature values are shown in Figure 3. 10 insert (b).

The Raman measurements were obtained asynchronously at a frame rate of about 6 fps, and subsequently synchronized with the applied voltage cycles to create plots similar to Figure 3. 10 insert (a). Each curve of Figure 3. 10 insert (a) includes 400 Raman measured temperature data points and approximately 110 cycles of electroosmosis-spray-simulated mass analysis process.

3.3   Results and discussion

3.3.1   Electroosmosis induced protein denaturation.

Bovine carbonic anhydrase II, a 29 kDa protein reported to have a melting point of 64 $^{\circ}$C, [41] has been the subject of folding/denaturation studies under a variety of conditions and several conformational states have been noted. [42-44] Mass spectrometry studies of conventional pH induced unfolding of carbonic anhydrase II was also reported. In its native state (i.e., the holo-carbonic anhydrase II (hCA II) form), a Zn^{2+} co-factor is present, although the presence of Zn^{2+} has not been observed to be key to folding of this protein. [45] When hCA II dissolved in a 5 mM NH_4OAc aqueous solution was subjected to nESI from a theta tip without an electroosmosis step, a narrow charge state distributions centered at +11 was observed containing the Zn^{2+} co-factor (Figure 3. 3 (a)). 100 ms of a 10 Hz square wave at +/-200 V resulted in the generation of higher charge states of hCA II (Figure 3. 3 (b)) with the +15 charge state being most abundant of the newly apparent charge states. The +/-200 V square wave with 50% duty cycle induced a bidirectional electroosmosis, which suppressed the bulk motion of the solutions from one channel to the other. Therefore, the small amount of denatured protein subjected to electroosmosis can be cleared up by applying a dump spray voltage for 200 ms to regain the pre-osmosis spectrum. At +/-230 V, a more extensive shift in charge states of hCA II was noted, along with low levels of

apo-carbonic anhydrase II (aCA II) ions over a wide range of charge states (Figure 3. 3 (c)). In this case, the +18 charge state was most abundant of the higher charge states. The abundance pattern of the higher charge states is also suggestive of the presence of several charge state distributions. In any case, the data of Figure 3. 3 clearly suggest that protein denaturation can take place upon electroosmosis in the theta tip and that the extent of denaturation increases with the square wave voltage.

Myoglobin is another extensively studied globular protein and has a reported melting temperature of 76 ^{o}C at neutral pH. [46] In its native state, myoglobin contains a non-covalently-bound heme ligand. It is referred to as holo-myoglobin (hMb) when the heme group is present and apo-myoglobin (aMb) when it is absent. When exposed to heat, hMb undergoes stepwise unfolding through a series of intermediates. [47] The initial stage of unfolding involves a slight extension of the tertiary structure while preserving the heme ligand. In the following phase, a dramatic tertiary structure alteration occurs resulting in the loss of the heme ligand and generation of unfolded aMb. Further heating of the protein may lead to polymerization of aMb before precipitation. Accumulated free heme ligand can also polymerize or nonspecifically attach to aMb and hMb. [48] The inserts of Figure 3. 4 show a selection of nESI spectra obtained as a function of square wave voltage in a theta tip. Both channels of the theta tip contained a myoglobin solution in 5 mM NH$_4$OAc solution. Figure 3. 4 (a) shows the spectrum of myoglobin sprayed after applying 100 ms of square wave at a voltage of +/-150 V. The spectrum, as well as those obtained at lower square wave voltages, is essentially identical to that obtained in the absence of electroosmosis (not shown) and clearly suggests that the native hMb conformation is preserved due to the retention of the heme group and the low charge state distributions centered at +8. The insert of Figure 3. 4 (b) shows the spectrum obtained after 100 ms electroosmosis induced by a 10

Hz +/-230 V square wave. At this voltage, a portion of the hMb cation population lost the heme

ligand to form aMb ions in two clearly apparent charge state distributions with maxima at +14 and

+9, respectively, as shown by the open, green circles in Figure 3. 4 (b). With the square wave

voltage increased to +/-300 V, the original hMb charge states were further depleted and the higher

charge state aMb peaks grew in relative abundance (see the insert of Figure 3. 4 (c)). Some of the

lost heme ligand was observed to attach to hMb to form a complex with two heme groups, as

indicated by the blue triangles. The attachment of more than one heme group to denatured hMb

has been noted in solution phase studies. [49, 50] The spectra of the inserts (b) and (c) show at

least two distinct charge state distributions for aMb ions, which likely reflects distinct folding

states of aMb. The plot of Figure 3. 4 shows the percentage of aMb ion signal relative to total

myoglobin ion signal (aMb+hMb ions) as a function of square wave voltage with the solid line

representing a sigmoidal fit to the data. While this plot does not reflect the evolution of different

folding states of aMb, the percentage of aMb ions provides an overall reflection of the extent of

denaturation of the protein. If the aMb ions are taken as representing any unfolded state while the

hMb ions are taken as representative of the native state, the plot of Figure 3. 4 treats myoglobin as

a two-state system (i.e., folded versus unfolded). A sigmoidal shape for the percentage of the

unfolded state is as a function of denaturation condition (e.g., temperature, pH, concentration of

denaturant, etc.) is expected for such a scenario. [51]

Similar phenomena were noted with equine cytochrome *c* (eCyt *c*), which has a reported

melting temperature of 85 $^{\circ}$C. [52] This protein contains a covalently bound heme ligand, which

remains bound to the protein upon denaturation. [53] Therefore, upon heating, eCyt *c* mainly

undergoes tertiary structure extension, reflected by an increase in charge states in nESI mass

spectra. In this case, we use the abundance weighted average charge state of the protein as a

reflection of the extent of denaturation as a function of square wave voltage in the plot of Figure 3. 5. These results were obtained from series of nESI mass spectra derived from eCyt c in an aqueous solution of 5 mM NH$_4$OAc as a function of square wave voltage. Inserts (a)-(c) show the mass spectra obtained using 100 ms of 10 Hz square wave at voltages of +/- 290 V, +/- 310 V, and +/- 340 V, respectively.

Collectively, the results for these proteins showed that protein denaturation under conditions of electroosmosis in a theta tip at relatively high square wave voltages is a general phenomenon. Furthermore, the extent of denaturation was found to be both condition dependent (e.g., the magnitude of the square wave voltage) and protein dependent (e.g., higher square wave voltages were required to denature proteins with higher melting temperatures). The results are consistent with thermal denaturation as a result of Joule heating at the end of the theta tip during electroosmosis.

3.3.2 Ammonium acetate concentration influence on protein denaturation

The addition of ammonium acetate is well known to stabilize the native conformation of proteins in solution through the pH buffering effect, [2] ionic specific interaction [54] and so forth. Throughout the electrospray ionization process the pH in the tip may decrease due to redox reactions [55, 56] which can induce protein denaturation. As such, it is common to buffer the solution, via the addition of ammonium acetate, to protect the native conformation of the protein from pH-induced unfolding. [2] It is also reported that cations and anions can stabilize or destabilize protein conformation in solution phase through ion-ion and ion-surface interactions. [57] The ionic effect is summarized as an empirical rule termed the Hofmeister series. Both ammonium and acetate ions are in the stabilizing end of the Hofmeister series, which helps maintain native conformation. Besides this effect, the protein-ligand dissociation constant also

decreases with higher ammonium acetate concentration, when the protein's isoelectric point is higher than the pH of the solution. [58] The isoelectric point of myoglobin is 6.8-7.4, while the ammonium acetate buffer pH is 6. At this pH, ammonium acetate enhances the retention of the heme in the myoglobin binding pocket. Since holo-myoglobin stability is determined by the heme ligand affinity, [59] the high binding affinity of the heme in ammonium acetate buffer can further stabilize myoglobin.

Based solely on the considerations mentioned above, an increase in ammonium acetate concentration in the theta tip under electroosmosis conditions might be expected to inhibit the extent of denaturation.   However, as demonstrated in Figure 3. 6, the extent of denaturation increases with a doubling of ammonium acetate concentration. Figure 3. 6 (a) shows a mass spectrum of myoglobin obtained using deionized water (i.e., no added ammonium acetate) after 100 ms of electroosmosis at +/-230 V. The result is consistent with the native protein (i.e., low charge state distributions of hMb ions), suggesting that denaturation does not take place to a detectable extent under such solution conditions. Using the same square wave voltage, the addition of 5 mM NH_4OAc to the protein solution results in the spectrum in Figure 3. 4 (b), which shows clear evidence for protein denaturation via the appearance of two aMb distributions. The hMb low charge state distributions remains highly abundant, however, which indicates that much of the protein in solution sampled by the mass spectrometer remains in the native state. Figure 3. 6 (b) shows the spectrum obtained using 10 mM NH_4OAc where significant myoglobin denaturation during electroosmosis was observed. The bimodal distribution of aMb peaks became dominant with only a small amount of hMb peaks remaining. The excess heme ligand formed via electroosmosis is observed to form a non-specific complex with hMb indicating further denaturation.

Electroosmosis using +/-200 V of bovine cytochrome c (bCyt c) in 5 mM and 10 mM NH_4OAc

solution showed the same trend, where the 10 mM NH_4OAc solution gave rise to higher bCyt c

denaturation (Figure 3. 7). These results are consistent with an increase in Joule heating due to an

increase in the conductivity of the solution with increasing electrolyte concentration (see Equation

1), which overcomes any stabilization effects that might otherwise arise with increasing

ammonium acetate concentration. The effect of electrolyte concentration, in addition to the

voltage effect described above, provides another indirect piece of evidence for Joule heating.

3.3.3 Ion type influence on protein denaturation

Protein thermal denaturation is influenced by solution pH [65] and ionic strength, both of

which are related to the ion type of the buffer. The thermal denaturation of ubiquitin under theta

tip electroosmosis demonstrated the ion type influence on protein stability. (Figure 3. 8) Ubiquitin

is a small globular protein with a molecular weight of 8564. Ubiquitin has a high pH and thermal

stability, and the reported ubiquitin melting temperature under neutral pH is above 100 ^{o}C. [64]

As mentioned above, ammonium acetate is a protein stabilizing salt based on Hofmeister series.

As a weak electrolyte, the ionic strength of ammonium acetate is relatively low, and as a neutral

buffer, the pH of 5 mM NH_4OAc is about 6. In 5 mM NH_4OAc without any electroosmosis,

ubiquitin stayed in native conformation, which showed a very narrow charge state distribution,

mainly including +5 and +6. (Figure 3. 8 a)) Even applying a high electroosmosis of +/- 300 V,

ubiquitin charge state distribution was not changed, and the protein stayed in the native

conformation. (Figure 3. 8 b) and c))

When the buffer was changed from ammonium acetate to ammonium formate, and the buffer

concentration was kept the same of 5 mM, ubiquitin denaturation started occurring. Starting from

a direct spray of ubiquitin in 5 mM ammonium formate in theta tip without applying any square

wave voltages, ubiquitin maintained its stable native state. The result showed that solution pH could not denature ubiquitin, although the pH of 5 mM ammonium formate (~5) is a little lower than that of 5 mM ammonium acetate solution. (Figure 3. 8 d)) When a 10 Hz, 200 V square wave was applied, protein charge state distribution was broadened. The center of the charge states shifted from +5 to +6 and the maximum charge increased from +6 to +8. (Figure 3. 8 e)) Under a continuous increasing of the square wave voltage amplitude from 200 V to 300 V, charge states of ubiquitin were further increased, which indicated protein further unfolding. (Figure 3. 8 f)) Ammonium formate is a stronger electrolyte than ammonium acetate, so the solution ionic strength is higher under the same salt concentration. Since Joule heating amount is proportional to solution ionic strength, the amount of Joule heating generated in 5 mM ammonium formate should be higher than in 5 mM ammonium acetate, which may contribute to ubiquitin denaturation. As mentioned above, solution pH of 5 mM ammonium formate is lower than that of 5 mM ammonium acetate. Under lower pH ubiquitin is less stable and thermal stability is lower.

When the salt is changed to an even stronger electrolyte ammonium chloride, ubiquitin denaturation under electroosmosis was even more significant. (Figure 3. 8) Ammonium chloride is a strong electrolyte formed by a strong acid and weak base, so the solution of ammonium chloride is more acidic. However, the acidity of the solution is not high enough to denature ubiquitin due to the high pH stability of the protein. Figure 3. 8 g) shows that in 5 mM ammonium chloride solution, ubiquitin stayed native and had a narrow low charge state distribution. When a +/- 200 V square wave was applied to induce in-tip electroosmosis, ubiquitin was highly denatured and a bimodal distribution was clearly observed. (Figure 3. 8 h)) The bimodal distribution indicated the coexistence of native and unfolded protein conformations, and protein denaturation was captured. Further increasing the square wave amplitude to 300 V, a complete high charge state

distribution was generated centered in +11 and all basic residues were protonated. This indicated ubiquitin full denaturation. (Figure 3. 8 i))

As a brief summary, salt type has a significant influence on protein denaturation extent under theta tip electroosmosis. Salt type influence may result from pH, ionic strength and ion-protein interactions. From ammonium acetate to ammonium chloride, the ionic strength become higher, and solution pH and ion stabilizing effect on protein becomes lower. Increasing ionic strength could increase Joule heating effect, and lower pH and lower ion stabilizing effect on protein could destabilize proteins. All of these effect lead to more protein denaturation upon electroosmosis. The results have shown that protein denaturation extent under the same electroosmosis condition but in different salt solution is that $NH_4OAc < HCOONH_4 < NH_4Cl$. In each salt solution, protein denaturation extent increase with electroosmosis voltage. These orders are consistent with the argument above and is also consistent with Joule heating effect.

3.3.4 Protein denaturation in basic condition and monitored by -nESI

Another argument for protein denaturation during electroosmosis may rise as surface-induced protein unfolding. Williams Group has reported a phenomenon that positively charged proteins can partially denature during +nESI ionization and spray process, and the denaturation extent is directly related to tip size. Proteins sprayed from a smaller tip could have a higher denaturation extent. However, negatively charged protein ions were not influenced by tip size. [66] This phenomenon was attributed to surface effect. Since the glass surface is negatively charged, it could interact with positively charged protein ions. The Coulomb force may tear proteins apart and unfold proteins. When tip size is smaller, the surface is larger so the surface-induced protein unfolding is stronger. When the protein is negatively charged, the Coulomb interaction is lost so negative protein ion conformation is not influenced by the surface area or tip size.

Considering this surface effect, electroosmosis of protein in basic condition was performed and -nESI was used to ionize protein. (Figure 3. 9) Myoglobin is a neutral reference protein with an isoelectric point of 6.8-7.4. Under basic condition adjusted by 5 mM piperidine, myoglobin is negatively charged and slightly denatured even without performing any electroosmosis. (Figure 3. 9 a)) Part of the holo-myoglobin lost the heme ligand and became apo-myoglobin, which is the most apparent evidence for protein denaturation. Starting from this point, when +/-230 V square wave was applied to one channel of a theta tip, in-tip electroosmosis was induced. Since myoglobin was negatively charged, protein-surface interaction should be very weak and the surface-induced protein unfolding should be very subtle. However, the data showed that under 230 V electroosmosis, myoglobin was significantly denatured and showed an apo-/holo- myoglobin ratio about 1/1. (Figure 3. 9 b)) Further increasing the voltage amplitude to 300V, the majority of the protein lost the heme ligand and showed a high charge state distribution centered in -16. (Figure 3. 9 c)) The negative mode protein denaturation results demonstrated that other factors beyond surface effect denatured the protein. The phenomenon is still able to be explained by Joule heating effect.

3.3.5   Temperature measurements using Raman spectroscopy

Protein denaturation can arise in a variety of ways and therefore provides only indirect evidence for Joule heating in a theta tip during electroosmosis. We therefore examined the temperature of the solution very near to the end of the tip as a function of operating conditions. The highest resistance to current flow is expected to be at the narrowest point of the channel, which is at the end of the tip, thus the Joule heating effect is the strongest at the end of the tip. It was therefore desirable to be able to measure temperature in a small volume at or near the end of the tip to minimize error associated with the bulk solution elsewhere in the theta tip. The measurement

of Raman scattering from a tightly focused laser spot, estimated to be 8-15 fL with our system, provides the needed spatial resolution. To measure the solution temperature during each step (electroosmosis, spray and mass analysis), a voltage supply and triggering system was established to mimic the procedure used in the mass spectrometry experiments, as described in Figure 3. 2. A 5 mM NH$_4$OAc solution was loaded into both channels of the theta tip. The duration of electroosmosis, spray, and mass analysis steps were set to 100 ms, 300 ms and 200 ms, respectively, as in the MS experiment. A 10 Hz square wave was used to induce 100 ms of electroosmosis with voltage values from +/-100 V to +/-500 V. The solution temperature was measured during this process and the resultant temperatures are shown in Figure 3. 10. During the electroosmosis step, the solution temperature increased from room temperature to a maximum temperature. When the square wave was completed, the solution temperature cooled down and reached the starting room temperature, as shown in Figure 3. 10 insert (a).

Figure 3. 10 shows how the maximum solution temperature obtained during the electroosmosis step is correlated to the applied square wave heating voltage. Based on the measured temperature, applying a +/-200 V square wave to one channel increased the solution temperature to about 44 ^{o}C, while +/-300 V voltage increased the solution temperature to 51 ^{o}C. Increasing the voltage amplitude to 500 V led to a maximum temperature at 77 ^{o}C. The small size of the theta tip, and the associated large resistance, implies that Joule heating is expected to produce a substantial temperature rise near the apex of a theta tip, although heat dissipation exists in the open system. The Raman laser measuring point is about 8 μm away from the end of the tip and the true maximum temperature at the tip apex may also be underestimated. Nevertheless, the Raman measurements directly show that the electroosmosis process gives rise to an increase in the solvent temperature that is directly related to the square wave voltage applied to induce electroosmosis.

When the electroosmosis time was increased to 500 ms (10 Hz, 5 cycles), the Raman thermometry measurement shows that the temperature reaches equilibrium. (Figure 3. 11) From the Raman data, it takes less than 300 ms for solution temperature to reach maximum. At the maximum temperature, heat generation and heat dissipation reaches equilibrium. 10 Hz, +/- 100 V electroosmosis for 500 ms can heat up the solution from room temperature to about 50 °C, and 200 V electroosmosis can heat up the solution up to 53 °C. (Figure 3. 11 insert a)) When the electroosmosis voltage increases, the temperature rising rate increases and 300 V square wave can heat up the solution to about 74 °C. (Figure 3. 11 insert b)) When 400 V electroosmosis was performed, the solution is highly boiled and bubbles were observed in tip. Measured solution temperature is above 100 °C, which can result from overheating. (Figure 3. 11 insert c))

3.3.6 Estimation of Joule heat amount in the theta tip apex during electroosmosis.

The tip portion of a theta capillary can be modeled by approximating each channel as a half cone (Figure 3. 12). Electroosmotic flow is induced with application of differential voltage between electrodes in each channel, where L is the electroosmosis flow path length between electrode tips and the radius of the capillary at the electrode tip is b. One may thus calculate the temperature in a small region of interest at the apex of the theta tip of length $\delta x = 10$ μm and an approximately half cylindrical shape of radius $a = 5$ μm. Thus, the region of interest has a volume of ~0.4 pL and a mass (m) obtained using the density of water (ρ). Given our experimentally measured flow rate of 1 nL/s (at an applied voltage of 300 V), we obtain a fluid exchange time of $t \sim 0.4$ ms.

The resistance along the x-axis is $R(x) = \frac{1}{\Lambda c A(x)}$, where $A(x)$ is the cross-sectional area. When calculating the resistance, the conductivity of the solution is described by using the molar conductivity of ammonium acetate ($\Lambda = 108.29$ S·m^2/mol) and electrolyte concentration ($c = 5$ mM).

Total resistance is obtained by integrating the resistance ($R(x)$) over the entire distance between the electrodes. The voltage drop across the region of interest is obtained from the applied voltage times the ratio of the resistance in the region of interest to the total resistance, and the resulting power deposited in the volume of interest is $P = V^2/R = V^2/[R(x)\delta x]$.

Finally, assuming that all the power generated is converted to heat ($Q = C_p m \Delta T = Pt$), and using the heat capacity (C_p) of water, the change in temperature at the theta tip (ΔT) may be obtained as follows:

$$\Delta T = \frac{Pt}{mC_p} = \frac{\Lambda ct}{\rho C_p L^2} \left(\frac{b}{a}\right)^2 V_0^2$$

Using parameters that approximate our experimental theta tip system, with an applied voltage of 300 V, the above expression predicts a temperature rise of about 174 °C. This temperature is in the scale of the measured temperature. Heat dissipation is a big factor contributing to the final solution temperature in the tip.

3.3.7 Correlation between protein melting temperature and denaturation voltage.

The melting temperature of a protein is a measure of its thermal stability towards denaturation and several reports have employed heated ESI or nESI emitters to examine thermal denaturation of proteins and protein complexes. [60, 61, 62] Therefore, the onset and extent of protein denaturation might be expected to correlate with theta tip heating voltage. Indeed, the extent of denaturation observed for the three proteins discussed above (viz., bovine CA II, myoglobin, and eCyt c) are consistent with this expectation. That is, the protein with the lowest reported melting temperature (CA II) showed extensive denaturation at the lowest square wave voltages and the protein with the highest reported melting temperature (eCyt c) required the greatest square wave voltages to lead to extensive denaturation. A more reliable comparison, however, can be made

with a mixture of proteins such that all experiments are conducted with the same theta tip and solution conditions, thereby ensuring that each protein is exposed to the same extent of Joule heating.

To study the correlation between protein melting temperature and heating voltage, a 5 mM NH$_4$OAc solution containing myoglobin (melting temperature of 76 ^{o}C [46]) bovine cytochrome *c* (melting temperature of 80 ^{o}C [63]) and ubiquitin (melting temperature of 100 ^{o}C [64]) was subjected to electroosmosis in a theta tip. Since the ionization efficiencies of these three proteins are different, the concentrations of myoglobin, cytochrome *c* and ubiquitin in the mixture were adjusted to 0.11, 0.07 and 0.02 mg/mL, respectively. Figure 3. 13 (a) shows the spectrum obtained when the protein mixture was subjected to 100 ms of electroosmosis using a 10 Hz +/-200 V square wave. No change in the mass spectrum was noted relative to the spectrum obtained without electroosmosis (not shown) suggesting that none of the proteins underwent measurable denaturation. Myoglobin showed signs of denaturation (viz., the appearance of aMb ions of relatively high charge states) using a +/-230 V square wave for heating (Figure 3. 13 (b)), while the bCyt *c* and ubiquitin ions remain unchanged at this voltage. The first sign of the denaturation of bCyt *c*, as reflected by the appearance of a higher charge state distributions, is observed at +/-250 V (Figure 3. 13 (c)). The abundances of the higher charge state distributions of myoglobin and bCyt *c* were observed to increase further at +/-300 V (Figure 3. 13 (d)) and +/-500 V (Figure 3. 13 (e)). Ubiquitin, which has the highest melting temperature in the mixture, showed no charge state distribution change until +/-500 V square wave voltage was applied. Figure 3. 13 (e) shows a modest charge state shift from +5 to +6 at +/-500 V heating which suggests that the ubiquitin tertiary structure might be perturbed under these conditions. Overall, these results are fully consistent with an increase in solution temperature with increasing square wave heating voltage

3.4   Conclusions

The effect is shown to arise from Joule heating via both direct and indirect evidence. Indirect evidence included an increase in the extent of protein denaturation with the magnitude of the voltage of a square wave used to effect electroosmosis. This effect was demonstrated for myoglobin, equine cytochrome *c*, and carbonic anhydrase II solutions. Joule heating is expected to increase with field strength. An increase in the extent of denaturation for myoglobin was also observed with an increase in the ammonium acetate concentration. Joule heating is expected to increase with solution conductivity. Using Raman spectroscopy temperature measurements near to the capillary tip, an increase in solution temperature, direct evidence for Joule heating, was found to correlate with the amplitude of the square wave voltage. Protein denaturation under electroosmosis in basic conditions ruled out the surface-induced protein denaturation effect, while further support the generation of Joule heat during electroosmosis. Ubiquitin denaturation experiment also demonstrated the influence of different salt type on protein thermal stability.

Electroosmosis-induced Joule heating was observed to be positively correlated to protein melting temperature when a solution of a mixture of proteins of known melting temperature was subjected to a series of experiments with increasing square wave heating voltage. This work points to the development of a convenient and efficient way to modulate solution temperature in a nano-ESI theta tip prior to spraying into a mass spectrometer. It represents a flexible approach for controlled protein denaturation that does not depend on changes in solution additives or solvent composition. With further development, this effect may serve as the basis for a method to study protein thermal stabilities on small quantities of materials and with mixtures of proteins. Given the ability to alter temperatures in a pulsed fashion on the time-scales of tenths of seconds, this effect may also prove to be useful in studying protein unfolding and refolding dynamics on such a

time-scale. In this report, we demonstrate protein denaturation resulting from electroosmosis in a theta tip nano-ESI capillary.

3.5   References

1. Fenn, J. B.; Mann, M.; Meng, C. K.; Wong, S. F.; Whitehouse, C. M. *Science* **1989**, *246*, 64-71.

2. Heck, A. J. R. *Nat. Methods* **2008**, *5*, 927-933.

3. Kaltashov, I. A.; Eyles, S. J. *Mass Spectrom. Rev.* **2002**, *21*, 37-71.

4. Liu, J.; Konermann, L. *J. Am. Soc. Mass Spectrom.* **2009**, *20*, 819-828.

5. Kaltashov, I. A.; Abzalimov, R. R. *J. Am. Soc. Mass Spectrom.* **2008**, *19*, 1239-1246.

6. Cassou, C. A.; Williams, E. R. *Anal. Chem.* **2014**, *86*, 1640-1647.

7. Reid, G. E.; Wu, J.; Chrisman, P. A.; Wells, J. M.; McLuckey, S. A. *Anal. Chem.* **2001**, *73,* 3274-3281.

8. Jockusch, R. A.; Schnier, P. D.; Price, W. D.; Strittmatter, E. F.; Demirev, P. A.; Williams, E. R. *Anal. Chem.* **1997**, *69*, 1119-1126.

9. Breuker, K.; Oh, H. B.; Horn, D. M.; Cerda, B. A.; McLafferty, F. W. *J. Am. Chem. Soc.* **2002**, *124*, 6407-6420.

10. Zubarev, R. A.; Kelleher, N. L.; McLafferty, F. W. *J. Am. Chem. Soc.* **1998**, *120*, 3265-3266.

11. Xu, D.; Tsai, C. J.; Nussinov, R. *Protein Eng.* **1997**, *10*, 999-1012.

12. Kumar, S.; Nussinov, R. *ChemBioChem* **2002**, *3*, 604-617.

13. Mirza, U. A.; Cohen, S. L.; Chait, B. T. *Anal. Chem.* **1993**, *65*, 1-6.

14. Sterling, H. J.; Williams, E. R. *J. Am. Soc. Mass Spectrom.* **2009**, *20*, 1933-1943.

15. Gratacós-Cubarsí, M.; Lametsch, R. *Meat Sci.* **2008**, *80*, 545-549.

16. Russo, N.; Estrin, D.; Martí, M.; Roitberg, A. *PLoS Comput. Biol.* **2012**, *8*, e1002761.

17. Park, Y.; Kim, K.; Lim, D.; Lee, E. K. *Process Biochem.* **2015**, *50*, 1379-1387.

18. Thakur, G.; Jiang, K.; Lee, D.; Prashanthi, K.; Kim, S.; Thundat, T. *Langmuir* **2014**, *30*, 2109-2116.

19. Ohyashiki, T.; Taka, M.; Mohri, T. *J. Biol. Chem.* **1985***, 260*, 6857-6861.

20. Iavarone, A. T.; Jurchen, J. C.; Williams, E. R. *J. Am. Soc. Mass Spectrom.* **2000**, *11*, 976-985.

21. Nemethy, G.; Peer, W. J.; Scheraga, H. A. *Annu. Rev. Biophys. Bioeng.* **1981**, *10*, 459-497.

22. Yu, Y.; Wang, J.; Shao, Q.; Shi, J.; Zhu, W. *Sci. Rep.* **2016**, *6*, 19500.

23. Mortensen, D. N.; Williams, E. R. *Anal. Chem.* **2016**, *88*, 9662-9668.

24. Sterling, H. J.; Cassou, C. A.; Susa, A. C.; Williams, E. R. *Anal. Chem.* **2012**, *84*, 3795-3801.

25. Kharlamova, A.; Prentice, B. M.; Huang, T.; McLuckey, S. A. *Anal. Chem.* **2010**, *82*, 7422-7429.

26. Kharlamova, A.; DeMuth, J. C.; McLuckey, S. A. *J. Am. Soc. Mass Spectrom.* **2012**, *23*, 88-101.

27. Girod, M.; Antoine, R.; Dugourd, P.; Love, C.; Mordehai, A.; Stafford, G. *J. Am. Soc. Mass Spectrom.* **2012**, *23*, 1221-1231.

28. Mortensen, D. N.; Williams, E. R. *Analyst* **2016**, *141*, 5598-5606.

29. Fisher, C. M.; Kharlamova, A.; McLuckey, S. A. *Anal. Chem.* **2014**, *86*, 4581-4588.

30. Mortensen, D. N.; Williams, E. R. *Anal. Chem.* **2015**, *87*, 1281-1287.

31. Fisher, C. M.; Hilger, R. T.; Zhao, F.; McLuckey, S. A. *J. Mass Spectrom.* **2015**, *50*, 1063-1070.

32. Mortensen, D. N.; Williams, E. R. *J. Am. Chem. Soc.* **2016**, *138*, 3453-3460.

33. Mortensen, D. N.; Williams, E. R. *Anal. Chem.* **2014**, *86*, 9315-9321.

34. Englander, S. W. *J. Am. Soc. Mass Spectrom.* **2006**, *17*, 1481-1489.

35. Blanco, E.; Ruso, J. M.; Sabín, J.; Prieto, G.; Sarmiento, F. *J. Therm. Anal. Calorim.* **2007**, *87*, 211-215.

36. Aseyev, V.; Hietala, S.; Laukkanen, A.; Nuopponen, M.; Confortini, O.; Prez, F. E. D.; Tenhu, H. *Polymer* **2005**, *46*, 7118-7131.

37. Upadhyay, S. K. *Chemical Kinetics and Reaction Dynamics.* Springer: New York, 2006.

38. Grossman, P. D.; Colburn, J. C. *Capillary Electrophoresis: Theory & Practice.* Academic Press, Inc.: Cambridge, 1992.

39. Whatley, H. *Basic Principles and Modes of Capillary Electrophoresis,* Humana Press Inc.: New York, 2001.

40. D'Arrigo, G.; Maisano, G.; Mallamace, F.; Migliardo, P.; Wanderlingh, F., *J. Chem. Phys.* **1981**, *75*, 4264-4270.

41. Sarraf, N.; Saboury, A.; Ranjbar, B.; Moosavi-Movahedi, A. *Acta Biochim. Pol.* **2004**, *51*, 665-671.

42. Gudiksen, K.L.; Urbach, A.R.; Gitlin, I.; Yang, J.; Vazquez, J.A.; Costello, C.E.; Whitesides, G.M. *Anal. Chem.* **2004**, *76*, 7151-7161.

43. Bushmarina, N. A.; Kuznetsova, I. M.; Biktashev, A. G.; Turoverov, K. T.; Uversky, V. N. *Chembiochem* **2001**, *2*, 813-821.

44. Semisotnov, G. V.; Rodionova, N. A.; Kutyshenko, V. P.; Ebert, B.; Blanck, J.; Ptitsyn, O. B. *FEBS Letters*, **1987**, *224*, 9-13.

45. Saito, R.; Sato, T.; Ikai, A.; Tanaka, N. *Acta Crystallogr.* **2004**, *D60*, 792-795.

46. Wan, L.; Twitchett, M.; Eltis, L.; Mauk, G.; Smith, M. *Proc. Natl. Acad. Sci.* **1998**, *95*, 12825-12831.

47. Awad, E. S.; Deranleau, D. A. *Biochemistry* **1968**, 7, 1791-1795.

48. Hargrove, M. S.; Barrick, D.; Olson, J. S. *Biochemistry* **1996**, *35*, 11293-11299.

49. Lee, V.W.S.; Chen, Y.-L.; Konermann, L. *Anal. Chem.* **1999**, *71*, 4154-4159.

50. Simmons, D.A.; Konermann, L. *Biochemistry* **2002**, *41*, 1906-1914.

51. Gillespie, B.; Plaxco, K.W. *Proc. Nat. Acad. Sci. USA* **2000**, *97*, 12014-12019.

52. Bágel'ová, J.; Antalík, M.; Tomori, Z. *Biochem. Mol. Biol. Int.* **1997**, *43*, 891-900.

53. Milne, J.; Xu, Y.; Mayne, L.; Englander, S. W. *J. Mol. Biol.* **1999**, *290*, 811-822.

54. Cacace, M. G.; Landau, E. M.; Ramsden, J. J. *Q. Rev. Biophys.* **1997**, *30*, 241-277.

55. Van Berkel, G.J.; Asano, K.G.; Schnier, P.D. *J. Am. Soc. Mass Spectrom.* **2001**, *12*, 853-862.

56. Van Berkel, G. J.; Zhou, F.; Aronson, J. T. *Int. J. Mass Spectrom. Ion Processes* **1997**, *162*, 55-67.

57. Salis, A.; Ninham, B. W. *Chem. Soc. Rev.* **2014**, *43*, 7358-7377.

58. Gavriilidou, A. F. M.; Gülbakan, B.; Zenobi, R. *Anal. Chem.*, **2015**, *87*, 10378-10384.

59. Hargrove, M. S.; Olson, J. S. *Biochemistry* **1996**, *35*, 11310-11318.

60. Benesch, J.L.; Sobott, F.; Robinson, C.V. *Anal. Chem.* **2003**, *75*, 2208-2214.

61. Geels, R.B.J.; Calmat, S.; Heck, A.J.R.; van der Vies, S.M.; Heeren, R.M.A. *Rapid Commun. Mass Spectrom.* **2008**, *22*, 3633-3641.

62. Wang, G.; Abzalimov, R.R.; Kaltashov, I. *Anal. Chem.* **2011**, *83*, 2870-2876.

63. Yang, F.; Zhou, B..; Zhang, P.; Zhao, Y.; Chen, J.; Liang, Y. *Chem.-Biol. Interact.* **2007**, *170*, 231-243.

64. Makhatadze, G.; Lopez, M.; Richardson, J.; Thmos, S. *Protein Sci.* **1998**, *7*, 689-697.

65. Law, A. J. R.; Leaver, J. *J. Agric. Food Chem.* **2000**, *48*, 672-679.

66. Mortensen, D. N.; Williams, E. R. *Anal. Chem.* **2016**, *88*, 9662-9668.
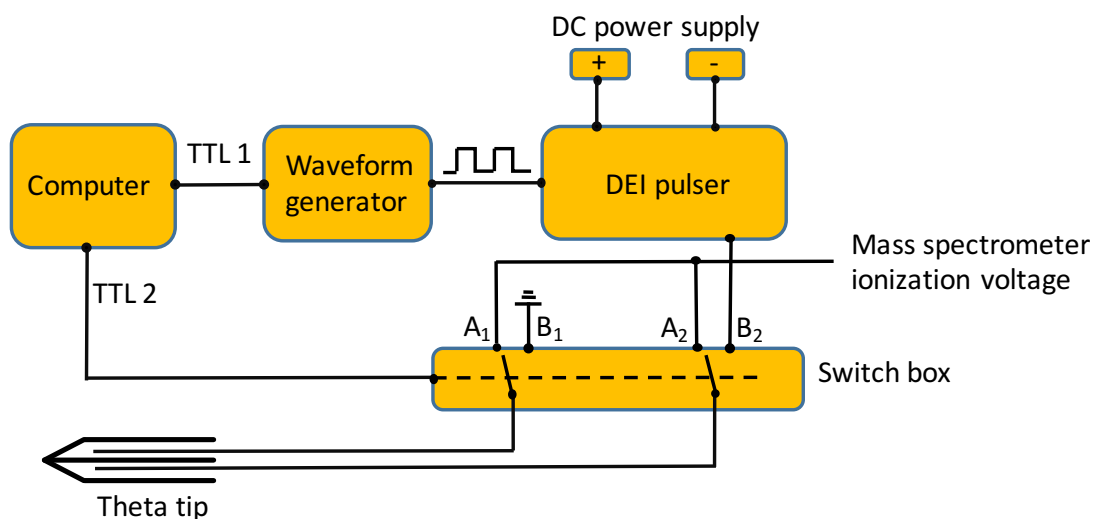
Figure 3. 1. Schematic of electroosmosis and spray power supply with triggering system.
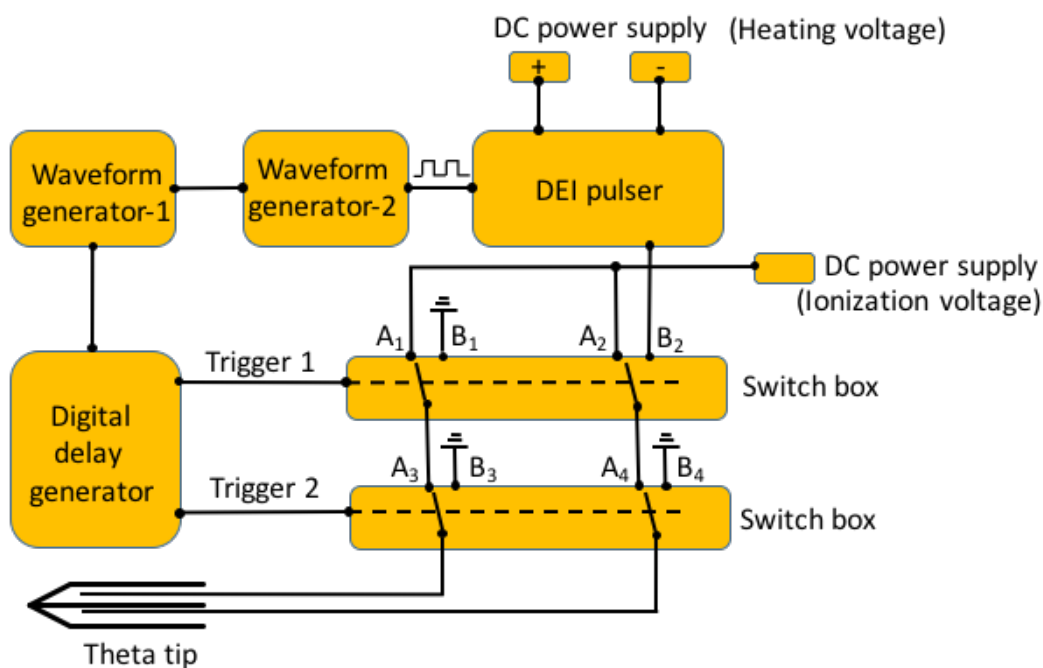
Figure 3. 2. Schematic of the voltage power supply and triggering setup used in Raman temperature measurements to initiate electroosmosis, spray and simulated mass analysis.
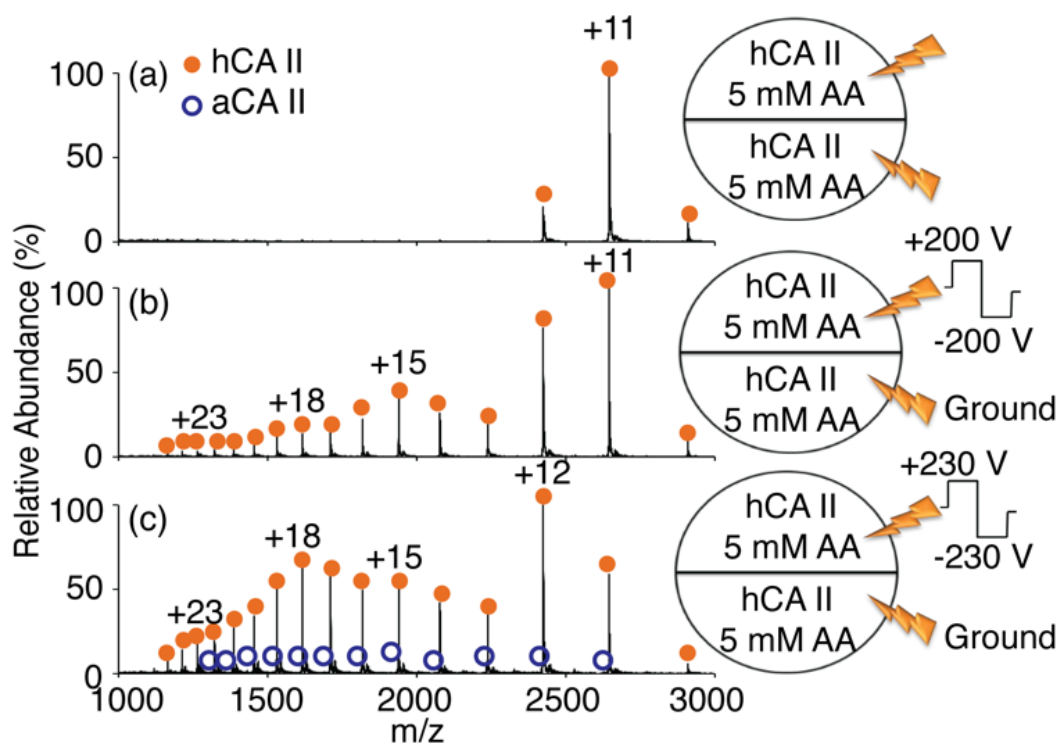
Figure 3. 3. (a) Positive nESI of a solution of bovine CA II in 5 mM NH_4OAc (AA) solution, sprayed out of a theta tip with no electroosmosis. Mass spectra of the same CA II solution after electroosmosis via 100 ms of a 10 Hz square wave at (b) +/-200 V and (c) +/-230 V. The circles at the right of the spectra indicate the theta tip schematic; an aliquot of the same sample was loaded in each channel, and the lightning bolts depict the voltage applied to each side.
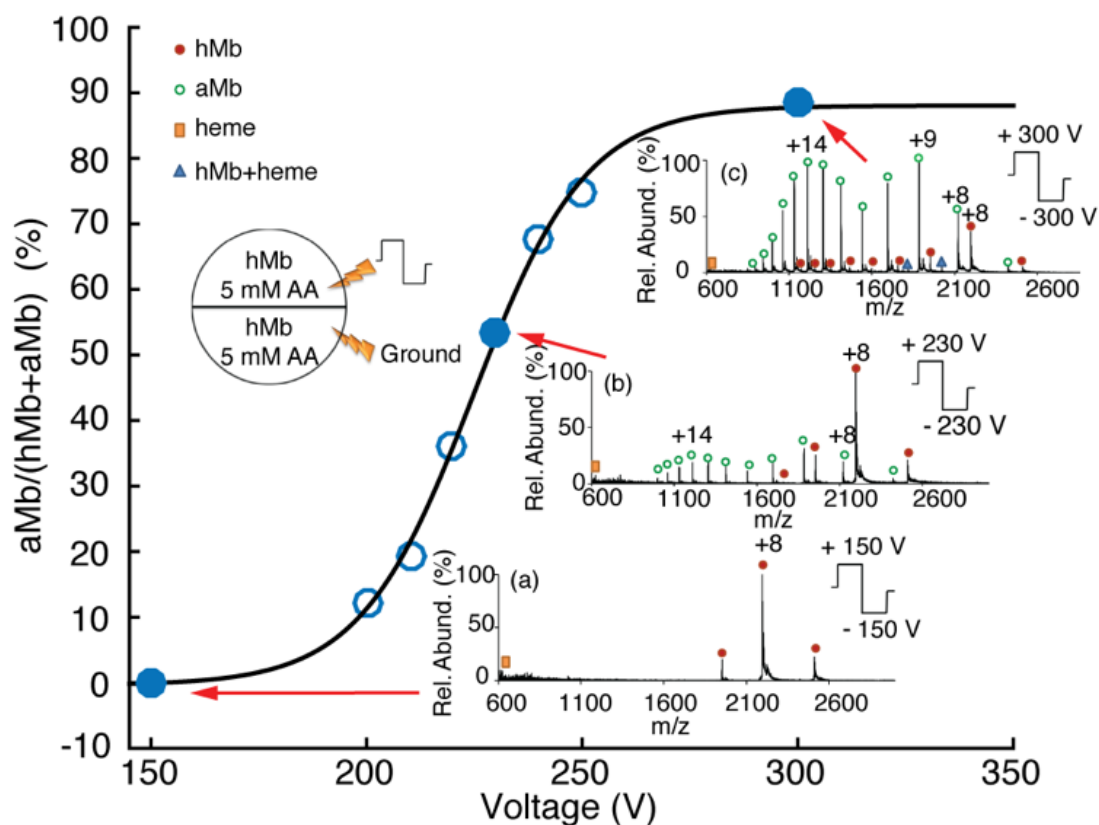
Figure 3. 4. A plot of the percentage of aMb ions relative to all myoglobin ions (aMb+hMb) as a function of square wave voltage.   Insert (a) - Positive nESI mass spectrum of a solution of hMb in 5 mM NH_4OAc (AA) solution, sprayed out of a theta tip with no electroosmosis. Insert (b) - Mass spectrum of the same hMb solution after electroosmosis via 100 ms of a 10 Hz square wave at +/-230 V. Insert (c) - Mass spectrum obtained with a square wave voltage of +/-300 V. Green open circles represent charge states of aMb, red closed circles represent charge states of hMb, blue triangles represent hMb with an additional heme group, filled gold square represents heme ion.
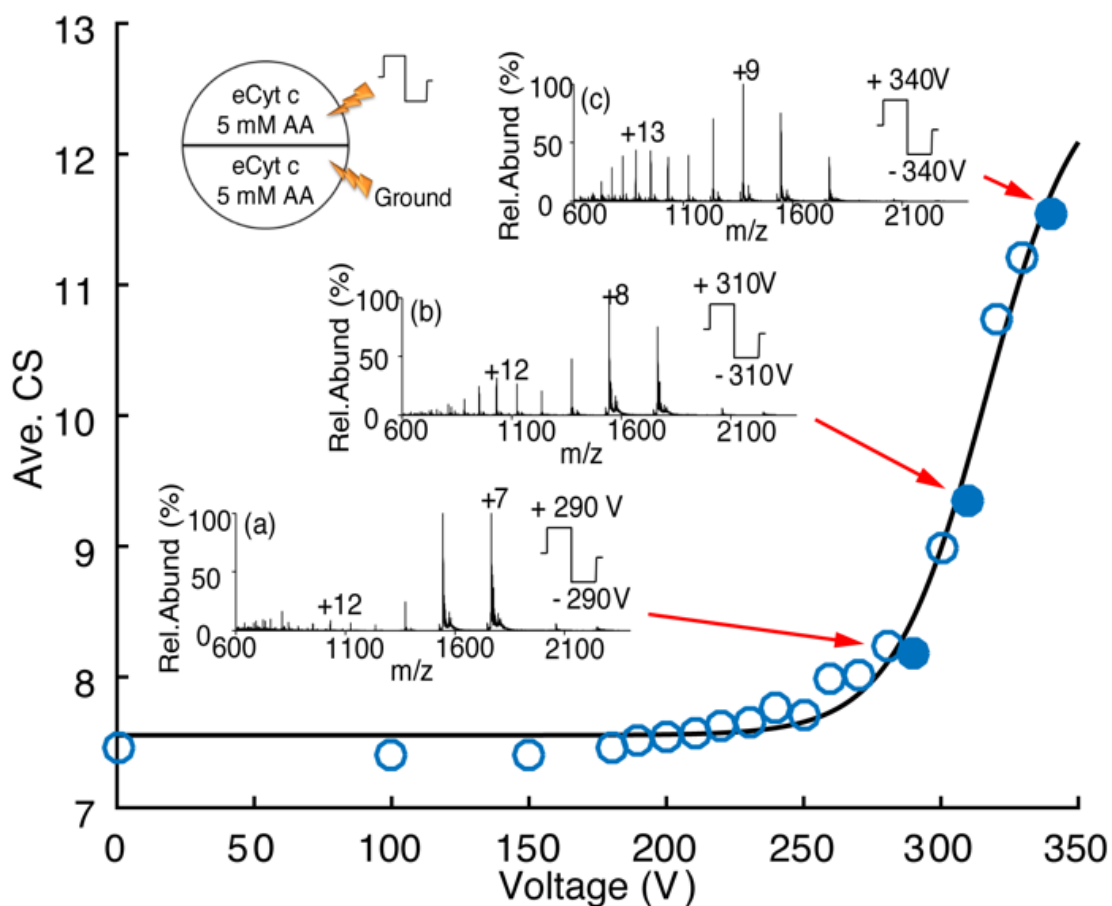
Figure 3. 5. A plot of the abundance weighted average charge state of eCyt *c* ions as a function of square wave voltage after 100 ms of a 10 Hz square wave applied to a solution of eCyt *c* in 5 mM NH$_4$OAc (AA) solution. Insert (a) Positive nESI mass spectrum obtained using +/-290 V. Insert (b) Mass spectrum obtained using +/-310 V. Insert (c) Mass spectrum obtained using +/-340 V
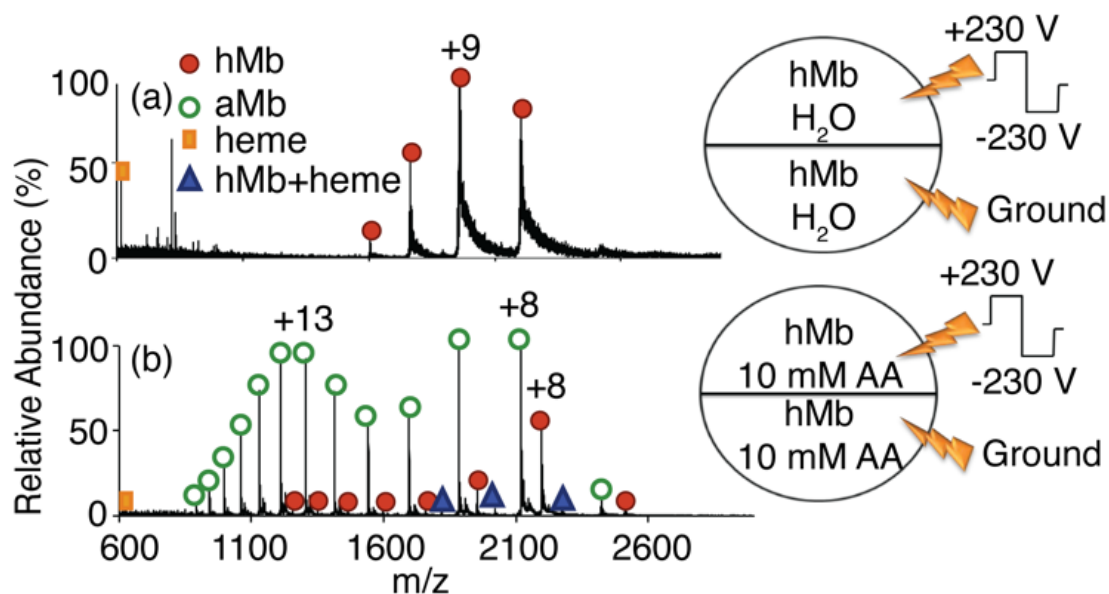
Figure 3. 6. Electroosmosis of myoglobin at +/-230 V for 100 ms in (a) de-ionized water; (b) 10 mM NH_4OAc (AA) solution. The circles at the right of the spectra indicate the theta tip schematic; an aliquot of the same sample was loaded in each channel, and the lightning bolts depict the voltage applied to each side
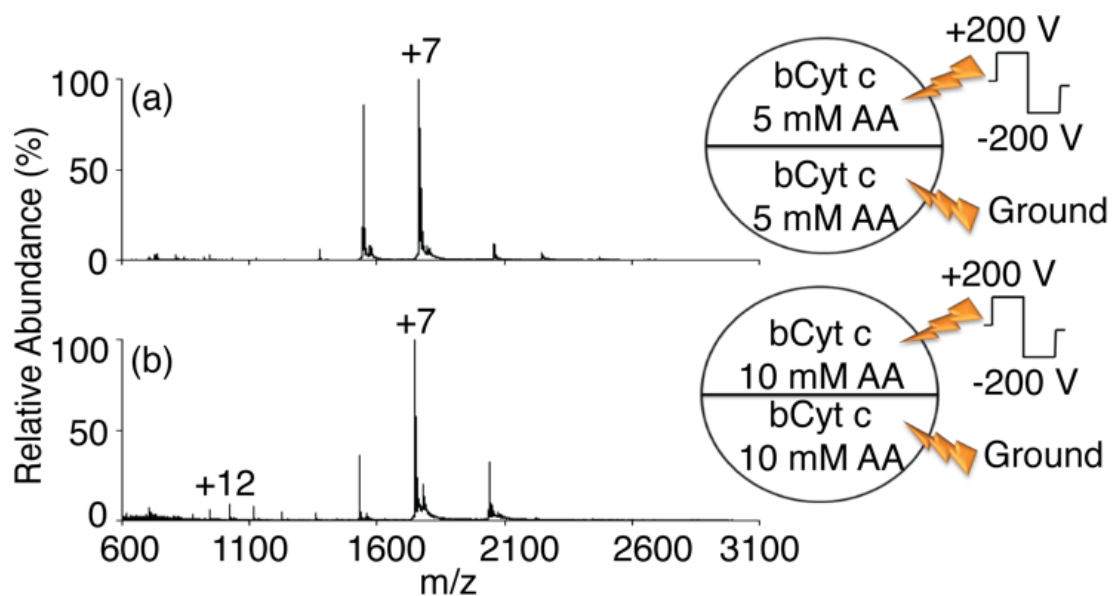
Figure 3. 7. Electroosmosis of bovine cytochrome c at +/- 200 V for 100 ms in (a) 5 mM NH_4OAc and (b) 10 mM NH_4OAc solution.
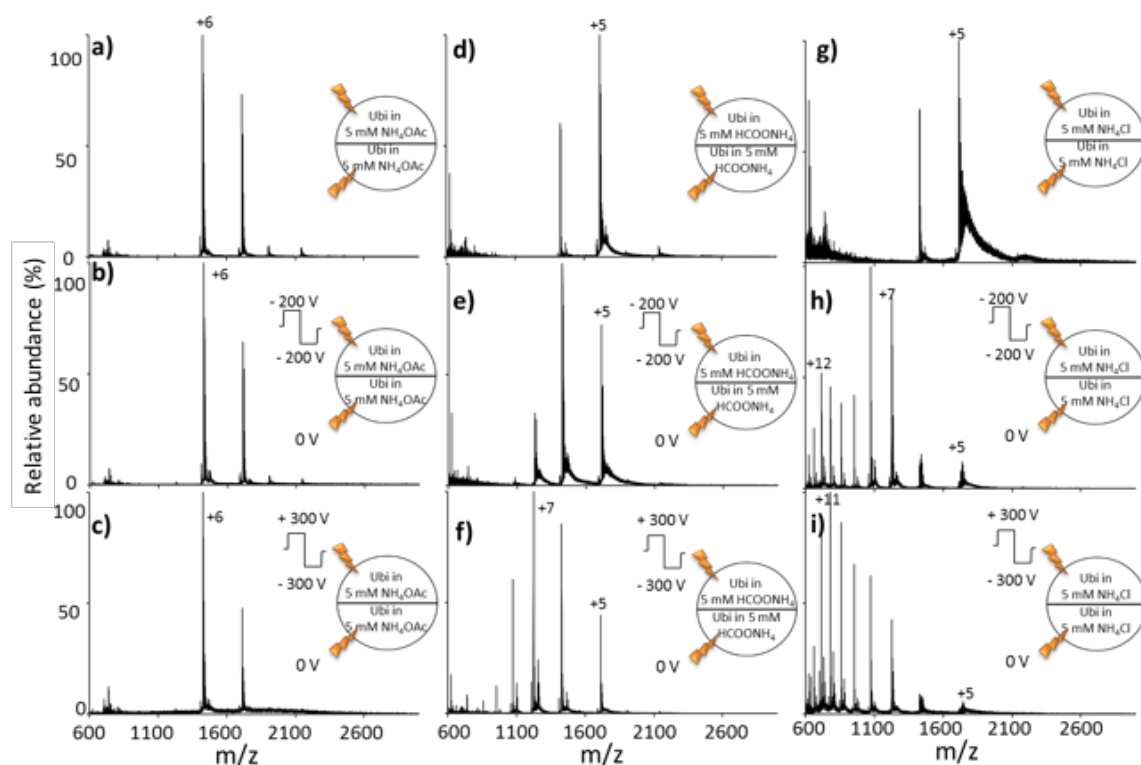
Figure 3. 8. Electroosmosis of ubiquitin in 5 mM of different salt solution for 100 ms. (a)-(c) show ubiquitin in 5 mM NH4OAc solution when applied (a) 0 V; (b) +/-200 V; (c) +/- 300 V square wave voltage for 100 ms. (d)-(f) show ubiquitin in 5 mM HCOONH4 solution when applied (d) 0 V; (e) +/-200 V; (f) +/- 300 V square wave voltage for 100 ms. (g)-(i) show ubiquitin in 5 mM NH4Cl solution when applied (g) 0 V; (h) +/-200 V; (i) +/- 300 V square wave voltage for 100 ms. The circles at the right of the spectra indicate the theta tip schematic; an aliquot of the same sample was loaded in each channel, and the lightning bolts depict the voltage applied to each side.
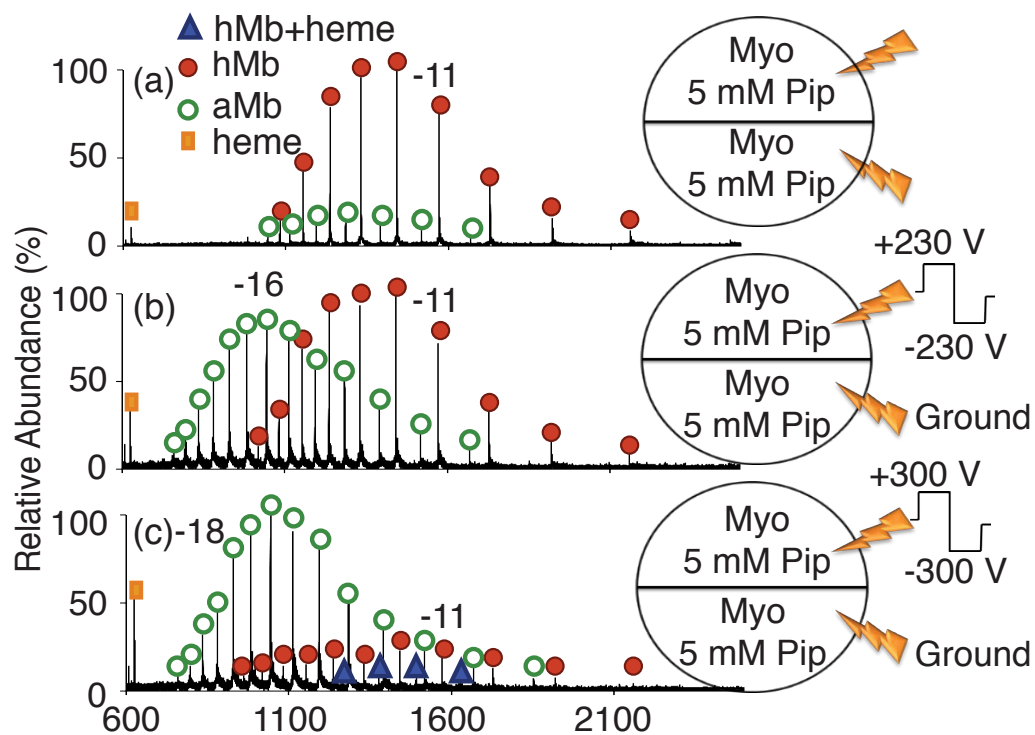
Figure 3. 9. -nESI analysis of protein thermal denaturation during theta tip electroosmosis. Electroosmosis of myoglobin in 5 mM piperidine for 100 ms under (a) 0 V; (b) 230 V; (c) 300 V. The circles at the right of the spectra indicate the theta tip schematic; an aliquot of the same sample was loaded in each channel, and the lightning bolts depict the voltage applied to each side
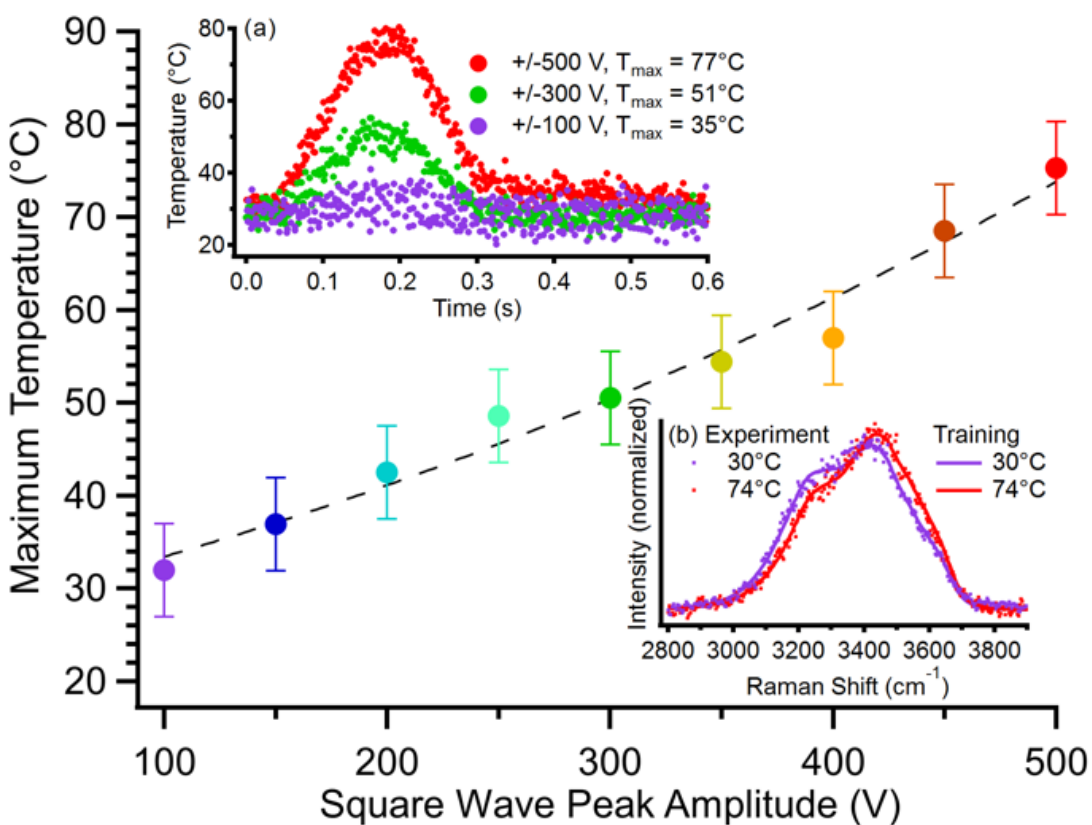
Figure 3. 10. Raman thermometry measurements of 5 mM NH$_4$OAc solution in a theta tip. Maximum temperature reached during the electroosmosis step is plotted with respect to the applied square wave peak amplitude. The dotted black line included to guide the eye is a quadratic fit to the data points. Insert (a) shows the temperature profile during the electroosmosis-spray-MS detection process with +/-100 V (violet), +/-300 V (green) and +/-500 V (red). Insert (b) shows representative training spectra (lines) for two temperature values and shows experimental spectra taken during electroosmosis (dots) to illustrate the sensitivity of the Raman measurements to temperature
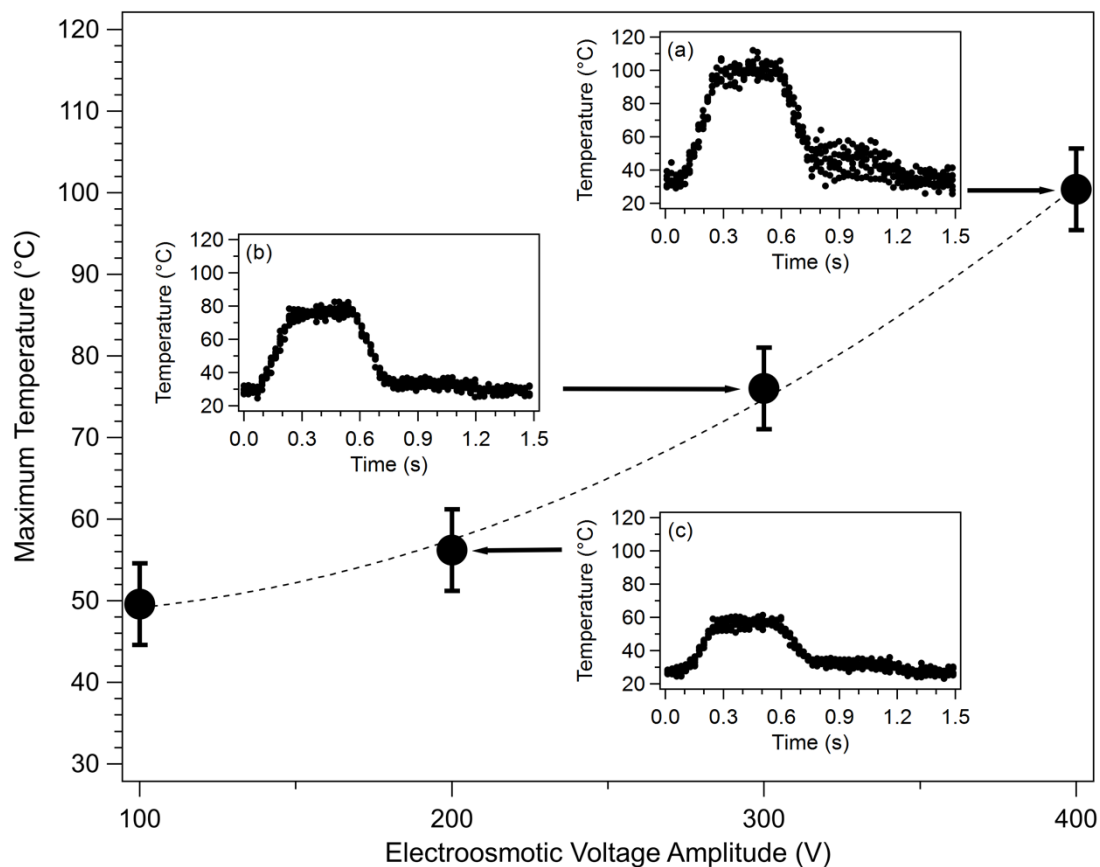
Figure 3. 11. Raman thermometry measurements of 5 mM NH₄OAc solution in a theta tip with 10 Hz electroosmosis step 500 ms. Maximum temperature reached during the electroosmosis step is plotted with respect to the applied square wave peak amplitude. The dotted black line included to guide the eye is a quadratic fit to the data points. Inserts show the temperature profile during the electroosmosis-spray-MS detection process with (a) +/-400 V, (b) +/-300 V and (c) +/-500 V.
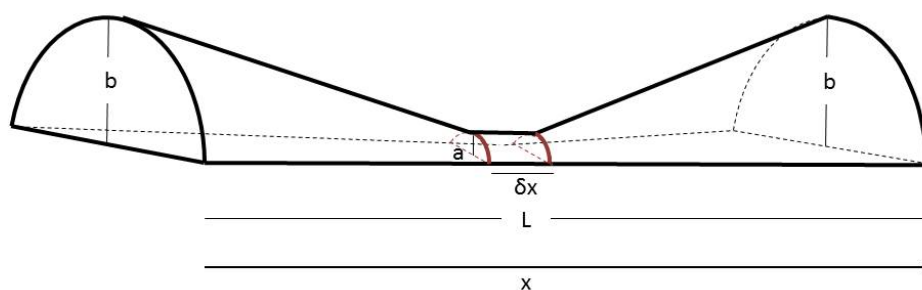
Figure 3. 12. Schematic illustration of theta tip model used for Joule heat calculation.
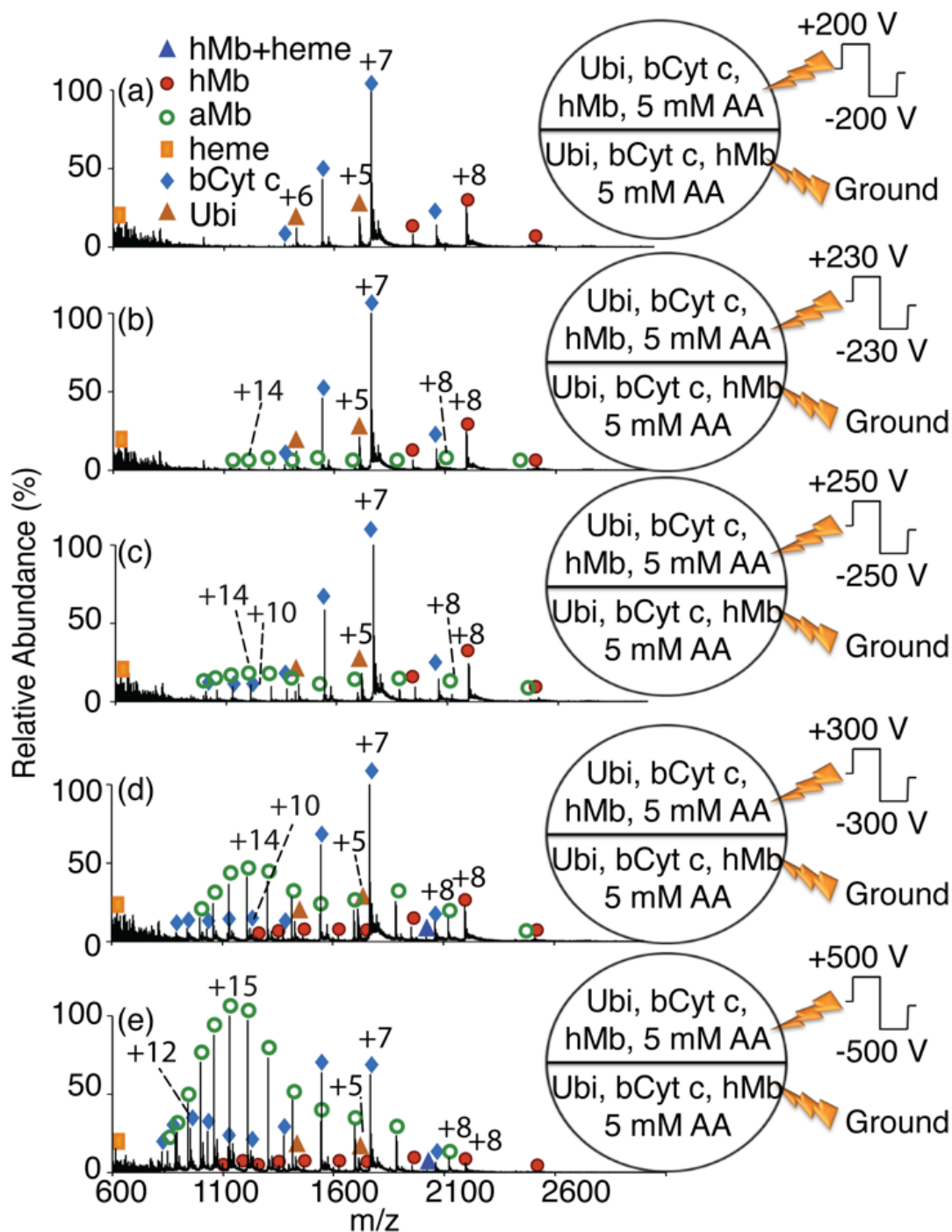
Figure 3. 13. Electroosmosis of a solution mixture of ubiquitin, bCyt *c* and myoglobin in 5 mM NH₄OAc solution in a theta tip at (a) +/- 200 V; (b) +/- 230 V; (c) +/-250 V; (d) +/-300 V and (e) +/-500 V. The circles at the right of the spectra indicate the theta tip schematic; an aliquot of the same sample was loaded in each channel, and the lightning bolts depict the voltage applied to each side

CHAPTER 4. PROTEIN MELTING TEMPERATURE MEASUREMENT USING THETA TIP JOULE HEATING EFFECT AND MASS SPECTROMETRY

4.1 Introduction

Protein thermal denaturation is an important biotransformation, which directly influences protein bioactivity. [1, 2] Protein thermal stability attracts a lot of attention in various biological fields including food science and pharmaceutical science. [2-5] The initial protein thermal denaturation at lower temperature are normally reversible, which involves a partially unfolding of the tertiary structure. [4., 6] In this stage, protein unfolding is easily analyzed. Upon higher temperature treatment of protein for longer time period, protein is further unfolded and intermolecular interaction increases. The intermolecular interactions including covalent reactions like disulfide bond formation and non-covalent interactions like hydrophobic interaction, hydrogen bonding etc.. These interactions could cause protein aggregation, and quickly leads to an irreversible end for the thermal denaturation. [3, 7, 8]

There are various techniques to investigate protein thermal denaturation. [2, 3] A direct analysis is based on microscopy, which is to measure the global change of chemical from solid to liquid. [9] In the case of solution phase protein melting, it measures the aggregation of unfolded proteins. [10] These methods require a macroscale of protein state change and don't probe detailed structural transformations. Therefore, the sensitivity is low and the initial unfolding processes can hardly be investigated. The results analysis can also be subjective. Chromatographic methods like reverse phase HPLC are able to distinguish unfolded and folded protein without the requirement of aggregation, but these methods are slow and is suitable for stead state analysis. [11] Differential Scanning Calorimetry (DSC) is a widely used method to measure protein melting temperature,

which measures the enthalpy change or protein heat capacity change during protein thermal denaturation. [12-14] To get a good conformational transition signal, protein sample concentration is relatively high and protein aggregation or fragmentation could occur. Furthermore, for DSC measurement, not a lot of detailed structural information can be extracted besides energy change. Optical methods provide an alternative analytical tool to monitor solution phase protein melting. UV-Vis and fluorescence analysis measures the absorption of fluorophore in protein during denaturation, which could report the globular conformation change. [2, 15, 16] However, these methods highly rely on the fluorophore amount and position. Another widely used optical analysis of protein thermal stability is circular dichroism spectroscopy (CD). [17, 18] CD monitors the absorption of the polarized light by an ordered secondary structure, like alpha helices and beta sheets. This measurement is very sensitive, so CD is widely applied to measure protein melting temperature in solution. However, CD is not appropriate for tertiary structure measurement.

Mass spectrometry is a widely used tool to study biomolecule structure, taking advantage of its high sensitivity and accuracy. [19, 23] Electrospray ionization mass spectrometry (ESI-MS) or nanoESI-MS is especially appropriate for protein conformational study, since it's a soft ionization method and protein charging extent is directly related to protein conformation. [24-27] It is normally accepted that high charge states correspond to more unfolded structure and low charge states correspond to more folded conformation. [28-30] With this property, ESI-MS has been applied to investigate protein folding and unfolding, including thermal denaturation. In most of the protein thermal denaturation study, protein is either denatured off-line in bulk solution before analysis, or denatured online slowly by heating the bulk solution in a heating block. [31, 32] In these cases, short-lived folding intermediates can also be missed and slow heating may still cause aggregation and fragmentation, although the low sample concentration may help reduce

aggregation chances.

The recent development of dual-channel theta tips provided a fast online protein manipulation method. [33] It can perform microseconds time scale reactions in the Taylor cone and droplets and also milliseconds or longer reactions inside of the tip by inducing in-tip electroosmosis. [34-42] Recently, Joule heating effect in theta tip electroosmosis has been reported and the Joule heating is significant enough to boil the aqueous solution and thermally denature proteins. [43] The theta tip thermal denaturation of protein allows a fast online manipulation of protein unfolding process and the results could be immediately and sensitively analyzed by mass spectrometry. Since the heating time is limited to milliseconds and the unfolded protein is directly sprayed into the mass spectrometer for analysis, protein aggregation, fragmentation and refolding are significantly eliminated. The fast heating also allows the MS method to capture short-lived protein unfolding intermediates, so that MS method is sensitive to multiple stage melting. Besides, since mass spectrometry measures ion mass, it is very sensitive to ligand loss, which is an indicator for protein denaturation and conformation change. Therefore, combination of theta tip Joule heating effect and mass spectrometry may provide a new way to characterize protein thermal unfolding.

4.2   Experimental

4.2.1   Reagent

Myoglobin from equine skeletal muscle, cytochrome *c* from equine heart, carbonic anhydrase II from bovine erythrocytes and ammonium formate were purchased from Sigma Aldrich (St. Louis, MO). HPLC grade water was purchased from Fisher Scientific (Fair Lawn, NJ). Protein stock solutions were desalted and purified by PD midiTrap G-25 columns from GE Healthcare Bio-Sciences (Pittsburgh, PA). After desalting, the protein solutions were diluted and mixed with

ammonium formate buffer to a final protein concentration of 2-5 μM and buffer concentration of 5 mM.

4.2.2 Capillaries and tip holders

One channel borosilicate theta glass capillaries (O.D./I.D. 1.5 mm/0.86 mm I.D., overall length 10 cm) and dual channel borosilicate theta glass capillaries (O.D./I.D. 1.5 mm/1.17 mm I.D., septum thickness 0.165 mm, overall length 10 cm) were purchased from Sutter Instrument Co. (Novato, CA). One channel capillaries were pulled to one channel normal tips (O.D. 3-5 μm) and dual channel theta capillaries were pulled to theta tips (O.D. 13 μm) using a Flaming/Brown micropipette puller (P-87) from Sutter Instrument Co. (Novato, CA).

Tip holders were purchased from Warner Instruments, LLC (Hamden, CT). Platinum wires were used as electrodes to apply voltages to sample solutions. The platinum wires used in theta tips were purchased as Teflon coated, so they are electrically isolated from each other and voltages can be applied to each wire independently.

4.2.3 Mass spectrometry

All mass spectrometry measurements were performed on a Sciex 5600 TripleTOF tandem mass spectrometer (Concord, ON, Canada). The electroosmosis setup is the same as that used in a previous publication. [43] Briefly, the thermal denaturation analysis consists of four steps: electroosmosis, ionization, dump spray and mass analysis. Electroosmosis step is the Joule heating generation step and protein is thermally denatured in tip prior to ionization and spray. In the electroosmosis step, one channel was grounded and the other channel was applied a square wave (10 Hz, 100 ms, 50% duty cycle). In the ionization step the heated protein analytes were ionized and sprayed into vacuum. An ionization voltage of 1.8-2.0 kV was applied to both channels simultaneously so that heated protein ions were sprayed out, transferred and trapped in Q2

quadrupole for cooling. In the dump spray step, residual heated protein ions were further sprayed out and any residual heated proteins were cleaned up from the tip. The ion path voltages were set so that no ions from dump spray step were transferred to Q2. In the end, the ions trapped in Q2 were transferred to TOF analyzer for analysis.

4.2.4   Heating tape thermal denaturation of proteins

Protein mixture solution was loaded in a one channel nESI tip and the tip was wrapped by a 64 W wraparound heating cord (OMEGA Engineering, Inc., Norwalk, CT). The heating voltage was adjusted to 60 V by a variac. The heated solution was continuously sprayed into MS for protein conformation analysis.

4.2.5   Circular dichroism (CD)

The CD measurement was performed on J-1500 circular dichroism spectrometer (Jasco, Easton, MD). Myoglobin, cytochrome *c* and carbonic anhydrase were diluted in 5 mM ammonium formate solution to a final concentration of 25 μM, 25 μM and 10 μM separately. The thermal stability measurement was performed in a standard rectangular spectrophotometer cell with stopper, and the path length is 2 mm. (Starna cells, Inc. Atascadero, CA) The temperature scanning range is 45-95 ^{o}C with the heating rate of 50 ^{o}C/h. Alpha helix absorption is measured at 222 nm and 209 nm.

4.2.6   Calculation of conformation contribution

Peak area of each protein charge state was calculated and correlation between peak area and charge state was established. The peak area-charge state correlation at each electroosmosis voltage was fitted with Gaussian function using the MatLab code published on http://terpconnect.umd.edu/~toh/spectrum/InteractivePeakFitter.htm#ipf_instructions   Each

conformation was isolated by Gaussian fitting. The fitting with the minimum error was used as the best fit. The area under each Gaussian curve was calculated and the percentage of each area in the total area was considered as the contribution of each conformation.

4.2.7 Determination of melting transition voltage

Correlation between conformation contribution and voltage was established. The most unfolded conformation was used as an indicator of protein unfolding extent, which was fitted using sigmoidal function. The sigmoidal fitting was performed using MatLab code published on http://terpconnect.umd.edu/~toh/spectrum/InteractivePeakFitter.htm#ipf_instructions   The midpoint of the sigmoidal curve is considered as the transition point, and the corresponding voltage is identified as the transition voltage.

4.3   Results

4.3.1   Measurement of the melting voltage for individual protein using theta tip Joule heating effect

To establish melting voltage determination method using theta tip Joule heating effect in combination with mass spectrometry, we started with a simple situation, which is individual protein denaturation. Three model proteins cytochrome *c*, myoglobin and carbonic anhydrase were selected as model proteins to establish and evaluate the protein transition voltage determination method.

4.3.1.1   Cytochrome *c* melting voltage identification

Cytochrome *c* is a relatively thermal stable protein. The initial thermal denaturation stage is reversible, when native compact conformation slightly unfolds and forms a molten globule state. Further heating of cytochrome *c* will unfold the protein to random coil which may aggregate and lead to an irreversible denaturation end. [44] Most thermal stability studies are based on thermal

equalization, like DSC and CD. The slow heating method is able to successfully measure the protein initial unfolding, but the high temperature unfolding information is normally lost due to quick aggregation. Theta tip electroosmosis could induce a significant Joule heating effect, which could *in situ* heat up the solution and thermally denature proteins. The resulted denatured protein is immediately sprayed into mass spectrometry for analysis. [43] Since the heating time is short and protein concentration for MS analysis is low, theta tip thermal denaturation method may preserve the high temperature unfolded conformation before aggregation.

To perform theta tip thermal denaturation of cytochrome *c*, 5 mM ammonium formate (AF) was added to the solution to increase ionic strength and facilitate Joule heating generation. Without running any electroosmosis, cytochrome *c* was preserved as native conformation in 5 mM ammonium formate (AF) with a low charge state distribution centered in +7. (Figure 4. 1 (a)) When 200V square wave was applied to induce electroosmosis, the solution was slightly heated and some higher charge state peaks showed up, indicating of protein slight melting. (Figure 4. 1 (b)) With the voltage further increases, the contribution from the high charge states keped increasing until solution boiled at 400 V. (Figure 4. 1 (c-f)) At each voltage, the charge state distribution was fitted using Gaussian function and a three state model was applied to get the lowest fitting error. The fitted three conformations should be corresponding to the native state, molten globule and denatured state. The conformation contribution of each state was calculated and plotted over the voltages. (Figure 4. 2)

$$\text{Conformation contribution} = \frac{\text{Gaussian area of each conformation}}{\text{Total area of all conformations}}$$

The results showed that with electroosmosis voltage increasing, the native conformation contribution kept decreasing and the unfolded conformation kept increasing, indicating protein denaturation. The intermediate state amount was relatively stable, which indicated that the rate to

form the intermediates and intermediate consumption were relatively the same and the intermediate amounts reached equilibrium. The generation of unfolded conformation was used as a direct indicator of protein denaturation, so the correlation between unfolded conformation contribution and electroosmosis voltages was fitted into a sigmoidal curve. The midpoint was determined at 328 V, which was considered as the melting voltage.

4.3.1.2 Myoglobin melting voltage identification

Myoglobin is a globular protein, which is full of α-helix structures. Native myoglobin has a heme ligand in it, which is called holo-myoglobin. Myoglobin thermal denaturation undergoes a sequential unfolding steps involving the loosen of the globular structure, loss of ligand and stepwise extension of α-helices. [45] In most myoglobin thermal denaturation studies, the unfolding intermediates will interact with each other and form aggregates before full denaturation. [45-47] The aggregation phenomenon put a strong challenge in the study of protein thermal unfolding process from native to full denaturation. Here we use theta tip Joule heating effect in combination of mass spectrometry to investigate myoglobin thermal unfolding process, and expect to reduce or avoid protein aggregation.

Myoglobin was dissolved in 5 mM ammonium formate buffer, in which myoglobin maintained its native holo-myoglobin conformation. (Figure 4. 3 (a)) When a 220 V square wave voltage was applied to induce in-tip electroosmosis, myoglobin was slightly denatured, losing heme ligand and generating some apo-myoglobin. (Figure 4. 3 (b)) Further increasing the square wave voltage to 240 V resulted in a higher extent of myoglobin denaturation. (Figure 4. 3 (c)) Holo-myoglobin was further extended and also more apo-myoglobin was generated. Under this condition, there was a coexistence of four conformations: folded holo-myoglobin, unfolded holo-myoglobin, folded apo-myoglobin and unfolded apo-myoglobin. Along with the increase of

electroosmosis voltages, the protein unfolding process continued. By 400 V electroosmosis, the majority of myoglobin in solution was fully denatured, and the major CSDs is high charge state unfolded apo-myoglobin peaks. (Figure 4. 3 (d-f))

The charge state distribution of Joule heating denatured myoglobin spectra were fitted with Gaussian function using a four-state model to isolate each conformation and determine their amount. As shown in Figure 4. 4, with higher electroosmosis voltage, native conformation kept decreasing while the apo-myoglobin quickly increased. Unfolded holo-myoglobin as an unstable intermediate does not have a high contribution throughout the denaturation process. Sigmoidal fitting was performed on the most unfolded conformation, which is unfolded apo-myoglobin, and the midpoint was determined to be 255 V.

4.3.1.3   Carbonic anhydrase melting voltage identification

The same operation was performed on carbonic anhydrase. Carbonic anhydrase also has a noncovalently bound ligand, which is zinc. Upon denaturation, holo-carbonic anhydrase unfolds, followed by losing zinc ligand and form apo-carbonic anhydrase. In 5 mM ammonium formate, carbonic anhydrase could retain the zinc ligand, but the compact structure was slightly opened, showing a slightly bimodal charge state distribution. (Figure 4. 5 (a)) Upon Joule heating using 100 V square wave for 100 ms, holo-carbonic anhydrase conformation was further extended and a new high charge state distribution was observed, centered in +19. (Figure 4. 5 (b)) Slightly increasing the electroosmosis voltage from 100 V to 150 V, both folded and unfolded holo-carbonic anhydrase quickly lost zinc ligand and formed folded and unfolded apo-carbonic anhydrase. (Figure 4. 5 (c)) When the voltage kept increasing, the carbonic anhydrase denaturation extent further increased. At 300 V, all holo-protein lost the zinc ligand and formed apo-carbonic anhydrase. (Figure 4. 5 (d-f)) Gaussian fitting was performed in each charge state distribution and

identified five folding conformations, including folded holo-, intermediate holo-, unfolded holo-, folded apo-, unfolded apo- protein. Based on the final five state model Gaussian fitting results shown in Figure 4. 6, the most dramatic change is the decreasing of native protein and increasing of unfolded apo-carbonic anhydrase. The intermediate states are generally in a relatively stable concentration. Therefore, to determine the denaturation voltage, sigmoidal fitting was performed on the unfolded apo-carbonic anhydrase conformation and the midpoint was determined as 278 V.

In summary, using theta tip Joule heating effect, all three model proteins were successfully thermally denatured and stepwise unfolding was observed upon voltage increasing. No apparent protein aggregation occurred, so protein full denaturation process was monitored. Under this condition, by Gaussian fitting of protein charge state distribution, protein conformations were successfully isolated and conformation contribution was determined based on Gaussian area. The generation of the most unfolded conformation was used as an indicator for protein denaturation extent. Through sigmoidal fitting of the most unfolded conformation and finding the midpoint of the sigmoidal curve, protein melting voltages were successfully identified.

4.3.2   Measurement of protein melting voltage in a mixture

The individual protein melting voltage determination demonstrated the feasibility of the melting temperature measurement using theta tip Joule heating and mass spectrometry. A next requirement for the method development is to improve accuracy and reproducibility. Joule heating effect in theta tip electroosmosis can be affected by various factors, including voltage, time and also tip size, tip shape. The amount of Joule heat generated could directly influence the extent of protein denaturation, and thereby influence the absolute melting temperature measurement reproducibility. To eliminate the influence from all these parameters, temperature need to be

calibrated using internal standards. Therefore, protein mixture denaturation in theta tips were performed.

When myoglobin, carbonic anhydrase and cytochrome *c* were mixed in 5 mM ammonium formate and heated up by Joule heating, all the three proteins gradually unfolded. (Figure 4. 7) The protein behavior in a mixture was very similar to that in an individual solution. Using Gaussian fitting method, conformations of each protein could be isolated easily. The conformation contribution of the most unfolded conformation of each protein in the mixture was calculated and summarized in Figure 4. 8. Using the same method as used in individual protein melting voltage determination, sigmoidal fitting was performed for the most unfolded conformation of each protein. The denaturation voltage for carbonic anhydrase, myoglobin and cytochrome *c* were determined as 245 V, 235 V and 315 V separately. Therefore, protein mixture denaturation was successful in theta tips using Joule heating and absolute denaturation voltage can be determined. The electroosmosis voltage is positively correlated with solution temperature, [43] so in the future study, a theoretical temperature-voltage curve need to be established. Using two of the proteins as internal standard to calibrate the curve, the melting temperature of the third protein should be determined.

4.3.3   Measurement of protein melting temperature using CD

To evaluate the theta tip Joule heating based melting temperature measurement method, the results were compared with currently established melting temperature measurement method using CD. Here, the melting temperature of the three model protein carbonic anhydrase, myoglobin and cytochrome *c* were measured using CD. Since all of the three proteins are rich in alpha helix, 222 nm absorption is monitored and the melting temperature for carbonic anhydrase, myoglobin and

cytochrome c were identified as 63.2 $^{\circ}$C, 85.8 $^{\circ}$C and 82.8 $^{\circ}$C separately in 5 mM ammonium formate. (Figure 4. 11)

It was found that the melting trend measured by CD and theta tip Joule heating method for the three proteins are inconsistent. In the CD measurement, the order of the three protein melting temperature is carbonic anhydrase < cytochrome *c* < myoglobin; while using the theta tip-MS based method, the melting temperature trend is myoglobin < carbonic anhydrase < cytochrome *c*. A proposed explanation is that CD and theta tip-MS method measures different structural information, which gave different melting results. First, CD measures protein secondary structure while theta tip-MS method measures protein tertiary structure change including ligand loss. Therefore, their reported results could be different. Second, CD is a quantitative method, which measures the amount of alpha helix in the solution. However, after heating, a very apparent precipitation of cytochrome *c* and carbonic anhydrase were observed in the cuvettes. CD cannot distinguish the alpha helix loss from protein unfolding and protein aggregation, so the CD results are reporting a combined effect of unfolding and aggregation. However, for mass spectrometry, the heating time is very short and protein concentration is very low. Therefore, protein aggregation is minimized. The MS result reported the individual protein unfolding, without influence from intermolecular aggregation. Third, theta tip-MS method uses protein mixture denaturation, while CD measurement uses individual protein. Protein may interact with each other or transfer charges with each other in a mixture and result in a different melting temperature. CD is not able to study protein mixture behavior, since all alpha helix have the same absorption wavelength. Forth, during theta tip electroosmosis, other forces beyond Joule heating influenced protein denaturation.

4.3.4 Thermal denaturation of protein mixture using heating tape

To investigate if thermal effect is the major reason causing protein denaturation during electroosmosis, a control experiment is using heating tape to thermally denature protein mixture and use the same analyzer MS to analyze protein denaturation behavior. Using a heating block to denature protein in ESI capillary followed by MS analysis to study protein thermal denaturation has been investigated before. [32] Comparing to the theta tip Joule heating method, the heating block method has its weakness in the aspects of destroying the bulk solution in the emitter and thermal fragmentation during the slow heating process. However, the heating tape denaturation experiment could provide important supporting information for protein mixture thermal behavior monitored by MS, since the only unfolding force that proteins are exposed to is the thermal effect. Comparing the protein behavior during heating tape heating and theta tip electroosmosis could help elucidating protein denaturation reasons during theta tip electroosmosis.

When the protein mixture of carbonic anhydrase, myoglobin and cytochrome c were loaded in a nESI emitter and heated up to 4 min, no denaturation was observed and all three proteins maintained in the native conformation. (Figure 4. 9 (a)) The bulk solution was boiled by this time, but the temperature in the taper may be lower, which preserved the native conformation of proteins. When the solution was heated for 14-16 min, some apo-myoglobin and a small amount of carbonic anhydrase showed up, (Figure 4. 9 (b)) but the myoglobin and carbonic anhydrase peaks were quickly suppressed by the cytochrome c peaks. (Figure 4. 9 (c)) After heated for 16 min, the charge state distribution of cytochrome c was increased. The unfolding of cytochrome c may facilitate its chain ejection ionization mechanism and led to the signal suppression phenomenon. Further heating of the solution mixture for 18-20 min, cytochrome c charge states were shifted higher and the major two charge state distributions were centered in +9 and +16. (Figure 4. 9 (d)) The higher charge state peaks slowly grew when the heating time was elongated. (Figure 4. 9 (e)(f))

To look closely into the suppressed myoglobin and carbonic anhydrase peaks, the spectra were vertically zoomed in. (Figure 4. 9 (g-j)) Myoglobin almost completely lost the holo-conformation and became apo-myoglobin when heated for longer than 16 min. The apo-myoglobin charge state distribution was also broadened. (Figure 4. 9 (g)) 18-20 min of heating could significantly unfold apo-myoglobin and the charge state center was shifted to +20. (Figure 4. 9 (h)) Increasing the heating time generated a dominant high charge state distribution centered in +25. (Figure 4. 9 (i-j))

For carbonic anhydrase, the significant denaturation required a longer time than myoglobin, which was 18-20 min. (Figure 4. 9 (h)) By this time, carbonic anhydrase lost the zinc ligand and became highly charged apo-carbonic anhydrase. However, along with the unfolding, carbonic anhydrase thermal fragmentation was observed, which was labeled in Figure 4. 9 (h-j)

Using the same data analysis method as used in theta tip electroosmosis protein denaturation, protein conformations from heating tape denaturaiton were isolated using Gaussian fitting and the conformation contribution was calculated. The most unfolded conformation contribution of each protein was summarized in Figure 4. 10. The correlation showed that the protein denaturation is in the order of myoglobin, carbonic anhydrase and cytochrome *c*. This order is consistent with the transition voltage order when protein was denatured by theta tip electroosmosis. Since in heating tape experiment, the only factor inducing protein denaturation is thermal effect, the consistency in protein unfolding order between heating tape and electroosmosis induced denaturation supported that the electroosmosis induced protein unfolding is mainly due to Joule heating thermal effect.

4.4   Conclusions

Protein melting temperature measurement was performed using theta tip Joule heating effect and mass spectrometry. Individual protein melting voltage was identified by sigmoidal fitting of

the most unfolded conformation contribution at different voltage. The midpoint was identified as the melting voltage. To eliminate influences from various environmental factors including tip size, tip shape, tip-interface distance, heat dissipation etc., internal standard calibration method was introduced, which means a protein mixture of at least three need to be manipulated in a single theta tip. The results showed that protein mixture denaturation in a theta tip was successful. However, the trend for protein denaturation voltage measured by theta tip-MS methods and denaturation temperature measured by CD was different. Proposed explanations are that CD and MS are different read out methods, which report quantitative secondary structural change and tertiary structural change separately. Also, as a slow heating method using higher protein concentration, CD measurement cannot quite avoid protein aggregation, while in MS method protein aggregation can be significantly eliminated attributing to the short heating time and lower protein concentration. Another possibility is that there are other forces other than Joule heating is inducing protein denaturation during theta tip electroosmosis. Online thermal denaturation of proteins using heating tape combining MS readout showed consistent protein denaturation order, which provided some supporting information that protein denaturation in theta tip is mainly from thermal effect.

4.5   References

1. Singh, A. P.; Saxena, K. D. Effect of temperature, pH and denaturing agents on biological activity of MCJ lectin. Chem Sci Trans., 2013, 2, 1508-1512.

2. Sousa, F.; Sarmento, B.; Neves-Petersen, M. T. Biophysical study of bevacizumab structure and bioactivity under thermal and pH-stresses. Eur. J. Pharm. Sci. 2017, 105, 127-136.

3. Boye, J. I.; Ma, C. Y.; Harwalkar, V. R. Thermal denaturation and coagulation of proteins. In: Damodaran, S.; Paraf, A. (eds) Food Proteins and Their Applications. CRC Press: Marcel Dekker, Inc. 1997.

4. Mulvihill, D. M.; Donovan. M. Whey proteins and their thermal denaturation - A review. Irish J. Food Sci. Tech. 1987, 11, 43-75.

5. Wijayanti, H. B.; Bansal, N.; Deeth, H. C. Stability of whey proteins during thermal processing: A review. Compr. Rev. Food Sci. Food Saf. 2014, 13, 1235-1251.

6. Tanford, C. Protein denaturation. Adv. Protein Chem. 1968, 23, 121-282.

7. Yan, Y.; Wang, Q.; He, H.; Zhou, H. Protein thermal aggregation involves distinct regions: Sequential events in the heat-induced unfolding and aggregation of hemoglobin. Biophys. J. 2004, 86, 1682-1690.

8. Borzova, V. A.; Markossian, K. A.; Chebotareva, N. A.; Kleymenov, S. Y.; Poliansky, N. B.; Muranov, K. O.; Stein-Margolina, V. A.; Shubin, V. V.; Markov, D. I.; Kurganov, B. I. Kinetics of thermal denaturation and aggregation of bovine serum albumin. PLoS One. 2016, 11, e0153495.

9. Zscheile, F. P.; White Jr., J. W. Microscope hot stage for determination of melting points: Application to carotenoid pigments. Ind. Eng. Chem. Anal. Ed. 1940, 12, 436-438.

10. Harwalkar, V. R.; Kalab, M. Thermal denaturation and aggregation of β-lactoglobulin in solution. Electron microscopic study. Milchwissenschaft 1985, 40, 65-68.

11. Parris, N.; Purcell, J. M.; Ptashkin, S. M. Thermal denaturation of whey proteins in skim milk. J. Agric. Food Chem. 1991, 39, 2167-2170.

12. Durowoju, I. B.; Bhandal, K. S.; Hu, J.; Carpick, B.; Kirktadze, M. Differential scanning calorimetry - A method for assessing the thermal stability and conformation of protein antigen. J. Vis. Exp. 2017, 121, e55262.

13. Johnson, C. M. Differential scanning calorimetry as a tool for protein folding and stability. Arch. Biochem. Biophys. 2013, 531, 100-109.

14. Michnik, A. Thermal stability of bovine serum albumin DSC study. J. Therm. Anal. Cal. 2003, 71, 509-519.

15. Stros, M. Kleinwaichter, V. Thermal denaturation and fluorescence study of nucleosomes containing non-histone chromosomal protein HMG2. Biochim. Biophys. Acta 1987, 910 163-170.

16. Cimmperman, P.; Matulis, D. Protein thermal denaturation measurements via a fluorescent dye. In: Podjarny, A.; Dejaegere, A. P.; Kieffer, B. (eds) Biophysical Approaches Determining Ligand Binding to Biomolecular Targets: Detection, Measurement and Modelling. The Royal Society of Chemistry: Cambridge, UK, 2011.

17. Greenfield, N. J. Using circular dichroism collected as a function of temperature to determine the thermodynamics of protein unfolding and binding interactions. Nat. Protoc. 2006, 1, 2527-2535.

18. Ireland, S. M.; Sula, A.; Wallace, B. A. Thermal melt circular dichroism spectroscopic studies for identifying stabilizing amphipathic molecules for the voltage gated sodium channel NavMs. Biopolymers 2018,109, e23067.

19. Glish, G. L.; Vachet, R. W. The basics of mass spectrometry in the twenty first century. Nat. Rev. Drug Discov. 2003, 2, 140-150.

20. Roux, A.; Lison, D.; Junot, C.; Heilier, J. Applications of liquid chromatography coupled to mass spectrometry-based metabolomics in clinical chemistry and toxicology: A review. Clin. Biochem. 2011, 44, 119-135.

21. Bantscheff, M.; Schirle, M.; Sweetman, G.; Rich, J.; Kuster, B. Quantitative mass spectrometry in proteomics: A critical review. Anal. Bioanal. Chem. 2007, 389, 1017-1031.

22. Benson, S.; Lennard, C.; Maynard, P.; Roux, C. Forensic applications of isotope ratio mass spectrometry-A review. Forensic. Sci. Int. 157, 2006, 1-22.

23. Jackson, S. E.; Pearson, N. J.; Griffin, W. L.; Belousova, E. A. The application of laser ablation-inductively coupled plasma-mass spectrometry to in situ U-Pb zircon geochronology. Chem. Geol. 2004, 211, 47-69.

24. Fenn, J. B.; Mann, M.; Meng, C. K.; Wong, S. F.; Whitehouse, C. M. Electrospray ionization for mass spectrometry of large biomolecules. Science 1989, 246, 64-71.

25. Wilm, M.; Mann, M. Analytical properties of the nanoelectrospray ion source. Anal. Chem. 1996, 68, 1-8.

26. Pan, P.; Guawardena, H. P.; Xia, Y.; McLuckey, S. A. Nanoelectrospray ionization of protein mixtures: solution pH and protein pI. Anal. Chem. 2004, 76, 1165-1174.

27. Chen, S. Rapid protein identification using direct infusion nanoelectrospray ionization mass spectrometry. Proteomics 2006, 6, 16-25.

28. Kaltashov, I. A.; Eyles, S. J. Studies of biomolecular conformations and conformational dynamics by mass spectrometry. Mass Spectrom. Rev. 2002, 21, 37-71.

29. Fenn, J. B. Ion formation from charged droplets: Roles of geometry, energy, and time. J. Am. Soc. Mass Spectrom. 1993, 4, 524-535.

30. Loo, J. A.; Loo, R. R.; Udseth, H. R.; Edmonds, C. G.; Smith, R. D. Solvent-induced conformational changes of polypeptides probed by electrospray-ionization mass spectrometry. Rapid Commun. Mass Spectrom. 1991, 5, 101-105.

31. Le Blanc, J. C. Y.; Beuchemin, D.; Siu, K. W. M.; Guevremont, R.; Berman, S. S. Thermal denaturation of some proteins and its effect on their electrospray mass spectra. J. Mass Spectr.1991, 26, 831-839.

32. El-Baba, T. J.; Woodall, D. W.; Raab, S. A.; Fuller, D. R.; Laganowsky, A.; Russell, D. H.; Clemmer, D. E. Melting proteins: Evidence for multiple stable structures upon thermal denaturation of native ubiquitin from ion mobility spectrometry-mass spectrometry measurements. J. Am. Chem. Soc. 2017, 139, 6306-6309.

33. Mark, L. P.; Gill, M. C.; Mahut, M.; Derrick, P. J. Dual nano-electrospray for probing solution interactions and fast reactions of complex biomolecules. Eur. J. Mass Spectrom. 2012, 18, 439-446.

34. Fisher, C. M.; Kharlamova, A.; McLuckey, S. A. Affecting protein charge state distributions in nano-electrospray ionization via in-spray solution mixing using theta capillaries. Anal. Chem. 2014, 86, 4581-4588.

35. Mortensen, D. N.; Williams, E. R. Theta-glass capillaries in electrospray ionization: Rapid mixing and short droplet lifetimes. Anal. Chem. 2014, 86, 9315-9321.

36. Mortensen, D. N.; Williams, E. R. Investigating protein folding and unfolding in electrospray nanodrops upon rapid mixing using theta-glass emitters. Anal. Chem. 2015, 87, 1281-1287.

37. Mortensen, D. N.; Williams, E. R. Ultrafast (1 μs) mixing and fast protein folding in nanodrops monitored by mass spectrometry. J. Am. Chem. Soc. 2016, 138, 3453-3460.

38. Jansson, E. T.; Lai, Y.; Santiago, J. G.; Zare, R. N. Rapid hydrogen-deuterium exchange in liquid droplets. J. Am. Chem. Soc. 2017, 139, 685-6854.

39. Walker, K. L.; Dornan, L. M.; Zare, R. N.; Waymouth, R. M.; Muldoon, M. J. Mechanism of catalytic oxidation of styrenes with hydrogen peroxide in the presence of cationic palladium(II) complexes. J. Am. Chem. Soc. 2017, 139, 12495-12503.

40. Miller, C. F.; Kulyk, D. S.; Kim, J. W.; Badu-Tawiah, A. K. Re-configurable, multi-mode contained electrospray ionization for protein folding and unfolding on the millisecond time scale. Analyst 2017, 142, 2152-2160.

41. Liu, F.; Lu, W.; Yin, X.; Liu, J. Mechanistic and kinetic study of singlet O_2 oxidation of methionine by on-line electrospray ionization mass spectrometry. J. Am. Soc. Mass Spectrom. 2016, 27, 59-72.

42. Fisher C. M.; Hilger, R. T.; Zhao, F.; McLuckey, S. A. Electroosmotically driven solution mixing in borosilicate theta glass nESI emitters. J. Mass Spectrom. 2015, 50, 1063-1070.

43. Zhao, F.; Matt, S. M.; Bu, J.; Rehrauer, O. G.; Ben-Amotz, D.; McLuckey, S. A. Joule heating and thermal denaturation of proteins in nano-ESI theta tips. J. Am. Soc. Mass Spectrom. 2017, 28, 2001-2010.

44. Mehta, R.; Kundu, A.; Kishore, N. A mechanistic study on the thermal unfolding of cytochrome *c* in presence of 4-chlorobutan-1-ol: Differential scanning calorimetric and spectroscopic approach. Phys. Chem. Chem. Phys. 2003, 5, 5514-5522.

45. Yan, Y.; Wang, Q.; He, H.; Hu, X.; Zhang, R.; Zhou, H. Two-dimensional infrared correlation spectroscopy study of sequential events in the heat-induced unfolding and aggregation process of myoglobin. Biophys. J. 2003, 85, 1959-1967.

46. Fandrich, M.; Forge, V.; Buder, K.; Kittler, M.; Dobson, C. M.; Diekmann, S. Myoglobin forms amyloid fibrils by association of unfolded polypeptide segments. Proc. Natl. Acad. Sci. U.S.A. 2003, 100, 15463-15468.

47. Meersman, F.; Smeller, L.; Heremans, K. Comparative Fourier transform infrared spectroscopy study of cold-, pressure-, and heat-induced unfolding and aggregation of myoglobin. Biophys. J. 2002, 82, 2635-2644.
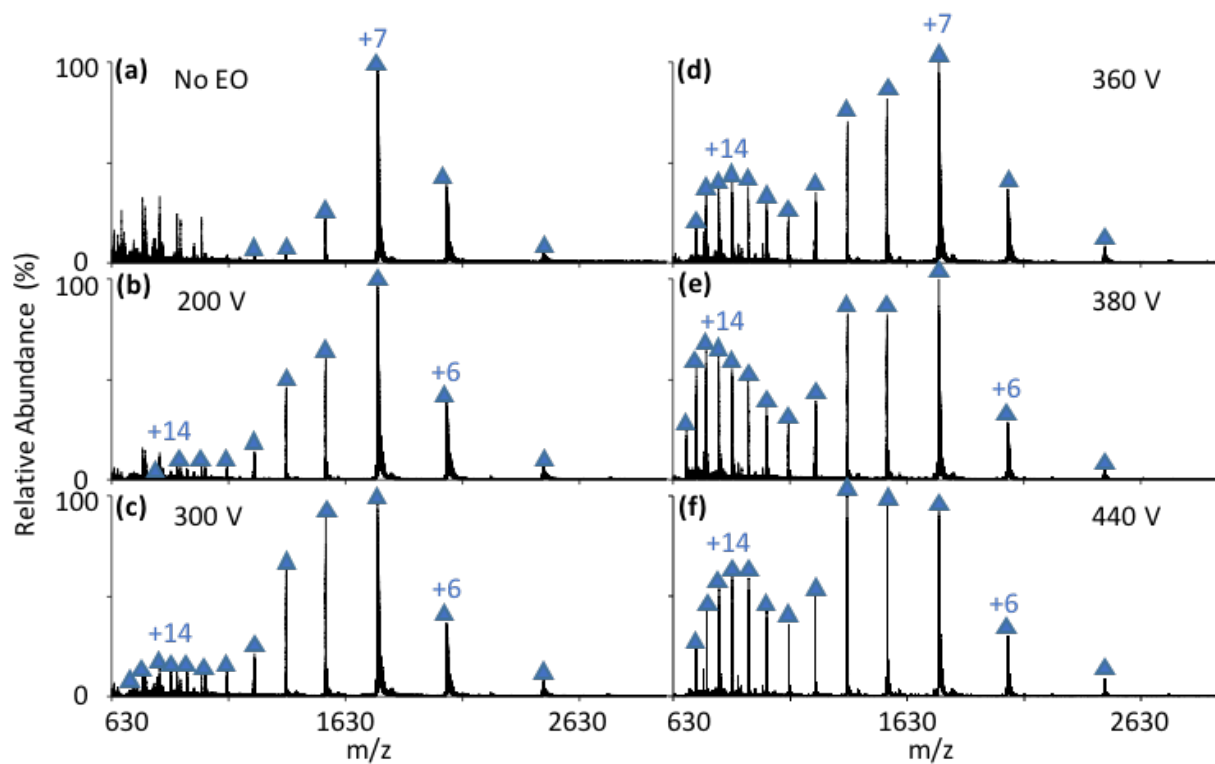
Figure 4. 1. Thermal denaturation of equine cytochrome *c* through theta tip Joule heating effect. (a) Control spectrum of cytochrome *c* in 5 mM ammonium formate sprayed from a theta tip without electroosmosis. Cytochrome *c* heated by theta tip Joule heating under a square wave of (b) 200 V; (c) 300 V; (d) 360 V; (e) 380 V; (f) 440 V. The blue triangles indicate cytochrome *c* peaks.
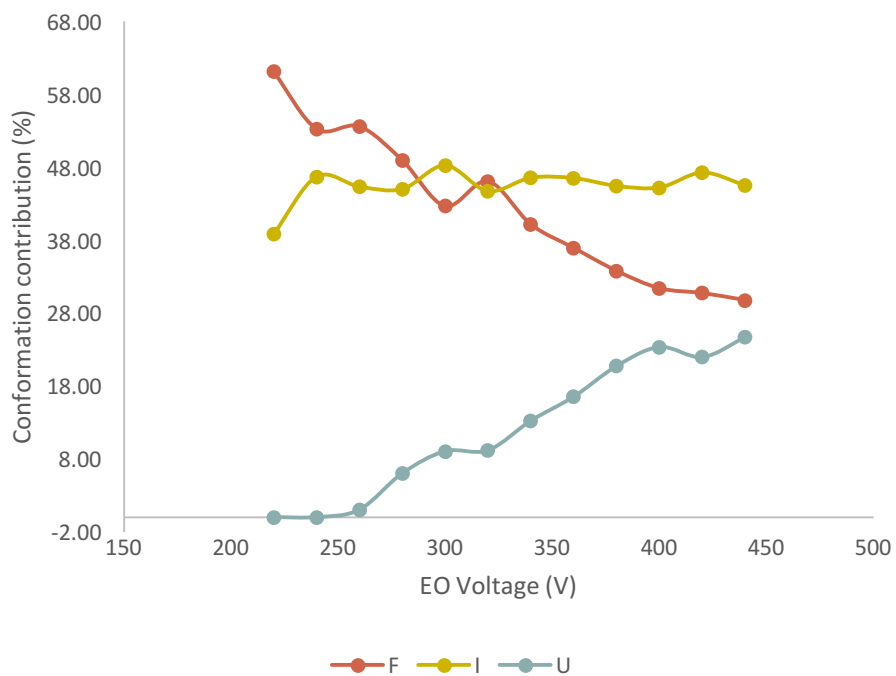
Figure 4. 2. Correlation of cytochrome *c* conformation contribution with electroosmosis voltage. The red line and dots indicate folded cytochrome *c*; the yellow line and dots indicate intermediate cytochrome *c*; the blue line and dots indicate unfolded cytochrome *c*.
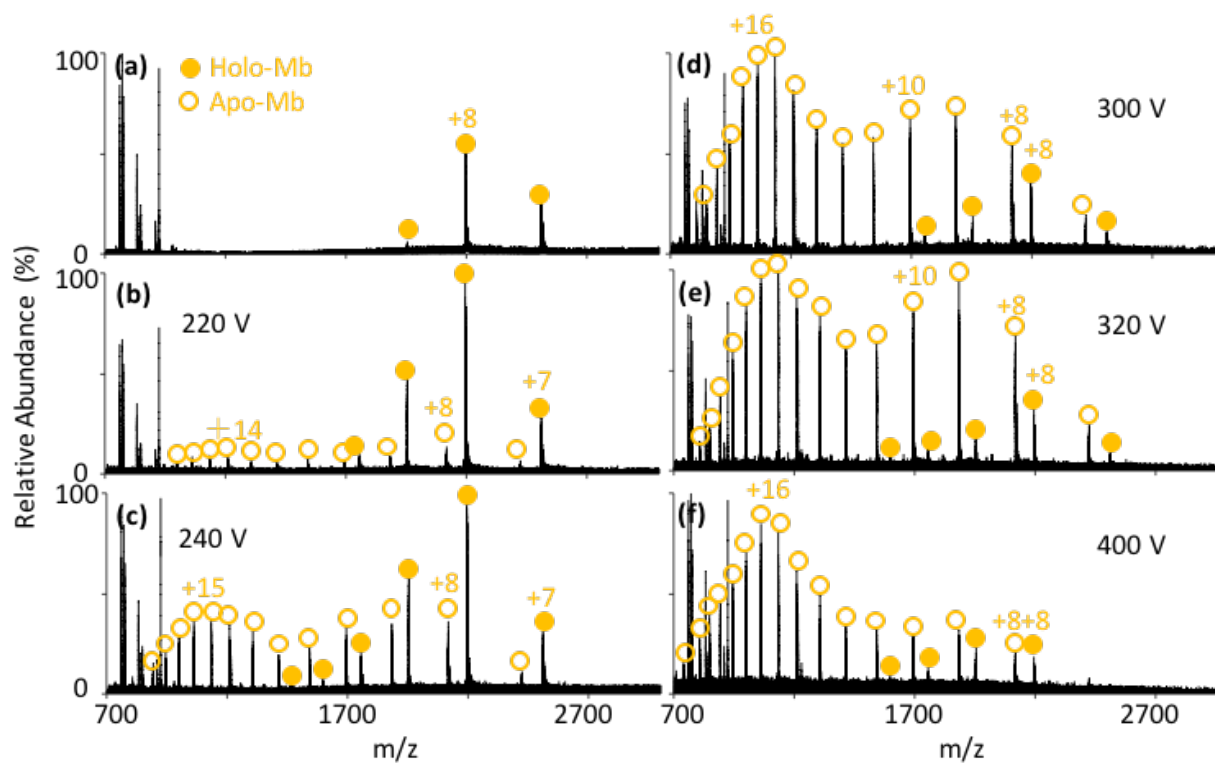
Figure 4. 3. Thermal denaturation of myoglobin through theta tip Joule heating effect. (a) Control spectrum of myoglobin in 5 mM ammonium formate sprayed from a theta tip without electroosmosis. Myoglobin heated by theta tip Joule heating under a square wave of (b) 200 V; (c) 300 V; (d) 360 V; (e) 380 V; (f) 440 V. The filled yellow dots indicate holo-myoglobin peaks. The hollow yellow circles indicate apo-myoglobin peaks.
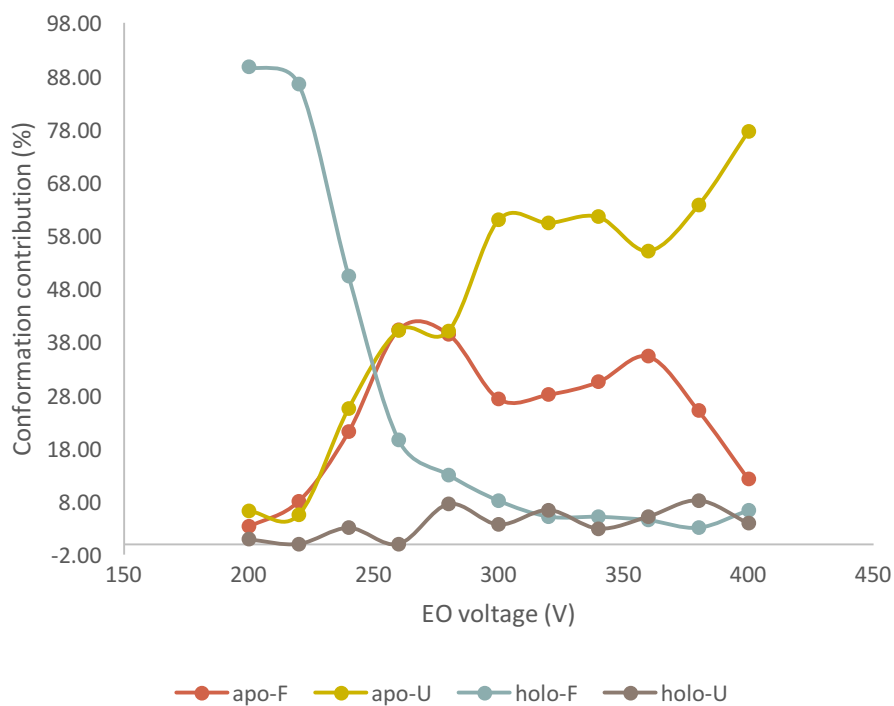
Figure 4. 4. Correlation of myoglobin conformation contribution with electroosmosis voltage. The red line and dots indicate folded apo-myoglobin; the yellow line and dots indicate unfolded apo-myoglobin; the blue line and dots indicate folded holo-myoglobin; the purple line and dots indicate unfolded holo-myoglobin.
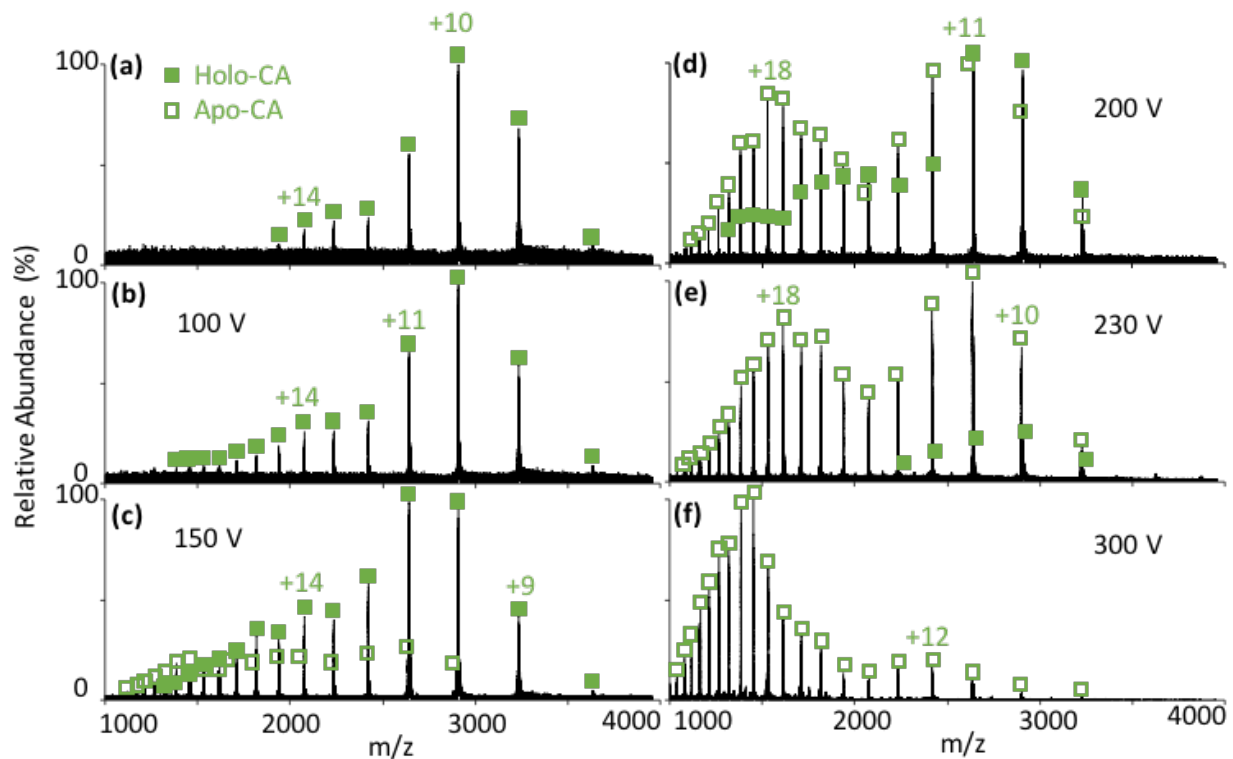
Figure 4. 5. Thermal denaturation of carbonic anhydrase through theta tip Joule heating effect. (a) Control spectrum of carbonic anhydrase in 5 mM ammonium formate sprayed from a theta tip without electroosmosis. Carbonic anhydrase heated by theta tip Joule heating under a square wave of (b) 200 V; (c) 300 V; (d) 360 V; (e) 380 V; (f) 440 V. The filled green squares indicate holo-carbonic anhydrase peaks. The hollow green square indicate apo-carbonic anhydrase peaks.
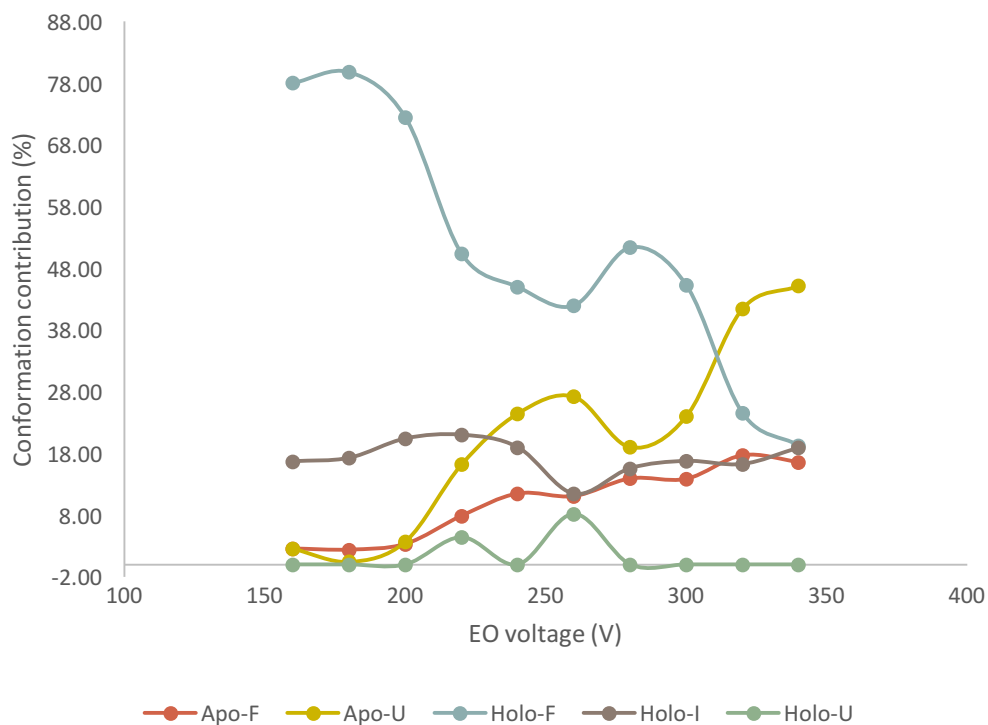
Figure 4. 6. Correlation of carbonic anhydrase conformation contribution with electroosmosis voltage. The red line and dots indicate folded apo-carbonic anhydrase; the yellow line and dots indicate unfolded apo-carbonic anhydrase; the blue line and dots indicate folded holo-carbonic anhydrase; the purple line and dots indicate intermediate holo-carbonic anhydrase; the green line and dots indicate unfolded holo-carbonic anhydrase.
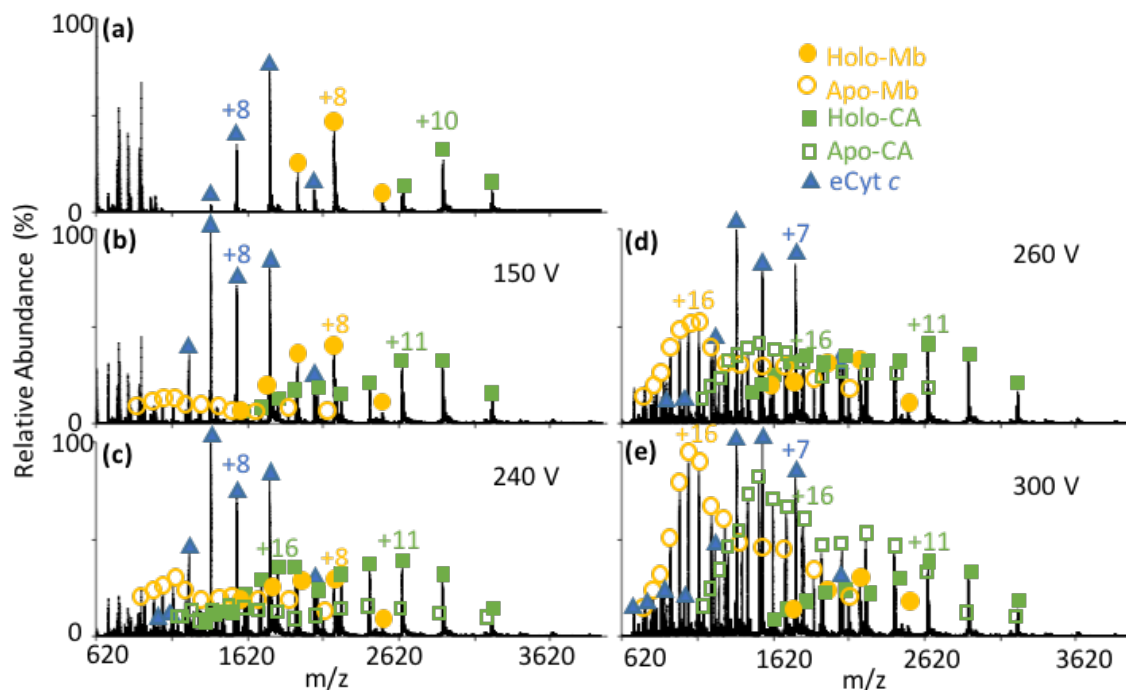
Figure 4. 7. Thermal denaturation of protein mixture of carbonic anhydrase, myoglobin and cytochrome *c* through theta tip Joule heating effect. (a) Control spectrum of protein mixture in 5 mM ammonium formate sprayed from a theta tip without electroosmosis. Protein mixture heated by theta tip Joule heating under a square wave of (b) 200 V; (c) 300 V; (d) 360 V; (e) 380 V; (f) 440 V. The filled green squares indicate holo-carbonic anhydrase peaks. The hollow green square indicate apo-carbonic anhydrase peaks. The filled yellow dots indicate holo-myoglobin peaks. The hollow yellow circles indicate apo-myoglobin peaks. The blue triangles indicate cytochrome *c*.
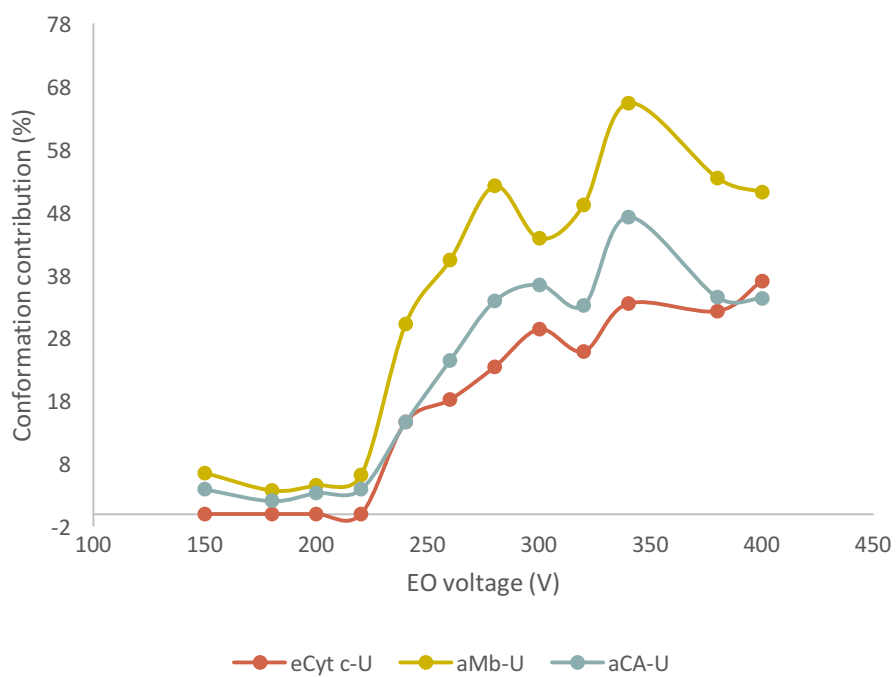
Figure 4. 8. Conformation contribution of the most unfolded conformation of each protein in a mixture corelates with electroosmosis voltage. The red line and dots indicate cytochrome *c*; the yellow line and dots indicate myoglobin; the blue line and dots indicate carbonic anhydrase.
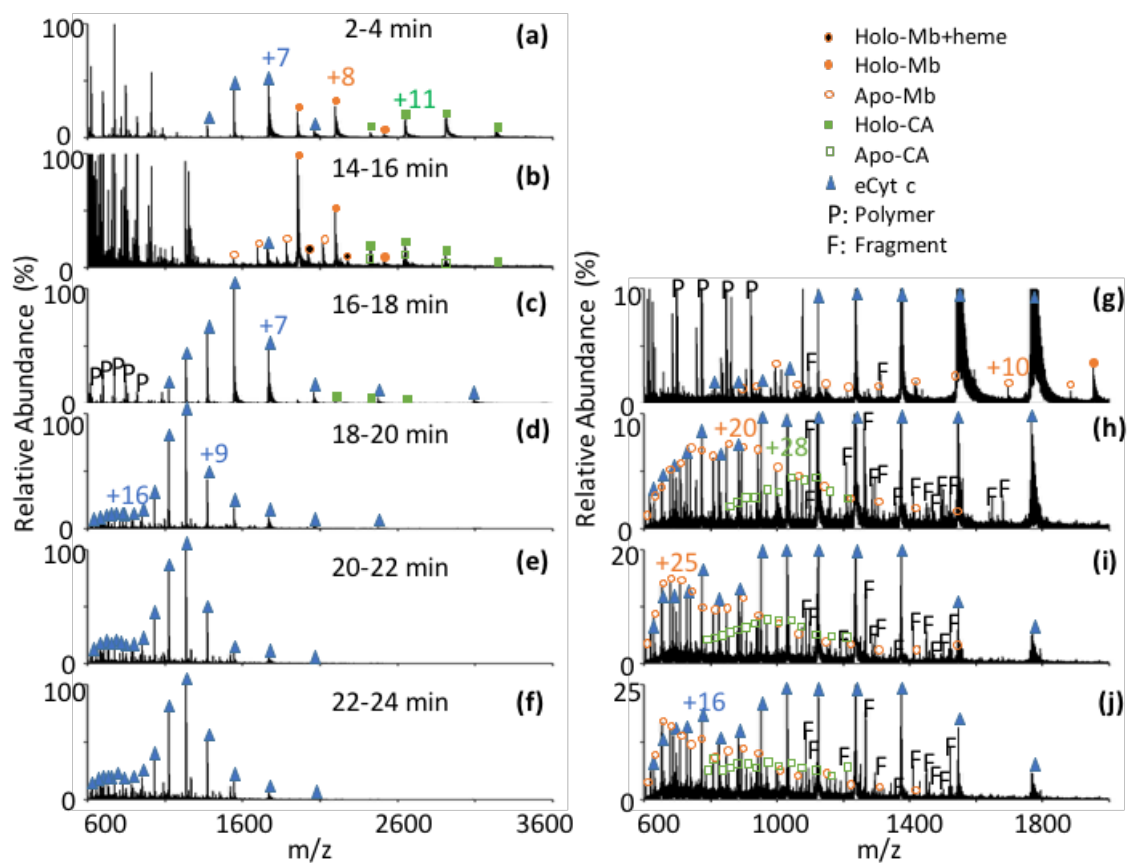
Figure 4. 9. Thermal denaturation of protein mixture of carbonic anhydrase, myoglobin and cytochrome *c in* 5 mM AF using heating tape. The figures show averaged spectra collected during heating time of (a) 2-4 min; (b) 14-16 min; (c) 16-18 min; (d) 18-20 min; (e) 20-22 min); (f) 22-24 min. The vertically zoomed spectra (c)-(f) were shown as figure (g)-(j). The filled green squares indicate holo-carbonic anhydrase peaks. The hollow green square indicate apo-carbonic anhydrase peaks. The filled yellow dots indicate holo-myoglobin peaks. The hollow yellow circles indicate apo-myoglobin peaks. The blue triangles indicate cytochrome *c*. The letter "P" indicates silicone polymer impurities; Letter "F" indicates protein fragments.
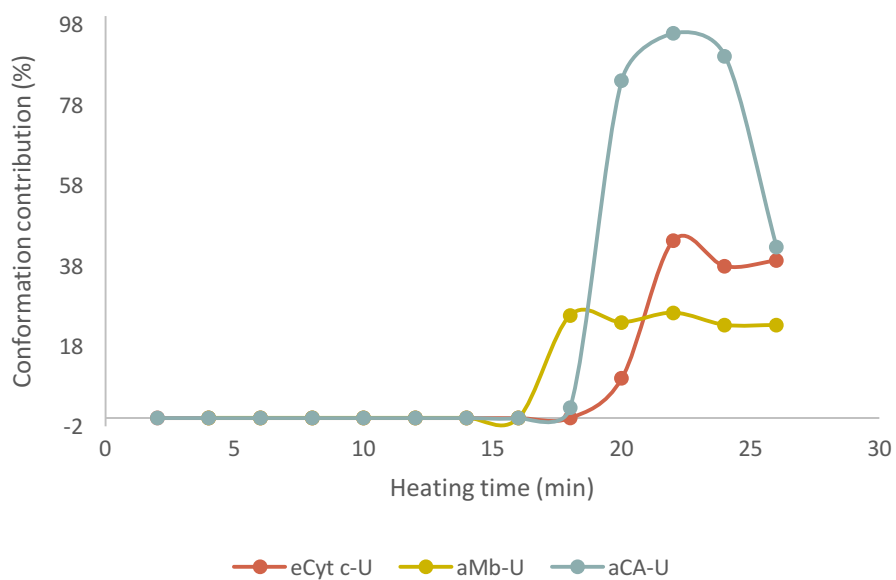
Figure 4. 10. Conformation contribution of the most unfolded conformation of each protein in a mixture corelates with heating time when the bulk solution was heated by heating tape. The red line and dots indicate the most unfolded conformation of cytochrome *c*; the yellow line and dots indicate the most unfolded conformation of myoglobin; the blue line and dots indicate the most unfolded conformation of carbonic anhydrase.
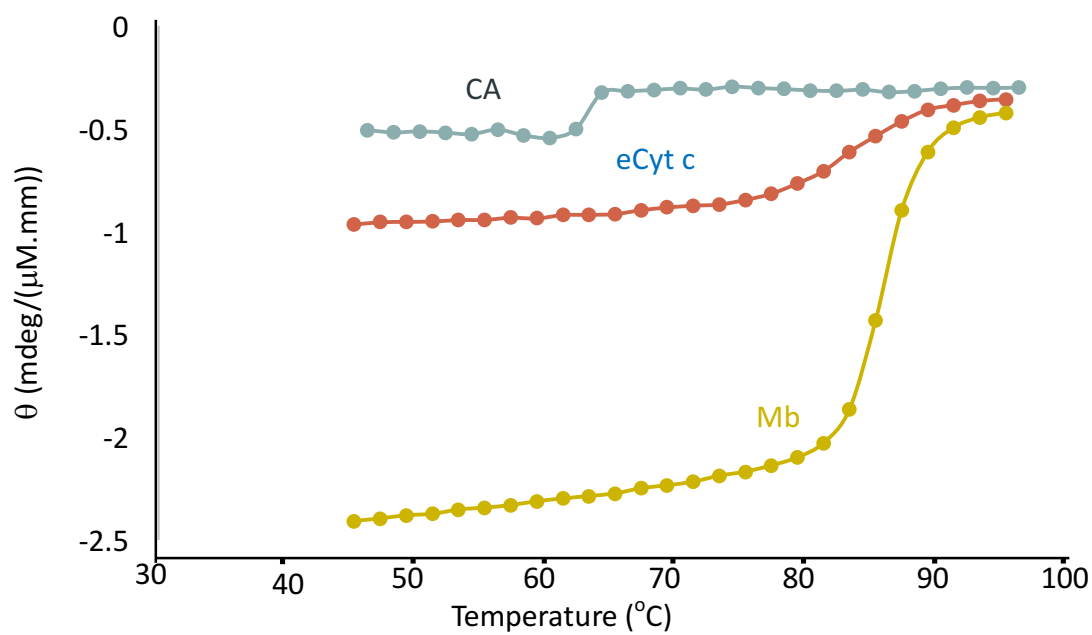
Figure 4. 11. CD measurement of protein melting temperature. The red line and dots indicate cytochrome *c*; the yellow line and dots indicate myoglobin; the blue line and dots indicate carbonic anhydrase.

CHAPTER 5. PROTEIN IDENTIFICATION USING LIMITED TRYPSIN DIGESTION AND MASS SPECTROMETRY

5.1   Introduction

Proteomics is a large scale protein identification and characterization study and is an essential topic to investigate protein composition and biological control in biological system. [1-3] Proteomics techniques can be used to identify proteome, post translational modification, protein-protein interaction, etc. [1] The protein identification process normally includes protein purification, degradation, database search and target identification based on matching score calculation. [4] Since the protein sample composition is complex and analytical workload is high, high throughput analysis is preferred. [5, 6] The traditional protein identification is based on protein gel electrophoresis or membrane electrophoresis in combination of blotting methods for protein separation. [7] The purified proteins are then degraded by chemical (eg. Edmann degradation) [8] or enzymatic digestion [9] to generate enough sequence information for database search. However, these methods are not suitable for high throughput applications limited by their slow analysis speed, besides other problems including low sensitivity, reaction blocking after certain degradation cycles and high protein concentration requirement, etc. [4]

Mass spectrometry is a widely used tool to quickly analyze chemicals, taking advantage of its high analytical speed, high accuracy and efficiency, low sample amount requirement, etc. [10-14] The development of soft ionization methods of matrix assisted laser desorption ionization (MALDI) and electrospray ionization (ESI) extended the application area of mass spectrometry to bioanalysis fields. [15-18] MALDI-MS and ESI-MS also promoted the development of mass spectrometry based protein identification methods, which is now the most widely used protein identification strategy. [19, 20]

The currently widely used protein identification methods based on mass spectrometry mainly include top-down, bottom-up and middle-down. [25] Bottom-up is the most widely used method, which involves fully digestion of intact protein in solution, measurement of the obtained peptide masses using MS and searching the peptide masses in database to identify proteins. This method has a high identification accuracy, but the intact protein mass is lost, thereby direct information about protein size and post translational modification is missed. [22-25] Top-down method is to spray the intact protein into mass spectrometer followed by tandem MS dissociation. This method could well preserve the intact protein mass information. However, for the following protein identification, it requires efficient gas phase dissociation to generate enough fragments for protein identification. The sequence coverage is quite limited by dissociation efficiency, so normally a combination of several different fragmentation methods is required. [26-29] Middle-down is a compromised method between top-down and bottom-up, which involves cutting proteins to big pieces using "rare-cutter" enzymes before tandem mass spectrometry. [30-33] However, the loss of intact protein and high efficient gas phase fragmentation requirement are still limitations.

To develop a good mass spectrometry based protein identification method and prepare it as a future proteomics technique, besides the need of both intact mass and fragment information, we also need to consider the amount of information to be extracted. In proteomics, one big challenge is the complexity of information. [21] Therefore, the current pursue of increasing sequence coverage by generating more fragments may also lead to new challenges in proteomics study. Limited trypsin digestion as one of the limited proteolysis methods [34, 35], could provide a new protein identification method. In this method, protein is partially digested to preserve both intact protein and some fragments. By controlling the digestion time, a proper amount of peptides will

be generated for database search. Here in this thesis, we combined limited trypsin digestion and mass spectrometry to develop a protein identification method.

5.2 Experimental

5.2.1 Reagent

Apo-myoglobin from equine skeletal muscle, cytochrome c from bovine heart, ammonium bicarbonate and perfluorooctane (PFO) were purchased from Sigma Aldrich (St. Louis, MO). Immobilized trypsin was purchased from Thermo Fisher Scientific (Lombard, IL). HPLC grade water and methanol were purchased from Fisher Scientific (Fair Lawn, NJ). Aqueous stock solutions of proteins were diluted to a final concentration of 10 μM in a solvent mixture. The final optimized reaction condition is that final protein concentration 10 μM, final immobilized trypsin suspension amount 1.4 mL/1μmol protein, final buffer condition 10 mM NH_4HCO_3. The optimized solvent mixture for apo-myoglobin is 80% 10 mM NH_4HCO_3 and 20% MeOH; while for cytochrome c the optimized solvent condition is 50% 10 mM NH_4HCO_3 and 50% MeOH.

5.2.2 Limited trypsin digestion

In a series of Ependorf tubes were added 7 μL acetic acid to prepare for trypsin digestion quenching. In another Ependorf tube, protein was dissolved in ammonium bicarbonate buffer (10 mM) in a mixed water/organic solvent (1.4 mL) to a final protein concentration of 10 μM. The denatured protein was added to prewashed immobilized trypsin (20 μL). The reaction mixture was vigorously shaken at room temperature up to 6 h and aliquots of 70 μL were collected at different time points for reaction monitoring. The aliquots were directly added to the prepared acetic acid to get the trypsin digestion reaction quenched. The quenched reaction mixture was filtered to remove the trypsin resin and the solvent of the filtrate was removed by vacuum concentrator. The

obtained residue was reconstituted by water/methanol/acetic acid 50/49/1 (v/v/v) and subjected for MS analysis.

5.2.3   Mass spectrometry and ion/ion reaction

All mass spectra were collected using a TripleTOF mass spectrometer (5600, Sciex, Concord, ON, Canada), previously modified for ion/ion reactions. Protein and tryptic peptides were sprayed in positive mode using an ionization voltage of 1600-2000 V. For non-ion/ion reaction experiments, ions were transferred to TOF for analysis. For ion/ion proton transfer reactions, the protein and peptide cations were transferred to and trapped in q2 quadrupole. Perfluorooctane was used as proton transfer reagent, which was sprayed using –nESI and isolated in Q1. The isolated perfluorooctane anions and protein/ tryptic peptide cations were mutually stored in q2 reaction cell for proton transfer reaction. The resulted charge reduced protein/peptide ions were transferred to TOF for analysis.

5.2.4   Data processing

The obtained post-ion/ion reaction data were deconvoluted to singly charged peaks using Sciex customized software based on THRASH algorithm. Tryptic peptide database for limited trypsin digestion was created. MOWSE score were calculated and hit proteins were ranked based on the score.

5.3   Results

5.3.1   Limited trypsin digestion

Trypsin is one of the most widely used proteases for protein structure analysis, which is also applied in bottom-up protein identification studies. [36-38] Trypsin selectively cleaves peptides from lysine and arginine residue sites. Based on this cleavage rule, theoretical tryptic peptide

database can be generated with known protein sequences. [39] Normal trypsin digestion time is hours or overnight. The development of immobilized trypsin on resin or membrane has accelerated the digestion period. [40-42] Trypsin digestion rate is also related to pH, buffer and solvent, which factors influence both trypsin bioactivity and analyte protein conformation. Protein conformation could influence trypsin accessibility to the cleavage sites, and therefore change the digestion efficiency. [36, 43] Limited trypsin digestion is to partially digest protein, so a limited amount of fragment information is generated for protein identification and intact protein is preserved for protein size and post-translational modification identification.

Myoglobin is a common model protein used in a lot of biological or analytical studies. The native myoglobin has a heme ligand, which is called holo-myoglobin. Removing of the heme ligand generates apo-myoglobin. Apo-myoglobin molecular weight is 16941 Da and it has 19 lysine and 2 arginine residues. Apo-myoglobin was subjected to trypsin digestion in 10 mM ammonium bicarbonate buffer and the solvent is 50/50 water/methanol. Ammonium bicarbonante adjusted the solution pH to slightly basic, which is optional for trypsin digestion reaction, and the solvent mixture will partially unfold myoglobin and promote the trypsin digestion. The trypsin was immobilized on agarose resin, which not only has a higher reaction efficiency, but also simplify the tryptic peptide purification process. The results have shown that after 1 min of trypsin digestion, the majority of apo-myoglobin is intact, with minimum amount of tryptic peptides generated. The multiply charged small amount of tryptic peptides were easily buried in the baseline. (Figure 5. 1 (a)) 6 min of trypsin digestion can generate a descent amount of tryptic peptides, and most of the intact proteins were preserved. (Figure 5. 1 (b)) After 6 h of digestion, the trypsin digestion is complete and all intact proteins were consumed. Fully cleaved tryptic peptides were generated. (Figure 5. 1 (c))

The limited trypsin digestion was also successfully performed on equine cytochrome *c*. (Figure 5. 2) Cytochrome *c* is a 12351 Da protein with a covalently bound heme ligand. The cytochrome *c* sequence is

GDVEKGKKIFVQKCAQCHTVEKGGKHKTGPNLHGLFGRKTGQAPGFSYTDANKNKGIT WGEETLMEYLENPKKYIPGTKMIFAGIKKKGEREDLIAYLKKATNE.

Similar to apomyoglobin digestion, 1 min of trypsin digestion generated few tryptic peptides, which were buried in baseline. (Figure 5. 2 (a)) 6 min is long enough to generate an apparent amount of tryptic peptides, with the majority of protein keeping its intact primary structure. (Figure 5. 2 (b)) After 6 h of complete trypsin digestion, all intact protein were digested to small peptides, which were mixed in the low molecular weight salt clusters and impurities.

5.3.2 Proton transfer reaction to reduce protein charge states

Based on apo-myoglobin and cytochrome *c* digestion data, limited trypsin digestion could be successfully performed in a controlled reaction time frame. However, due to the property for electrospray ionization, protein and peptide peaks were multiply charged. Multiply charging lead to more peak overlapping in low m/z range, which obstacle the peptide peak isolation. It also reduces peptide peak intensity due to the dispersity into multiple charge states, which reduces the sensitivity for tryptic peptide detection. Gas phase proton transfer reaction could reduce analyte charge state and increase the resolution and sensitivity for tryptic peptide detection. Here perfluorooctane (PFO) was used as a gas phase proton transfer reagent and reacted with the protein-peptide mixture. The results have shown that for both apo-myoglobin (Figure 5. 3) and cytochrome *c* (Figure 5. 4), protein/peptide charge states were reduced and spectra were simplified. After proton transfer, the buried tryptic peptide peaks clearly show up in the spectra, and peptide peaks were spread out.

5.3.3 Deconvolution to further simplify trypsin digestion spectra

With the enhanced resolution from proton transfer reaction, deconvolution algorithm was well performed on the raw MS data. After calculation, protein and peptide charge states were all reduced to +1. This charge state reduction not only better resolved different peptide peaks, it also significantly increased the database search speed and accuracy. Figure 5. 5 and Figure 5. 6 show that in less than 6 min, intact protein information is well preserved and peptide peaks were also generated for later database search.

5.3.4 Protein identification and post-translational modification analysis

To increase the search accuracy using limited trypsin digestion peaks, a tryptic peptide database including multiple missed cleavages were established. MOWSE score was calculated to determine the protein ranking in the matching results. When the fully digested apo-myoglobin peaks were searched in the database, protein was identified, with a score of 14.49. (Figure 5. 5 (d), Table 5.4) However, since no intact protein was preserved, no protein molecular weight or post translational modification information was indicated. When apo-myoglobin was limited digested by immobilized trypsin for only one minute, a large amount of intact protein was preserved, while 11 matched tryptic peptides were also generated. (Figure 5. 5 (a), Table 5.1) By searching the obtained tryptic peptide mass in database, myoglobin was identified as the top hit and the MOWSE score was calculated as 9.09. When the digestion time was elongated to 6 min, the majority of intact protein still existed, but 37 matched fragment peptides were generated. (Figure 5. 5 (b) Table 5.2) With the increased number of tryptic peptides, myoglobin was identified with a searching score of 22.05, which is higher than other cases. With the preserved intact protein, the protein molecular weight was identified as 16941 Da. However, from database search, protein molecular weight was fed back as 17072 Da, which is 131 Da higher than the measured mass. The mass

difference indicated the existence of post-translational modification. Based on mass calculation, the mass difference is attributed to the loss of N-terminal methionine residue.

Cytochrome *c* digestion data were also searched in database. When cytochrome *c* was fully digested by immobilized trypsin in 6 h, the obtained tryptic peptides can be used to identify the protein with a calculated MOWSE score of 23.46. (Figure 5. 6 (c), Table 5. 7) However, since all intact protein was digested, without running tandem MS, no post-translational-modification can be indicated from the data. When the protein digestion time was reduced to 1 min, intact protein could be preserved, and cytochrome *c* was identified with the limited tryptic peptide mass. (Figure 5. 6 (b) Table 5.5) However, when the digestion time was slightly elongated to 6 min, more tryptic peptides were obtained, which resulted in a higher MOWSE score of 24.59 for protein identification comparing to the score of 11.16 with 1 min digestion. (Figure 5. 6 (c)) In 6 min digestion, 47 tryptic peptides were generated and contributed to the searching score. (Table 5.6) This MOWSE score does not increase upon longer digestion. With the intact protein, the protein molecular weight was identified as 12351 Da, which is 526 Da higher than the database mass 11825 Da. Besides the known heme addition modification (+616 Da), there is still a mass difference of 90, which indicates the existence of other PTMs. Removal of N-terminal methionine (-132 Da) and N-terminal acetylation (+43 Da) could change the mass to 12352 Da, which is 1 Da higher than the measured molecular weight. This mass difference may result from Asp-Asn isomerization (-1 Da).

Carbonic anhydrase is a compact globular protein (29 kDa), which contains a noncovalent zinc ligand. Its 3D structure contains two big modules, which are the compact core structure and a flexible N-terminus (27 residues). In aqueous buffer or MeOH/H_2O (50/50), carbonic anhydrase core structure could not be well denatured based on the tryptic peptide peak assignment and the

digestion rate was much lower than myoglobin and cytochrome c. Acetonitrile/H_2O (50/50) could better denature carbonic anhydrase and get the core structure digested to increase sequence coverage, which facilitated protein identification. In acetonitrile/H_2O (50/50), limited digestion of carbonic anhydrase for 10 min can generate enough tryptic peptides to get carbonic anhydrase identified as a top hit protein based on MOWSE score ranking and also preserved the intact protein mass. For carbonic anhydrase digestion, some other unclear processes like aggregation may go on, which prevented the observation of big complementary tryptic peptide pieces. It also makes the optimum reaction time not very reproducible.

5.4   Conclusions

Protein identification using limited trypsin digestion and mass spectrometry is successful. Limited trypsin digestion was successfully performed by controlling reaction condition and reaction time. Proton transfer reaction and deconvolution algorithm reduced protein and peptide charges to increase resolution, sensitivity and database searching accuracy. Through short time digestion of proteins, enough tryptic peptides were generated and protein can be identified by searching the mass in database. Along with the tryptic peptides, the majority of intact protein was preserved, which can be used to identify protein molecular weight. Protein post translational modification was indicated by the difference between measured molecular weight and the reported mass from database search. Both apo-myoglobin and cytochrome c were identified using limited trypsin digestion and corresponding PTMs were deduced with the intact protein mass.

5.5 References

1. Chandramouli, K.; Qian, P. Proteomics: Challenges, techniques and possibilities to overcome biological sample complexity. Hum. Genomics Proteomics 2009, 2009, 239204.

2. Graves, P. R.; Haystead, T. A. J. Molecular biologist's guide to proteomics. Microbiol. Mol. Biol. Rev. 2002, 66, 39-63.

3. Norman, K. C.; Moore, B. B.; Arnold, K. B.; O'Dwyer, D. N. Proteomics: Clinical and research applications in respiratory diseases. Respirology 2018, 23, 993-1003.

4. Gevaert, K.; Vandekerckhove, J. E. Protein identification methods in proteomics. Electrophoresis 2000, 21, 1145-1154.

5. Wilkins, M.R.; Gasteiger. E.; Gooley. A. A.; Herbert, B. R.; Molloy, M. P.; Binz, P. A.; Ou, K.; Sanchez, J. C.; Bairoch, A.; Williams, K. L; Hochstrasser, D. F. High-throughput mass spectrometric discovery of protein post-translational modifications. J. Mol. Biol. 1999, 289, 645-657.

6. Godovac-Zimmermann, J.; Brown, L. R. Perspectives for mass spectrometry and functional proteomics. Mass Spectrom. Rev. 2001, 20, 1-57.

7. Rabilloud, T.; Chevallet, M.; Luche, S.; Lelong, C. Two-dimensional gel electrophoresis in proteomics: Past, present and future. J. Proteomics 2010, 73, 2064-2077.

8. Klemm, P. Manual Edman degradation of proteins and peptides. Methods Mol. Biol. 1984, 1, 243-254.

9. Williams, K. R.; Stone, K. L. Enzymatic cleavage and HPLC peptide mapping of proteins. Mol. Biotechnol. 1997, 8, 155-167.

10. Glish, G. L.; Vachet, R. W. The basics of mass spectrometry in the twenty first century. Nat. Rev. Drug Discov. 2003, 2, 140-150.

11. Roux, A.; Lison, D.; Junot, C.; Heilier, J. Applications of liquid chromatography coupled to mass spectrometry-based metabolomics in clinical chemistry and toxicology: A review. Clin. Biochem. 2011, 44, 119-135.

12. Bantscheff, M.; Schirle, M.; Sweetman, G.; Rich, J.; Kuster, B. Quantitative mass spectrometry in proteomics: A critical review. Anal. Bioanal. Chem. 2007, 389, 1017-1031.

13. Benson, S.; Lennard, C.; Maynard, P.; Roux, C. Forensic applications of isotope ratio mass spectrometry-A review. Forensic Sci. Int. 2006, 157, 1-22.

14. Jackson, S. E.; Pearson, N. J.; Griffin, W. L.; Belousova, E. A. The application of laser ablation-inductively coupled plasma-mass spectrometry to in situ U-Pb zircon geochronology. Chem. Geol. 2004, 211, 47-69.

15. Fenn, J. B.; Mann, M.; Meng, C. K.; Wong, S. F.; Whitehouse, C. M. Electrospray ionization for mass spectrometry of large biomolecules. Science 1989, 246, 64-71.

16. Wilm, M.; Mann, M. Analytical properties of the nanoelectrospray ion source. Anal. Chem. 1996, 68, 1-8.

17. Pan, P.; Guawardena, H. P.; Xia, Y.; McLuckey, S. A. Nanoelectrospray ionization of protein mixtures: solution pH and protein pI. Anal. Chem. 2004, 76, 1165-1174.

18. Chen, S. Rapid protein identification using direct infusion nanoelectrospray ionization mass spectrometry. Proteomics 2006, 6, 16-25.

19. Hardouin, J. Protein sequence information by matrix-assisted laser desorption/ ionization in-source decay mass spectrometry. Mass Spectrom. Rev. 2007, 26, 672-682.

20. Medzihradszky, K. F. Peptide sequence analysis. Methods Enzymol. 2005, 402, 209-244.

21. Kislinger, T.; Emili, A. Multidimensional protein identification technology: Current status and future prospects. Expert Rev. Proteomics 2005, 2, 27-39.

22. Zhang, Y.; Fonslow, B. R.; Shan, B.; Baek, M.; Yates, J. R. Protein analysis by shotgun/bottom-up proteomics. Chem. Rev. 2013, 113, 2343-2394.

23. Gillet, L. C.; Leitner, A.; Aebersold, R. Mass spectrometry applied to bottom-up proteomics: Entering the high-throughput era for hypothesis testing. Annu. Rev. Anal. Chem. 2016, 9, 449-472.

24. Bogdanov, B.; Smith, R. D. Proteomics by FTICR mass spectrometry: Top down and bottom up. Mass Spectrom. Rev. 2005, 24, 168-200.

25. Moradian, A.; Kalli, A.; Sweredoski, M. J.; Hess, S. The top-down, middle-down, and bottom-up mass spectrometry approaches for characterization of histone variants and their post-translational modifications. Proteomics 2014, 14, 489-497.

26. McLafferty, F. W.; Breuker, K.; Jin, M.; Han, X.; Infusini, G.; Jiang, H.; Kong, X.; Begley, T. P. Top-down MS, a powerful complement to the high capabilities of proteolysis proteomics. FEBS J. 2007, 274, 6256-6268.

27. Armirotti, A.; Damonte, G. Achievements and perspectives of top-down proteomics. Proteomics 2010, 10, 3566-3576.

28. Toby, T. K.; Fornelli, L.; Kelleher, N. L. Progress in top-down proteomics and the analysis of proteoforms. Annu. Rev. Anal. Chem. 2016, 9, 499-519.

29. Gregorich, Z. R.; Ge, Y. Top-down proteomics in health and disease: Challenges and opportunities. Proteomics 2014, 14, 1195-1210.

30. Sidoli, S.; Garcia, B. A. Middle-down proteomics: A still unexploited resource for chromatin biology. Expert. Rev. Proteomics 2017, 14, 617-626.

31. Xu, P.; Peng, J. Characterization of polyubiquitin chain structure by middle-down mass spectrometry. Anal. Chem. 2008, 80, 3438-3444.

32. Sweredoski, M. J.; Moradian, A.; Raedle, M.; Franco, C.; Hess, S. High resolution parallel reaction monitoring with electron transfer dissociation for middle-down proteomics. Anal. Chem., 2015, 87, 8360-8366.

33. Laskay, Ü. A.; Lobas, A. A.; Srzentić, K.; Gorshkov, M. V.; Tsybin, Y. O. Proteome digestion specificity analysis for rational design of extended bottom-up and middle-down proteomics experiments. Proteome Res. 2013, 12, 5558-5569.

34. Schopper, S.; Kahraman, A.; Leuenberger, P.; Feng, Y.; Piazza, I.; Müller, O.; Boersema, P. J.; Picotti, P. Measuring protein structural changes on a proteome-wide scale using limited proteolysis-coupled mass spectrometry. Nat. Protoc. 2017, 12, 2391-2410.

35. Yamaguchi, H.; Miyazaki, M.; Maeda, H. Limited proteolysis in proteomics using protease-immobilized microreactors. In: Kaufmann M., Klinger C. (eds) Functional Genomics. Methods in Molecular Biology (Methods and Protocols). Springer: New York, NY, 2012.

36. Gundry, R. L.; White, M. Y.; Murray, C. I.; Kane, L. A.; Fu, Q.; Stanley, B. A.; Van Eyk, J. E. Preparation of proteins and peptides for mass spectrometry analysis in a bottom-up proteomics workflow. Curr. Protoc. Mol. Biol. 2009, Chapter Unit 10.25.

37. Lowenthal, M. S.; Liang, Y.; Phinney, K. W.; Stein, S. E. Quantitative bottom-up proteomics depends on digestion conditions. Anal. Chem. 2014, 86, 551-558.

38. Huynh, M. L.; Russell, P.; Walsh, B. Tryptic digestion of in-gel proteins for mass spectrometry analysis. Methods Mol. Biol. 2009, 519, 507-513.

39. Olsen, J. V.; Ong, S.; Mann, M. Trypsin cleaves exclusively C-terminal to arginine and lysine residues. Mol. Cell Proteomics 2004, 3, 608-614.

40. Calleri, E.; Temporini, C.; Perani, E.; Stella, C.; Rudaz, S.; Lubda, D.; Mellerio, G.; Veuthey, J.-L.; Caccialanza, G.; Massolinia, G. Development of a bioreactor based on trypsin immobilized on monolithic support for the on-line digestion and identification of proteins. J. Chromatogr. A 2004, 1045, 99-109.

41. Massolini, G.; Calleri, E. Immobilized trypsin systems coupled on-line to separation methods: Recent developments and analytical applications. J. Sep. Sci. 2005, 28, 7-21.

42. Wang, C.; Oleschuk, R.; Ouchen, F.; Li, J.; Thibault, P.; Harrison, D. J. Integration of immobilized trypsin bead beds for protein digestion within a microfluidic chip incorporating capillary electrophoresis separations and an electrospray mass spectrometry interface. Rapid Commun. Mass Spectrom. 2000, 14, 1377-1383.

43. Turapov, O. A.; Mukamolova, G. V.; Bottrill, A. R.; Pangburn, M. K. Digestion of native proteins for proteomics using a thermocycler. Anal. Chem. 2008, 80, 6093-6099.
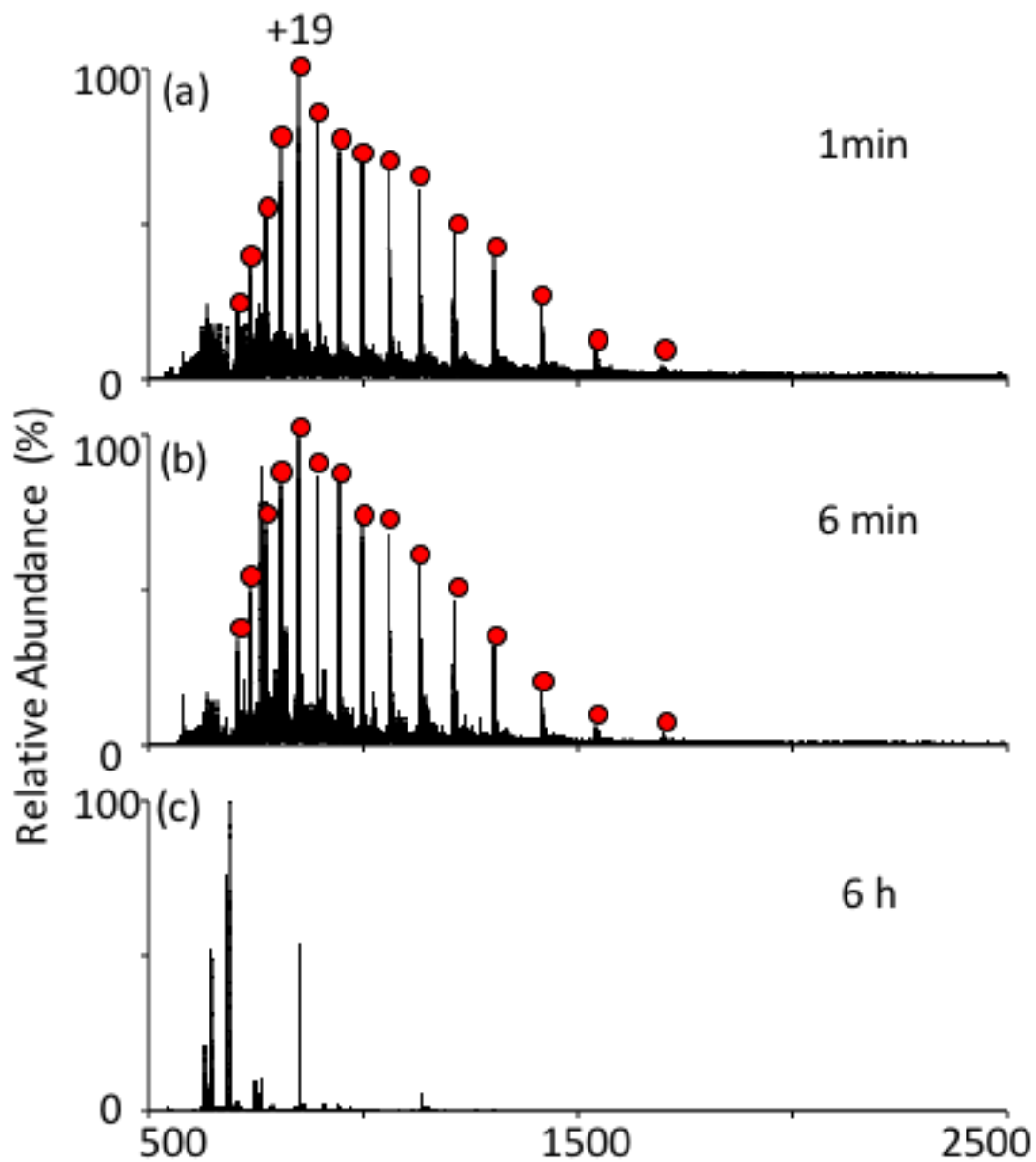
Figure 5. 1. Limited trypsin digestion of apo-myoglobin for (a) 1 min; (b) 6 min; (c) 6 h. The red dots indicate intact protein ions.
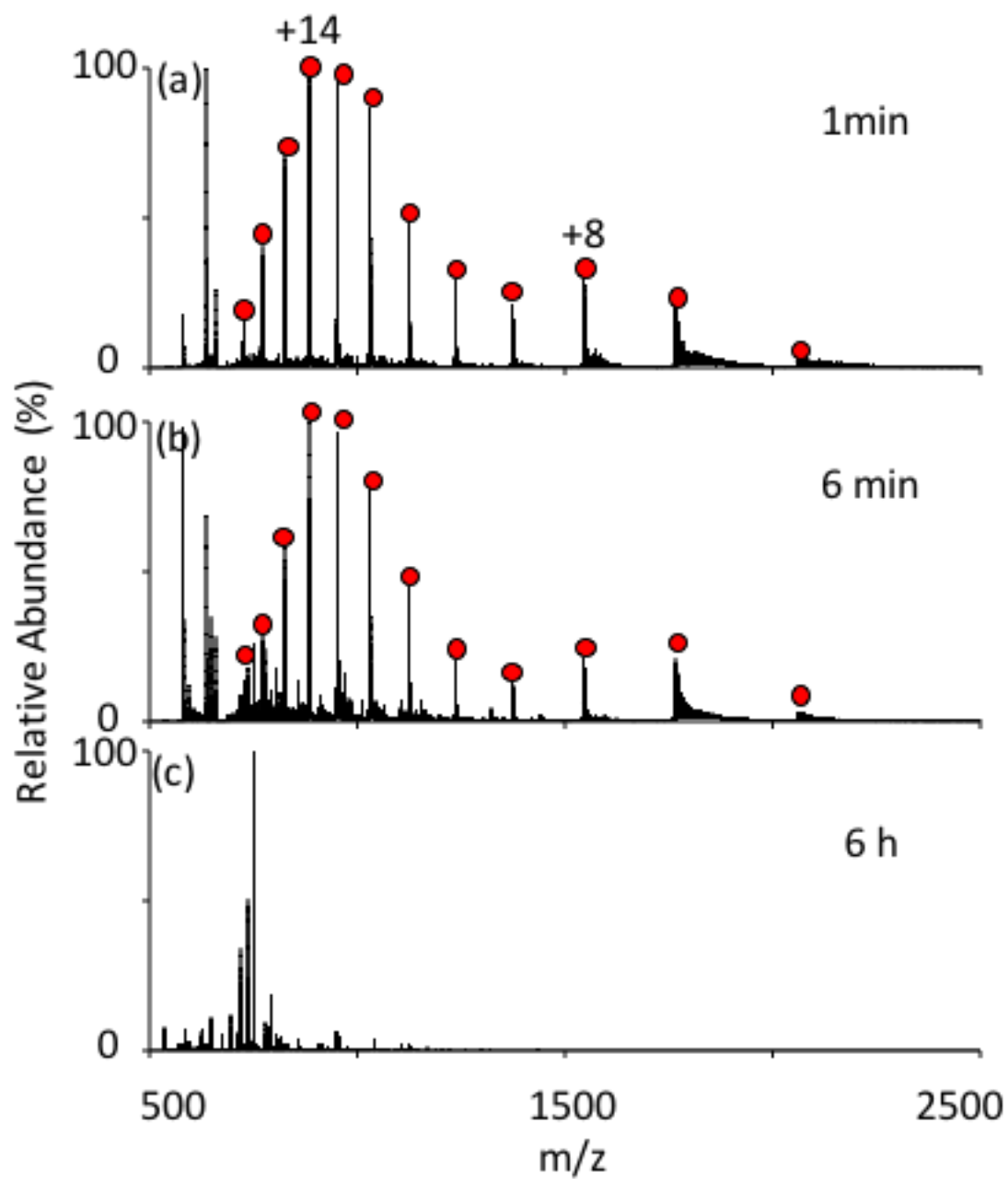
Figure 5. 2. Limited trypsin digestion of cytochrome *c* for (a) 1 min; (b) 6 min; (c) 6 h. The red dots indicate intact protein ions.
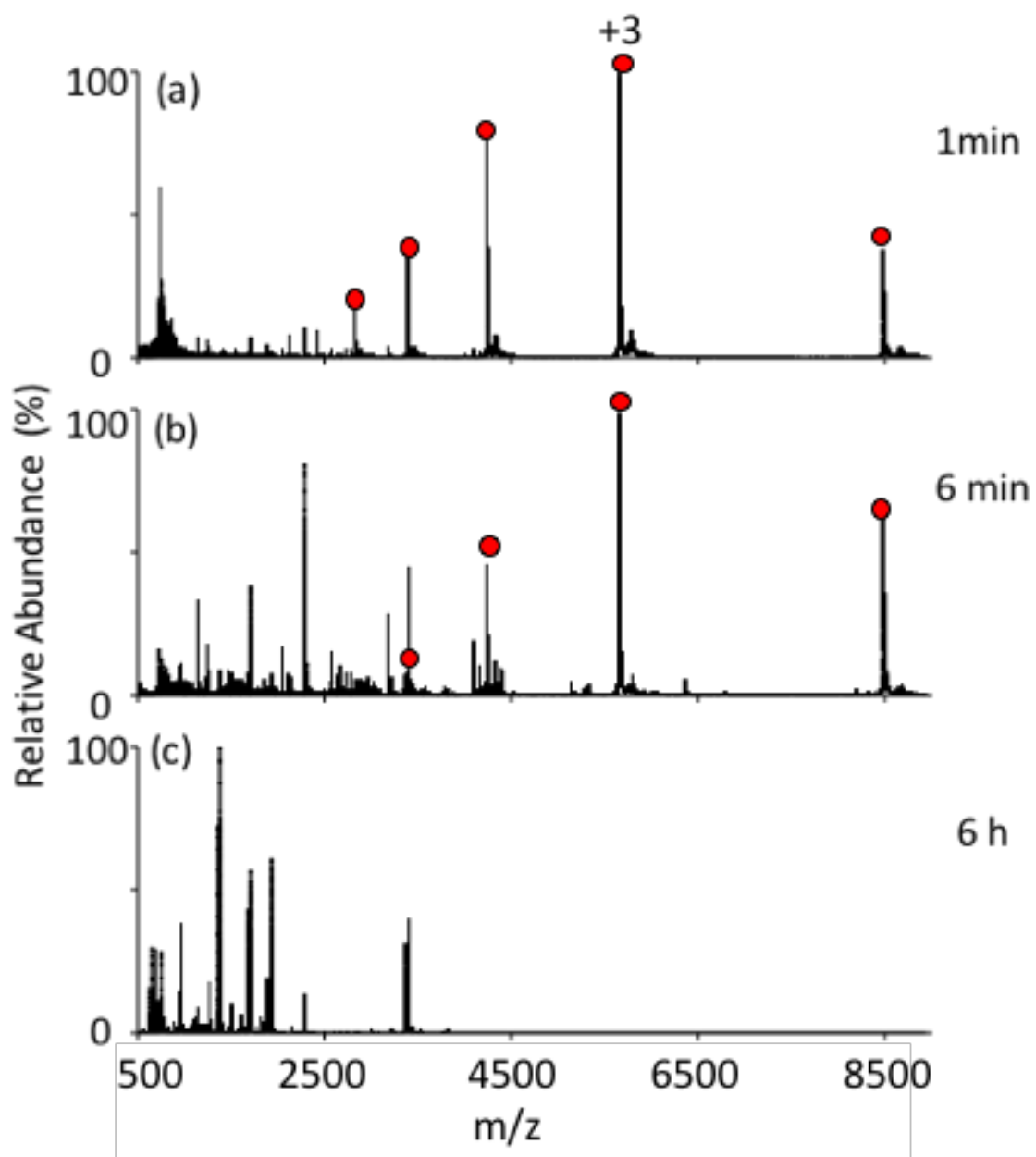
Figure 5. 3. Reducing charge state of apo-myoglobin tryptic peptides by gas phase proton transfer reaction. The limited trypsin digestion time is (a) 1 min; (b) 6 min; (c) 6 h. The red dots indicate intact protein ions.
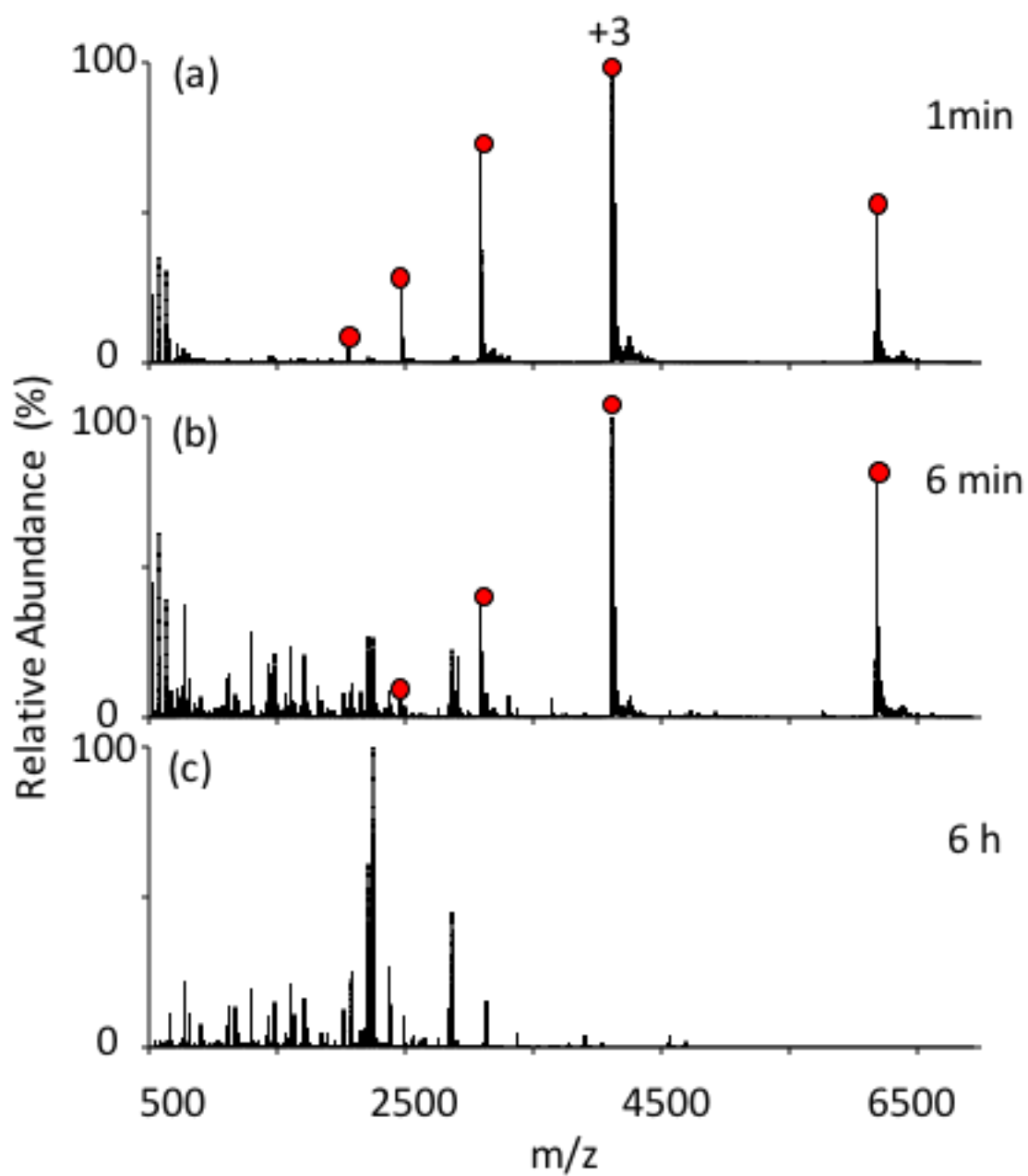
Figure 5. 4. Reducing charge state of cytochrome *c* tryptic peptides by gas phase proton transfer reaction. The limited trypsin digestion time is (a) 1 min; (b) 6 min; (c) 6 h. The red dots indicate intact protein ions.
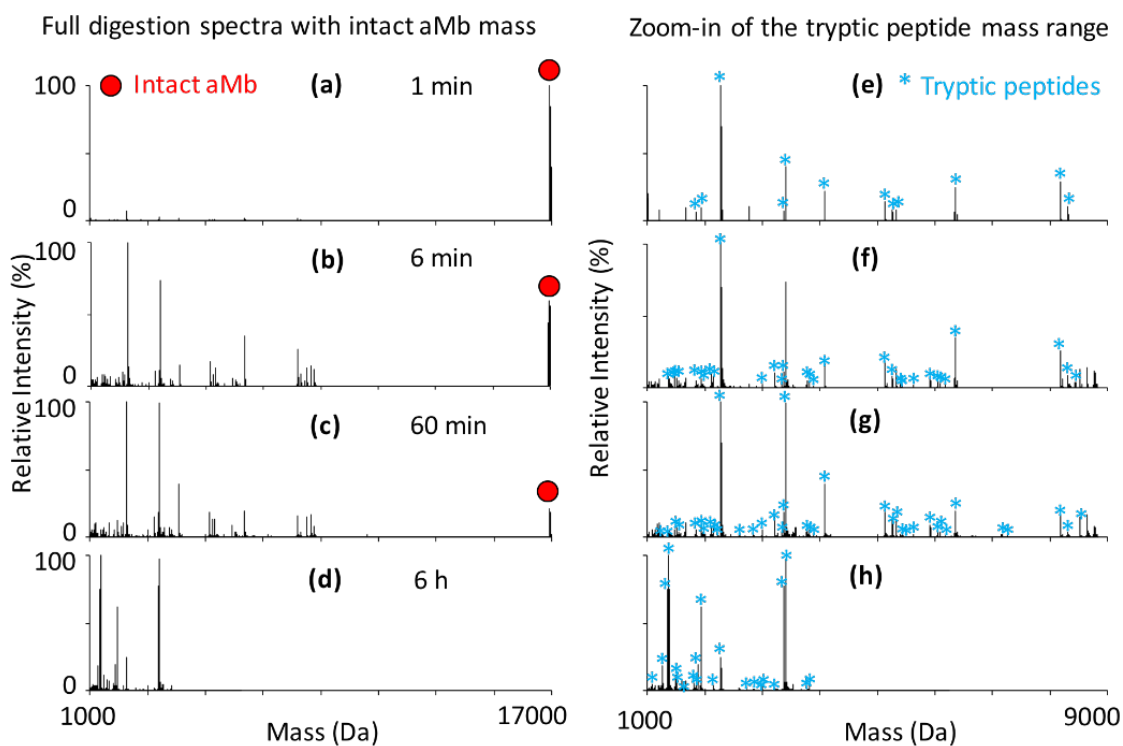
Figure 5. 5. Deconvolution of apomyoglobin limited trypsin digestion spectra. Apo-myoglobin was subjected to limited trypsin digestion for (a) 1 min; (b) 6 min; (c) 60 min; (d) 6 h and the spectra were simplified by gas phase proton transfer reaction before performing deconvolution algarithm. The low mass range peaks were zoomed in to identify the peptide peaks. (e)-(h)
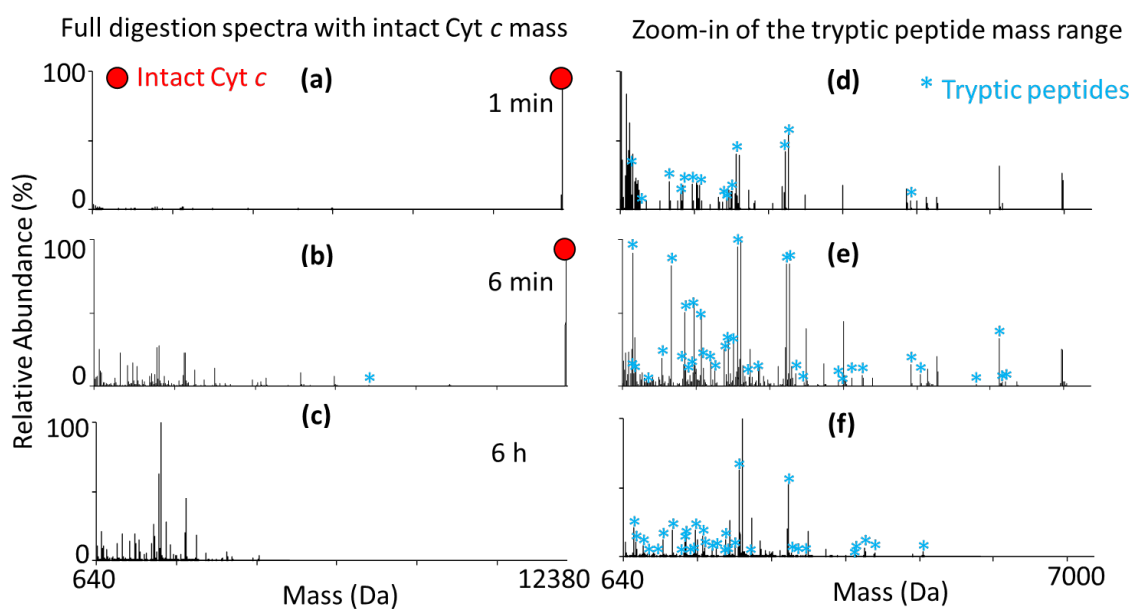
Figure 5. 6. Deconvolution of cytochrome *c* limited trypsin digestion spectra. Cytochrome *c* was subjected to limited trypsin digestion for (a) 1 min; (b) 6 min; (c) 6 h and the spectra were simplified by gas phase proton transfer reaction before performing deconvolution algarithm. The low mass range peaks were zoomed in to identify the peptide peaks. (d)-(f)

Table 5. 1 Myoglobin tryptic peptides generated in 1 min limited trypsin digestion.
Obs. Mass: observed mass; Theo. Mass: theoretical mass; error: matching error; start: start residue position; end: end residue position; mscl: missed cleavage number.
number of matched fragment peptides: 11; MOWSE score 9.09

Fragment sequence	Obs. Mass	Theo. Mass	Error	Start	End	mscl
'GHHEAELKPLAQSHATK'	'1852.93'	'1852.95'	'-10.96'	' 80'	' 96'	'0'
'YLEFISDAIIHVLHSKHPGDFGADAQGAMTK'	'3367.61'	'3367.67'	'-15.51'	'103'	'133'	'1'
'LFTGHPETLEKFDKFK'	'1936.01'	'1936.01'	' 1.06'	' 32'	' 47'	'2'
'HKIPIKYLEFISDAIIHVLHSKHPGDFGADAQGAMTK'	'4084.10'	'4084.14'	' -7.65'	' 97'	'133'	'3'
'ALELFRNDIAAKYKELGFQG'	'2282.17'	'2282.21'	'-14.20'	'134'	'153'	'3'
'ALELFRNDIAAKYKELGFQG'	'2282.22'	'2282.21'	' 5.80'	'134'	'153'	'3'
'LFTGHPETLEKFDKFKHLKTEAEMKASEDLKKHGTVVLTALGGILK'	'5134.80'	'5134.79'	' 1.36'	' 32'	' 77'	'7'
'HKIPIKYLEFISDAIIHVLHSKHPGDFGADAQGAMTKALELFRNDIAAKYKELGFQG'	'6348.24'	'6348.33'	'-13.89'	' 97'	'153'	'7'
'LFTGHPETLEKFDKFKHLKTEAEMKASEDLKKHGTVVLTALGGILKK'	'5262.89'	'5262.88'	' 0.71'	' 32'	' 78'	'8'
'GHHEAELKPLAQSHATKHKIPIKYLEFISDAIIHVLHSKHPGDFGADAQGAMTKALELFRNDIAAKYKELGFQG'	'8183.30'	'8183.27'	' 3.10'	' 80'	'153'	'8'
'KGHHEAELKPLAQSHATKHKIPIKYLEFISDAIIHVLHSKHPGDFGADAQGAMTKALELFRNDIAAKYKELGFQG'	'8311.29'	'8311.37'	' -9.07'	' 79'	'153'	'9'

Table 5. 2. Myoglobin tryptic peptides generated in 6 min limited trypsin digestion.

Obs. Mass: observed mass; Theo. Mass: theoretical mass; error: matching error; start: start residue position; end: end residue position; mscl: missed cleavage number.
number of matched fragment peptides: 37;
MOWSE score 22.05

Fragment sequence	Obs. Mass	Theo. Mass	Error	Start	End	mscl
'HGTVVLTALGGILK'	'1377.81'	'1377.83'	'-16.93'	' 65'	' 78'	' 0'
'GHHEAELKPLAQSHATK'	'1852.94'	'1852.95'	' -8.23'	' 81'	' 97'	' 0'
'KHGTVVLTALGGILK'	'1505.91'	'1505.93'	'-15.05'	' 64'	' 78'	' 1'
'HGTVVLTALGGILKK'	'1505.91'	'1505.93'	'-15.05'	' 65'	' 79'	' 1'
'KGHHEAELKPLAQSHATK'	'1981.02'	'1981.05'	'-14.25'	' 80'	' 97'	' 1'
'YLEFISDAIIHVLHSKHPGDFGADAQGAMTK'	'3367.62'	'3367.67'	'-12.78'	'104'	'134'	' 1'
'YLEFISDAIIHVLHSKHPGDFGADAQGAMTK'	'3367.69'	'3367.67'	' 7.22'	'104'	'134'	' 1'
'LFTGHPETLEKFDKFK'	'1936.02'	'1936.01'	' 3.78'	' 33'	' 48'	' 2'
'ASEDLKKHGTVVLTALGGILK'	'2149.23'	'2149.25'	' -5.97'	' 58'	' 78'	' 2'
'KKGHHEAELKPLAQSHATK'	'2109.12'	'2109.14'	'-10.52'	' 79'	' 97'	' 2'
'IPIKYLEFISDAIIHVLHSKHPGDFGADAQGAMTK'	'3818.99'	'3818.98'	' 2.02'	'100'	'134'	' 2'
'NDIAAKYKELGFQG'	'1552.79'	'1552.79'	' 2.48'	'141'	'154'	' 2'
'ASEDLKKHGTVVLTALGGILKK'	'2277.35'	'2277.34'	' 2.05'	' 58'	' 79'	' 3'
'HKIPIKYLEFISDAIIHVLHSKHPGDFGADAQGAMTK'	'4084.12'	'4084.14'	' -4.93'	' 98'	'134'	' 3'
'ALELFRNDIAAKYKELGFQG'	'2282.18'	'2282.21'	'-11.48'	'135'	'154'	' 3'
'LFTGHPETLEKFDKFKHLKTEAEMK'	'3003.53'	'3003.55'	' -7.60'	' 33'	' 57'	' 4'
'HLKTEAEMKASEDLKKHGTVVLTALGGILK'	'3216.74'	'3216.79'	'-16.52'	' 49'	' 78'	' 4'
'HLKTEAEMKASEDLKKHGTVVLTALGGILK'	'3216.80'	'3216.79'	' 3.48'	' 49'	' 78'	' 4'
'GHHEAELKPLAQSHATKHKIPIKYLEFISDAIIHVLHSKHPGDFGADAQGAMTK'	'5919.08'	'5919.08'	' 0.54'	' 81'	'134'	' 4'
'HLKTEAEMKASEDLKKHGTVVLTALGGILKK'	'3344.87'	'3344.89'	' -5.24'	' 49'	' 79'	' 5'

Table 5. 2 Continued

'KGHHEAELKPLAQSHAT KHKIPIKYLEFISDAIIHVL HSKHPGDFGADAQGAMT K'	'6047.11'	'6047.17'	' -9.86'	' 80'	'134'	' 5'
'HKIPIKYLEFISDAIIHVLH SKHPGDFGADAQGAMTK ALELFRNDIAAK'	'5425.78'	'5425.88'	'-17.04'	' 98'	'146'	' 5'
'YLEFISDAIIHVLHSKHPG DFGADAQGAMTKALELF RNDIAAKYKELGFQG'	'5631.76'	'5631.86'	'-18.01'	'104'	'154'	' 5'
'LFTGHPETLEKFDKFKHL KTEAEMKASEDLKK'	'3774.95'	'3774.97'	' -5.26'	' 33'	' 64'	' 6'
'FDKFKHLKTEAEMKASE DLKKHGTVVLTALGGILK'	'3882.14'	'3882.14'	' -1.91'	' 44'	' 78'	' 6'
'KKGHHEAELKPLAQSHA TKHKIPIKYLEFISDAIIHV LHSKHPGDFGADAQGAM TK'	'6175.20'	'6175.27'	'-11.46'	' 79'	'134'	' 6'
'IPIKYLEFISDAIIHVLHSK HPGDFGADAQGAMTKAL ELFRNDIAAKYKELGFQG'	'6083.14'	'6083.18'	' -5.91'	'100'	'154'	' 6'
'LFTGHPETLEKFDKFKHL KTEAEMKASEDLKKHGT VVLTALGGILK'	'5134.81'	'5134.79'	' 4.09'	' 33'	' 78'	' 7'
'HKIPIKYLEFISDAIIHVLH SKHPGDFGADAQGAMTK ALELFRNDIAAKYKELGF QG'	'6348.26'	'6348.33'	'-11.17'	' 98'	'154'	' 7'
'HKIPIKYLEFISDAIIHVLH SKHPGDFGADAQGAMTK ALELFRNDIAAKYKELGF QG'	'6348.39'	'6348.33'	' 8.83'	' 98'	'154'	' 7'
'LFTGHPETLEKFDKFKHL KTEAEMKASEDLKKHGT VVLTALGGILKK'	'5262.80'	'5262.88'	'-16.56'	' 33'	' 79'	' 8'
'LFTGHPETLEKFDKFKHL KTEAEMKASEDLKKHGT VVLTALGGILKK'	'5262.90'	'5262.88'	' 3.44'	' 33'	' 79'	' 8'
'GHHEAELKPLAQSHATK HKIPIKYLEFISDAIIHVLH SKHPGDFGADAQGAMTK ALELFRNDIAAKYKELGF QG'	'8183.16'	'8183.27'	'-14.18'	' 81'	'154'	' 8'

Table 5. 2 Continued

'GHHEAELKPLAQSHATK HKIPIKYLEFISDAIIHVLH SKHPGDFGADAQGAMTK ALELFRNDIAAKYKELGF QG'	'8183.32'	'8183.27'	' 5.82'	' 81'	'154'	' 8'
'LFTGHPETLEKFDKFKHL KTEAEMKASEDLKKHGT VVLTALGGILKKK'	'5390.95'	'5390.98'	' -4.63'	' 33'	' 80'	' 9'
'KGHHEAELKPLAQSHAT KHKIPIKYLEFISDAIIHVL HSKHPGDFGADAQGAMT KALELFRNDIAAKYKELG FQG'	'8311.32'	'8311.37'	' -6.35'	' 80'	'154'	' 9'
'KKGHHEAELKPLAQSHA TKHKIPIKYLEFISDAIIHV LHSKHPGDFGADAQGAM TKALELFRNDIAAKYKEL GFQG'	'8439.46'	'8439.46'	' -0.96'	' 79'	'154'	'10'

Table 5. 3. Myoglobin tryptic peptides generated in 60 min limited trypsin digestion.

Obs. Mass: observed mass; Theo. Mass: theoretical mass; error: matching error; start: start residue position; end: end residue position; mscl: missed cleavage number.
number of matched fragment peptides: 42;
MOWSE score 24.05

Fragment sequence	Obs. Mass	Theo. Mass	Error	Start	End	mscl
'LFTGHPETLEK'	'1270.65'	'1270.66'	' -2.76'	' 32'	' 42'	'0'
'HGTVVLTALGGILK'	'1377.83'	'1377.83'	' -3.44'	' 64'	' 77'	'0'
'GHHEAELKPLAQSHATK'	'1852.96'	'1852.95'	' 5.26'	' 80'	' 96'	'0'
'KHGTVVLTALGGILK'	'1505.93'	'1505.93'	' -1.56'	' 63'	' 77'	'1'
'HGTVVLTALGGILKK'	'1505.93'	'1505.93'	' -1.56'	' 64'	' 78'	'1'
'KGHHEAELKPLAQSHATK'	'1981.05'	'1981.05'	' -0.76'	' 79'	' 96'	'1'
'YLEFISDAIIHVLHSKHPGD FGADAQGAMTK'	'3367.67'	'3367.67'	' 0.71'	'103'	'133'	'1'
'LFTGHPETLEKFDKFK'	'1936.00'	'1936.01'	' -2.73'	' 32'	' 47'	'2'
'ASEDLKKHGTVVLTALGG ILK'	'2149.22'	'2149.25'	'-12.48'	' 57'	' 77'	'2'
'ASEDLKKHGTVVLTALGG ILK'	'2149.26'	'2149.25'	' 7.52'	' 57'	' 77'	'2'
'KKGHHEAELKPLAQSHAT K'	'2109.15'	'2109.14'	' 2.97'	' 78'	' 96'	'2'
'HKIPIKYLEFISDAIIHVLHS K'	'2600.50'	'2600.48'	' 5.50'	' 97'	'118'	'2'
'IPIKYLEFISDAIIHVLHSKH PGDFGADAQGAMTK'	'3818.96'	'3818.98'	' -4.49'	' 99'	'133'	'2'
'ALELFRNDIAAKYK'	'1650.88'	'1650.91'	'-18.52'	'134'	'147'	'2'
'NDIAAKYKELGFQG'	'1552.78'	'1552.79'	' -4.03'	'140'	'153'	'2'
'LFTGHPETLEKFDKFKHLK '	'2314.25'	'2314.25'	' -0.17'	' 32'	' 50'	'3'
'TEAEMKASEDLKKHGTVV LTALGGILK'	'2838.58'	'2838.55'	' 8.08'	' 51'	' 77'	'3'
'ASEDLKKHGTVVLTALGG ILKK'	'2277.33'	'2277.34'	' -4.46'	' 57'	' 78'	'3'
'HKIPIKYLEFISDAIIHVLHS KHPGDFGADAQGAMTK'	'4084.17'	'4084.14'	' 8.56'	' 97'	'133'	'3'
'ALELFRNDIAAKYKELGFQ G'	'2282.21'	'2282.21'	' 2.01'	'134'	'153'	'3'
'LFTGHPETLEKFDKFKHLK TEAEMK'	'3003.57'	'3003.55'	' 5.89'	' 32'	' 56'	'4'
'HLKTEAEMKASEDLKKHG TVVLTALGGILK'	'3216.78'	'3216.79'	' -3.03'	' 48'	' 77'	'4'

Table 5. 3 Continued

'GHHEAELKPLAQSHATKH KIPIKYLEFISDAIIHVLHSK HPGDFGADAQGAMTK'	'5919.04'	'5919.08'	' -5.98'	' 80'	'133'	'4'
'GHHEAELKPLAQSHATKH KIPIKYLEFISDAIIHVLHSK HPGDFGADAQGAMTK'	'5919.16'	'5919.08'	' 14.02'	' 80'	'133'	'4'
'HPGDFGADAQGAMTKAL ELFRNDIAAKYKELGFQG'	'3765.87'	'3765.86'	' 3.95'	'119'	'153'	'4'
'HLKTEAEMKASEDLKKHG TVVLTALGGILKK'	'3344.85'	'3344.89'	'-11.75'	' 48'	' 78'	'5'
'KGHHEAELKPLAQSHATK HKIPIKYLEFISDAIIHVLHS KHPGDFGADAQGAMTK'	'6047.20'	'6047.17'	' 3.63'	' 79'	'133'	'5'
'HKIPIKYLEFISDAIIHVLHS KHPGDFGADAQGAMTKA LELFRNDIAAK'	'5425.86'	'5425.88'	' -3.55'	' 97'	'145'	'5'
'YLEFISDAIIHVLHSKHPGD FGADAQGAMTKALELFRN DIAAKYKELGFQG'	'5631.84'	'5631.86'	' -4.52'	'103'	'153'	'5'
'LFTGHPETLEKFDKFKHLK TEAEMKASEDLKK'	'3775.00'	'3774.97'	' 8.22'	' 32'	' 63'	'6'
'FDKFKHLKTEAEMKASED LKKHGTVVLTALGGILK'	'3882.11'	'3882.14'	' -8.42'	' 43'	' 77'	'6'
'KKGHHEAELKPLAQSHAT KHKIPIKYLEFISDAIIHVLH SKHPGDFGADAQGAMTK'	'6175.28'	'6175.27'	' 2.03'	' 78'	'133'	'6'
'GHHEAELKPLAQSHATKH KIPIKYLEFISDAIIHVLHSK HPGDFGADAQGAMTKALE LFRNDIAAK'	'7260.82'	'7260.82'	' 0.16'	' 80'	'145'	'6'
'IPIKYLEFISDAIIHVLHSKH PGDFGADAQGAMTKALEL FRNDIAAKYKELGFQG'	'6083.22'	'6083.18'	' 7.58'	' 99'	'153'	'6'
'LFTGHPETLEKFDKFKHLK TEAEMKASEDLKKHGTVV LTALGGILK'	'5134.78'	'5134.79'	' -2.42'	' 32'	' 77'	'7'
'LFTGHPETLEKFDKFKHLK TEAEMKASEDLKKHGTVV LTALGGILK'	'5134.88'	'5134.79'	' 17.58'	' 32'	' 77'	'7'
'HKIPIKYLEFISDAIIHVLHS KHPGDFGADAQGAMTKA LELFRNDIAAKYKELGFQG'	'6348.35'	'6348.33'	' 2.32'	' 97'	'153'	'7'

Table 5. 3 Continued

'LFTGHPETLEKFDKFKHLK TEAEMKASEDLKKHGTVV LTALGGILKK'	'5262.87'	'5262.88'	' -3.07'	' 32'	' 78'	'8'
'GHHEAELKPLAQSHATKH KIPIKYLEFISDAIIHVLHSK HPGDFGADAQGAMTKALE LFRNDIAAKYKELGFQG'	'8183.27'	'8183.27'	' -0.69'	' 80'	'153'	'8'
'LFTGHPETLEKFDKFKHLK TEAEMKASEDLKKHGTVV LTALGGILKKK'	'5391.03'	'5390.98'	' 8.86'	' 32'	' 79'	'9'
'KGHHEAELKPLAQSHATK HKIPIKYLEFISDAIIHVLHS KHPGDFGADAQGAMTKA LELFRNDIAAKYKELGFQG'	'8311.26'	'8311.37'	'-12.86'	' 79'	'153'	'9'
'KGHHEAELKPLAQSHATK HKIPIKYLEFISDAIIHVLHS KHPGDFGADAQGAMTKA LELFRNDIAAKYKELGFQG'	'8311.43'	'8311.37'	' 7.14'	' 79'	'153'	'9'

Table 5. 4. Myoglobin tryptic peptides generated in 6 h limited trypsin digestion.

Obs. Mass: observed mass; Theo. Mass: theoretical mass; error: matching error; start: start residue position; end: end residue position; mscl: missed cleavage number.
number of matched fragment peptides: 26;
MOWSE score 14.49

Fragment sequence	Obs. Mass	Theo. Mass	Error	Start	End	mscl
'LFTGHPETLEK'	'1270.65'	'1270.66'	'-6.57'	' 33'	' 43'	'0'
'HGTVVLTALGGILK'	'1377.82'	'1377.83'	'-7.25'	' 65'	' 78'	'0'
'GHHEAELKPLAQSHATK'	'1852.96'	'1852.95'	' 1.45'	' 81'	' 97'	'0'
'YLEFISDAIIHVLHSK'	'1884.01'	'1884.01'	'-2.29'	'104'	'119'	'0'
'HPGDFGADAQGAMTK'	'1501.65'	'1501.66'	'-7.59'	'120'	'134'	'0'
'LFTGHPETLEKFDK'	'1660.84'	'1660.85'	'-3.29'	' 33'	' 46'	'1'
'HLKTEAEMK'	'1085.55'	'1085.55'	'-2.28'	' 49'	' 57'	'1'
'KHGTVVLTALGGILK'	'1505.92'	'1505.93'	'-5.37'	' 64'	' 78'	'1'
'HGTVVLTALGGILKK'	'1505.92'	'1505.93'	'-5.37'	' 65'	' 79'	'1'
'IPIKYLEFISDAIIHVLHSK'	'2335.35'	'2335.33'	' 7.07'	'100'	'119'	'1'
'YLEFISDAIIHVLHSKHPGDFGADAQGAMTK'	'3367.66'	'3367.67'	'-3.10'	'104'	'134'	'1'
'ALELFRNDIAAK'	'1359.76'	'1359.75'	' 4.23'	'135'	'146'	'1'
'LFTGHPETLEKFDKFK'	'1936.00'	'1936.01'	'-6.54'	' 33'	' 48'	'2'
'ASEDLKKHGTVVLTALGGILK'	'2149.26'	'2149.25'	' 3.71'	' 58'	' 78'	'2'
'HKIPIKYLEFISDAIIHVLHSK'	'2600.49'	'2600.48'	' 1.69'	' 98'	'119'	'2'
'IPIKYLEFISDAIIHVLHSKHPGDFGADAQGAMTK'	'3818.95'	'3818.98'	'-8.30'	'100'	'134'	'2'
'IPIKYLEFISDAIIHVLHSKHPGDFGADAQGAMTK'	'3819.03'	'3818.98'	'11.70'	'100'	'134'	'2'
'NDIAAKYKELGFQG'	'1552.78'	'1552.79'	'-7.84'	'141'	'154'	'2'
'LFTGHPETLEKFDKFKHLK'	'2314.24'	'2314.25'	'-3.98'	' 33'	' 51'	'3'
'TEAEMKASEDLKKHGTVVLTALGGILK'	'2838.56'	'2838.55'	' 4.27'	' 52'	' 78'	'3'
'ASEDLKKHGTVVLTALGGILKK'	'2277.32'	'2277.34'	'-8.27'	' 58'	' 79'	'3'
'ALELFRNDIAAKYKELGFQG'	'2282.20'	'2282.21'	'-1.80'	'135'	'154'	'3'
'LFTGHPETLEKFDKFKHLKTEAEMK'	'3003.56'	'3003.55'	' 2.08'	' 33'	' 57'	'4'
'HLKTEAEMKASEDLKKHGTVVLTALGGILK'	'3216.77'	'3216.79'	'-6.85'	' 49'	' 78'	'4'
'TEAEMKASEDLKKHGTVVLTALGGILKK'	'2966.66'	'2966.65'	' 5.55'	' 52'	' 79'	'4'

Table 5. 4 Continued

| 'HPGDFGADAQGAMTKAL ELFRNDIAAKYKELGFQG' | '3765.86' | '3765.86' | ' 0.14' | '120' | '154' | '4' |

Table 5. 5. Cytochrome *c* tryptic peptides generated in 1 min limited trypsin digestion.

 Obs. Mass: observed mass; Theo. Mass: theoretical mass; error: matching error; start: start residue position; end: end residue position; mscl: missed cleavage number.
number of matched fragment peptides: 18;
MOWSE score 11.16

Fragment sequence	Obs. Mass	Theo. Mass	Error	Start	End	mscl
'TGQAPGFTYTDANK'	'1469.68'	'1469.68'	' 2.19'	'40'	' 53'	' 0'
'MIFAGIK'	' 778.44'	' 778.44'	' -5.78'	'80'	' 86'	' 0'
'TGPNLHGLFGRK'	'1295.70'	'1295.71'	'-11.47'	'28'	' 39'	' 1'
'TGQAPGFTYTDANKNK'	'1711.80'	'1711.82'	'-10.67'	'40'	' 55'	' 1'
'GITWKEETLMEYLENPK'	'2080.03'	'2080.02'	' 5.60'	'56'	' 72'	' 1'
'MIFAGIKK'	' 906.53'	' 906.54'	' -4.78'	'80'	' 87'	' 1'
'GITWKEETLMEYLENPKK'	'2208.12'	'2208.11'	' 3.28'	'56'	' 73'	' 2'
'KTEREDLIAYLK'	'1477.82'	'1477.81'	' 1.90'	'88'	' 99'	' 2'
'TEREDLIAYLKK'	'1477.82'	'1477.81'	' 1.90'	'89'	'100'	' 2'
'GITWKEETLMEYLENPKKYIPGTK'	'2867.44'	'2867.48'	'-13.60'	'56'	' 79'	' 3'
'GITWKEETLMEYLENPKKYIPGTK'	'2867.50'	'2867.48'	' 6.40'	'56'	' 79'	' 3'
'KKTEREDLIAYLK'	'1605.90'	'1605.91'	' -4.88'	'87'	' 99'	' 3'
'KTEREDLIAYLKK'	'1605.90'	'1605.91'	' -4.88'	'88'	'100'	' 3'
'KTEREDLIAYLKKATNE'	'2021.06'	'2021.08'	' -8.91'	'88'	'104'	' 4'
'TGQAPGFTYTDANKNKGITWKEETLMEYLENPKKYIPGTK'	'4561.33'	'4561.28'	' 10.49'	'40'	' 79'	' 5'
'KKTEREDLIAYLKKATNE'	'2149.17'	'2149.17'	' -1.55'	'87'	'104'	' 5'
'MIFAGIKKKTEREDLIAYLKKATNE'	'2909.61'	'2909.60'	' 1.85'	'80'	'104'	' 6'
'GITWKEETLMEYLENPKKYIPGTKMIFAGIKKKTEREDLIAYLKKATNE'	'5759.05'	'5759.07'	' -4.09'	'56'	'104'	'10'

Table 5. 6. Cytochrome *c* tryptic peptides generated in 6 min limited trypsin digestion.

 Obs. Mass: observed mass; Theo. Mass: theoretical mass; error: matching error; start: start residue position; end: end residue position; mscl: missed cleavage number.
number of matched fragment peptides: 47;
MOWSE score 24.59

Fragment sequence	Obs. Mass	Theo. Mass	Error	Start	End	mscl
'TGPNLHGLFGR'	'1167.62'	'1167.61'	' 1.80'	'28'	' 38'	' 0'
'TGQAPGFTYTDANK'	'1469.68'	'1469.68'	' -1.16'	'40'	' 53'	' 0'
'MIFAGIK'	' 778.43'	' 778.44'	' -9.13'	'80'	' 86'	' 0'
'GDVEKGK'	' 773.39'	' 773.39'	' -0.21'	' 1'	' 7'	' 1'
'TGPNLHGLFGRK'	'1295.72'	'1295.71'	' 5.18'	'28'	' 39'	' 1'
'KTGQAPGFTYTDANK'	'1597.79'	'1597.77'	' 10.61'	'39'	' 53'	' 1'
'TGQAPGFTYTDANKNK	'1711.79'	'1711.82'	'-14.02'	'40'	' 55'	' 1'
'GITWKEETLMEYLENPK'	'2080.02'	'2080.02'	' 2.25'	'56'	' 72'	' 1'
'KYIPGTK'	' 805.47'	' 805.47'	' -1.79'	'73'	' 79'	' 1'
'GDVEKGKK'	' 901.48'	' 901.49'	' -1.50'	' 1'	' 8'	' 2'
'HKTGPNLHGLFGRK'	'1560.87'	'1560.86'	' 2.68'	'26'	' 39'	' 2'
'KTGQAPGFTYTDANKNK'	'1839.92'	'1839.91'	' 2.89'	'39'	' 55'	' 2'
'GITWKEETLMEYLENPKK'	'2208.11'	'2208.11'	' -0.07'	'56'	' 73'	' 2'
'KTEREDLIAYLK'	'1477.81'	'1477.81'	' -1.45'	'88'	' 99'	' 2'
'TEREDLIAYLKK'	'1477.81'	'1477.81'	' -1.45'	'89'	'100'	' 2'
'EDLIAYLKKATNE'	'1506.79'	'1506.79'	' -1.17'	'92'	'104'	' 2'
'TGPNLHGLFGRKTGQAPGFTYTDANKNK'	'2989.53'	'2989.52'	' 4.07'	'28'	' 55'	' 3'
'GITWKEETLMEYLENPKKYIPGTK'	'2867.49'	'2867.48'	' 3.05'	'56'	' 79'	' 3'
'KKTEREDLIAYLK'	'1605.90'	'1605.91'	' -8.23'	'87'	' 99'	' 3'
'KTEREDLIAYLKK'	'1605.90'	'1605.91'	' -8.23'	'88'	'100'	' 3'
'TEREDLIAYLKKATNE'	'1892.96'	'1892.98'	'-14.53'	'89'	'104'	' 3'
'TEREDLIAYLKKATNE'	'1892.99'	'1892.98'	' 5.47'	'89'	'104'	' 3'
'KTGQAPGFTYTDANKNKGITWKEETLMEYLENPK'	'3901.94'	'3901.92'	' 4.20'	'39'	' 72'	' 4'
'TGQAPGFTYTDANKNKGITWKEETLMEYLENPKK'	'3901.94'	'3901.92'	' 4.20'	'40'	' 73'	' 4'
'NKGITWKEETLMEYLENPKKYIPGTK'	'3109.60'	'3109.62'	' -4.07'	'54'	' 79'	' 4'
'GITWKEETLMEYLENPKKYIPGTKMIFAGIK'	'3627.90'	'3627.91'	' -2.74'	'56'	' 86'	' 4'

Table 5. 6 Continued

'MIFAGIKKKTEREDLIAYLK'	'2366.32'	'2366.34'	' -6.43'	'80'	' 99'	' 4'
'KKTEREDLIAYLKK'	'1733.98'	'1734.00'	'-12.21'	'87'	'100'	' 4'
'KTEREDLIAYLKKATNE'	'2021.05'	'2021.08'	'-12.26'	'88'	'104'	' 4'
'KTEREDLIAYLKKATNE'	'2021.10'	'2021.08'	' 7.74'	'88'	'104'	' 4'
'TGQAPGFTYTDANKNKGITWKEETLMEYLENPKKYIPGTK'	'4561.32'	'4561.28'	' 7.14'	'40'	' 79'	' 5'
'GITWKEETLMEYLENPKKYIPGTKMIFAGIKK'	'3756.00'	'3756.00'	' -2.26'	'56'	' 87'	' 5'
'MIFAGIKKKTEREDLIAYLKK'	'2494.42'	'2494.43'	' -4.75'	'80'	'100'	' 5'
'KKTEREDLIAYLKKATNE'	'2149.16'	'2149.17'	' -4.90'	'87'	'104'	' 5'
'KKTEREDLIAYLKKATNE'	'2149.21'	'2149.17'	' 15.10'	'87'	'104'	' 5'
'KTGQAPGFTYTDANKNKGITWKEETLMEYLENPKKYIPGTK'	'4689.34'	'4689.38'	' -9.13'	'39'	' 79'	' 6'
'KTGQAPGFTYTDANKNKGITWKEETLMEYLENPKKYIPGTK'	'4689.43'	'4689.38'	' 10.87'	'39'	' 79'	' 6'
'MIFAGIKKKTEREDLIAYLKKATNE'	'2909.60'	'2909.60'	' -1.50'	'80'	'104'	' 6'
'TGPNLHGLFGRKTGQAPGFTYTDANKNKGITWKEETLMEYLENPKKYIPGTK'	'5838.94'	'5838.98'	' -7.85'	'28'	' 79'	' 7'
'TGPNLHGLFGRKTGQAPGFTYTDANKNKGITWKEETLMEYLENPKKYIPGTK'	'5839.05'	'5838.98'	' 12.15'	'28'	' 79'	' 7'
'KTGQAPGFTYTDANKNKGITWKEETLMEYLENPKKYIPGTKMIFAGIK'	'5449.86'	'5449.81'	' 8.86'	'39'	' 86'	' 7'
'TGQAPGFTYTDANKNKGITWKEETLMEYLENPKKYIPGTKMIFAGIKK'	'5449.86'	'5449.81'	' 8.86'	'40'	' 87'	' 7'
'YIPGTKMIFAGIKKKTEREDLIAYLKKATNE'	'3568.96'	'3568.97'	' -3.05'	'74'	'104'	' 7'
'GITWKEETLMEYLENPKKYIPGTKMIFAGIKKKTEREDLIAYLKKATNE'	'5759.03'	'5759.07'	' -7.43'	'56'	'104'	'10'

Table 5. 6 Continued

'GITWKEETLMEYLENP KKYIPGTKMIFAGIKKK TEREDLIAYLKKATNE'	'5759.14'	'5759.07'	' 12.56'	'56'	'104'	'10'
'NKGITWKEETLMEYLE NPKKYIPGTKMIFAGIK KKTEREDLIAYLKKAT NE'	'6001.25'	'6001.21'	' 7.41'	'54'	'104'	'11'
'TGQAPGFTYTDANKNK GITWKEETLMEYLENP KKYIPGTKMIFAGIKKK TEREDLIAYLKKATNE'	'7452.92'	'7452.88'	' 6.08'	'40'	'104'	'12'

Table 5. 7 Cytochrome *c* tryptic peptides generated in 6 h limited trypsin digestion.

 Obs. Mass: observed mass; Theo. Mass: theoretical mass; error: matching error; start: start residue position; end: end residue position; mscl: missed cleavage number.
number of matched fragment peptides: 47; MOWSE score 23.46

Fragment sequence	Obs. Mass	Theo. Mass	Error	Start	End	mscl
'CAQCHTVEK'	'1017.44'	'1017.44'	' 5.42'	'14'	' 22'	'0'
'TGPNLHGLFGR'	'1167.62'	'1167.61'	' 7.80'	'28'	' 38'	'0'
'TGQAPGFTYTDANK'	'1469.69'	'1469.68'	' 4.84'	'40'	' 53'	'0'
'EETLMEYLENPK'	'1494.70'	'1494.69'	' 8.79'	'61'	' 72'	'0'
'MIFAGIK'	' 778.44'	' 778.44'	'-3.13'	'80'	' 86'	'0'
'GDVEKGK'	' 773.40'	' 773.39'	' 5.79'	' 1'	' 7'	'1'
'KIFVQK'	' 761.47'	' 761.48'	'-13.38'	' 8'	' 13'	'1'
'TGPNLHGLFGRK'	'1295.72'	'1295.71'	' 11.18'	'28'	' 39'	'1'
'KTGQAPGFTYTDANK'	'1597.77'	'1597.77'	' -3.39'	'39'	' 53'	'1'
'TGQAPGFTYTDANKNK'	'1711.84'	'1711.82'	' 11.98'	'40'	' 55'	'1'
'GITWKEETLMEYLENPK'	'2080.04'	'2080.02'	' 8.25'	'56'	' 72'	'1'
'EETLMEYLENPKK'	'1622.79'	'1622.79'	' 3.08'	'61'	' 73'	'1'
'KYIPGTK'	' 805.47'	' 805.47'	' 4.21'	'73'	' 79'	'1'
'MIFAGIKK'	' 906.53'	' 906.54'	' -2.13'	'80'	' 87'	'1'
'TEREDLIAYLK'	'1349.74'	'1349.72'	' 12.98'	'89'	' 99'	'1'
'EDLIAYLKK'	'1091.63'	'1091.62'	' 6.31'	'92'	'100'	'1'
'GDVEKGKK'	' 901.49'	' 901.49'	' 4.50'	' 1'	' 8'	'2'
'HKTGPNLHGLFGRK'	'1560.88'	'1560.86'	' 8.68'	'26'	' 39'	'2'
'KTGQAPGFTYTDANKNK'	'1839.93'	'1839.91'	' 8.89'	'39'	' 55'	'2'
'NKGITWKEETLMEYLENPK'	'2322.17'	'2322.16'	' 7.72'	'54'	' 72'	'2'
'GITWKEETLMEYLENPKK'	'2208.13'	'2208.11'	' 5.93'	'56'	' 73'	'2'
'KTEREDLIAYLK'	'1477.82'	'1477.81'	' 4.55'	'88'	' 99'	'2'
'TEREDLIAYLKK'	'1477.82'	'1477.81'	' 4.55'	'89'	'100'	'2'
'EDLIAYLKKATNE'	'1506.80'	'1506.79'	' 4.83'	'92'	'104'	'2'
'KIFVQKCAQCHTVEKGGK'	'2003.08'	'2003.04'	' 17.28'	' 8'	' 25'	'3'
'TGPNLHGLFGRKTGQAPGFTYTDANKNK'	'2989.55'	'2989.52'	' 10.07'	'28'	' 55'	'3'
'TGQAPGFTYTDANKNKGITWKEETLMEYLENPK'	'3773.86'	'3773.82'	' 10.19'	'40'	' 72'	'3'
'NKGITWKEETLMEYLENPKK'	'2450.28'	'2450.25'	' 12.80'	'54'	' 73'	'3'

Table 5. 7 Continued

'GITWKEETLMEYLENPKKYIPGTK'	'2867.50'	'2867.48'	' 9.05'	'56'	' 79'	'3'
'KKTEREDLIAYLK'	'1605.91'	'1605.91'	' -2.23'	'87'	' 99'	'3'
'KTEREDLIAYLKK'	'1605.91'	'1605.91'	' -2.23'	'88'	'100'	'3'
'TEREDLIAYLKKATNE'	'1893.01'	'1892.98'	' 11.47'	'89'	'104'	'3'
'KTGQAPGFTYTDANKNKGITWKEETLMEYLENPK'	'3901.96'	'3901.92'	' 10.20'	'39'	' 72'	'4'
'TGQAPGFTYTDANKNKGITWKEETLMEYLENPKK'	'3901.96'	'3901.92'	' 10.20'	'40'	' 73'	'4'
'NKGITWKEETLMEYLENPKKYIPGTK'	'3109.62'	'3109.62'	' 1.93'	'54'	' 79'	'4'
'MIFAGIKKKTEREDLIAYLK'	'2366.39'	'2366.34'	' 19.57'	'80'	' 99'	'4'
'KKTEREDLIAYLKK'	'1734.03'	'1734.00'	' 13.79'	'87'	'100'	'4'
'KTEREDLIAYLKKATNE'	'2021.11'	'2021.08'	' 13.74'	'88'	'104'	'4'
'KTGQAPGFTYTDANKNKGITWKEETLMEYLENPKK'	'4030.05'	'4030.01'	' 8.52'	'39'	' 73'	'5'
'GITWKEETLMEYLENPKKYIPGTKMIFAGIKK'	'3756.02'	'3756.00'	' 3.75'	'56'	' 87'	'5'
'KKTEREDLIAYLKKATNE'	'2149.18'	'2149.17'	' 1.10'	'87'	'104'	'5'
'KTGQAPGFTYTDANKNKGITWKEETLMEYLENPKKYIPGTK'	'4689.36'	'4689.38'	' -3.13'	'39'	' 79'	'6'
'KTGQAPGFTYTDANKNKGITWKEETLMEYLENPKKYIPGTK'	'4689.46'	'4689.38'	' 16.87'	'39'	' 79'	'6'
'TGQAPGFTYTDANKNKGITWKEETLMEYLENPKKYIPGTKMIFAGIK'	'5321.72'	'5321.71'	' 0.22'	'40'	' 86'	'6'
'MIFAGIKKKTEREDLIAYLKKATNE'	'2909.62'	'2909.60'	' 4.50'	'80'	'104'	'6'
'KTGQAPGFTYTDANKNKGITWKEETLMEYLENPKKYIPGTKMIFAGIK'	'5449.89'	'5449.81'	' 14.86'	'39'	' 86'	'7'
'TGQAPGFTYTDANKNKGITWKEETLMEYLENPKKYIPGTKMIFAGIKK'	'5449.89'	'5449.81'	' 14.86'	'40'	' 87'	'7'

PUBLICATIONS

1. N. Wang, A. L. Pilo, F. Zhao, S. A. McLuckey. Gas-Phase Rearrangement Reaction of Schiff-Base-Modified Peptide Ions. Rap. Comm. Mass Spec. 32(2018), 2166-2173.

2. F. Zhao, S. M. Matt, J. Bu, O. G. Rehrauer, D. Ben-Amotz, S. A. McLuckey. Joule Heating and Thermal Denaturation of Proteins in Nano-ESI Theta Tips. J. Am. Soc. Mass Spectrom. 28(2017), 2001-2010.

3. J. Bu, Z. Peng, F. Zhao, S. A. McLuckey. Enhanced Reactivity in Nucleophilic Acyl Substitution Ion/Ion Reactions Using Triazole-Ester Reagents. J. Am. Soc. Mass Spectrom. 28(2017), 1254-1261.

4. L. Pilo, F. Zhao, S. A. McLuckey. Selective Gas-Phase Oxidation and Localization of Alkylated Cysteine Residues in Polypeptide Ions via Ion/Ion. Chemistry. J. Proteome. Res. 15(2016), 3139-3146.

5. M. Fisher, R. T. Hilger, F. Zhao, S. A. McLuckey. Electroosmotically Driven Solution Mixing in Borosilicate Theta Glass nESI Emitters. J. Mass Spectrom. 50(2015), 1063-1070.

CrossMark

RESEARCH ARTICLE

Joule Heating and Thermal Denaturation of Proteins in Nano-ESI Theta Tips

Feifei Zhao, Sarah M. Matt, Jiexun Bu, Owen G. Rehrauer, Dor Ben-Amotz, Scott A. McLuckey

Department of Chemistry, Purdue University, 560 Oval Drive, West Lafayette, IN 47907-2084, USA
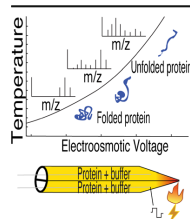
Abstract. Electro-osmotically induced Joule heating in theta tips and its effect on protein denaturation were investigated. Myoglobin, equine cytochrome *c*, bovine cytochrome *c*, and carbonic anhydrase II solutions were subjected to electro-osmosis in a theta tip and all of the proteins were denatured during the process. The extent of protein denaturation was found to increase with the applied square wave voltage and electrolyte concentration. The solution temperature at the end of a theta tip was measured directly by Raman spectroscopy and shown to increase with the square wave voltage, thereby demonstrating the effect of Joule heating through an independent method. The electro-osmosis of a solution comprised of myoglobin, bovine cytochrome *c*, and ubiquitin demonstrated that the magnitude of Joule heating that causes protein denaturation is positively correlated with protein melting temperature. This allows for a quick determination of a protein's relative thermal stability. This work establishes a fast, novel method for protein conformation manipulation prior to MS analysis and provides a temperature-controllable platform for the study of processes that take place in solution with direct coupling to mass spectrometry.

Keywords: Joule heating, Theta tip, Electro-osmosis, Protein denaturation

Introduction

Nano-electrospray ionization (nESI) is used to generate gaseous ions of biomolecules such as proteins, carbohydrates, lipids, etc. [1, 2]. Proteins normally result in multiply charged ions when subjected to electrospray ionization and charge state distributions are related to protein conformation. It is generally accepted, for example, the magnitude of charges is relatively high for unfolded conformations, which are described as high charge state distributions, while more folded conformations usually display relatively low charge state distributions [3–5]. For this reason, charge state distributions have been used in a biophysical context to monitor protein conformations using mass spectrometry. The magnitude of protein ion charge also has analytical implications. For example, high charge state ions are more efficiently detected by charge sensitive detectors like those used by Fourier transform based mass analyzers [6]. Furthermore, increasing the charge state of a protein ion can lead to improved sequence coverage in top-down analysis [7–9], especially when electron transfer dissociation (ETD) and electron capture dissociation (ECD) are used as dissociation methods [10]. Therefore, in-source protein denaturation can be desirable for the primary structural characterization of a protein via tandem mass spectrometry.

Tertiary and quaternary protein structures are stabilized by various interactions including salt bridges, hydrogen bonding, hydrophobic interactions and van der Waals interactions [11, 12]. These interactions can be affected by a variety of factors including temperature [4, 13–15], pH [16–18], ionic strength [19], solvent [20–22], surface effects [23], as well as instrumental parameters [24]. Most methods intended to change protein conformation involve bulk solution manipulations, such as the addition of acid, base, organic solvent, supercharging reagents [14] or other additives, as well as heating. These methods can be time consuming and require larger sample volumes. In recent years, fast conformation manipulation methods in conjunction with ESI have been developed, including vapor exposure [25–27], electrothermal denaturation [24, 28], and theta tip mixing [29–32]. During vapor exposure, the ESI droplets containing the protein are allowed to

Correspondence to: Scott McLuckey; *e-mail:* mcluckey@purdue.edu

interact with acidic or basic vapors added to the nitrogen curtain gas, leading to protein denaturation or refolding on the basis of pH changes [25, 26]. The electrothermal supercharging method manipulates protein conformation by changing the ionization voltage [24]. It has been reasoned that by applying a high spray voltage the droplet size is increased, thereby elongating its lifetime in the hot capillary interface and maximizing the thermal denaturation of the protein in the droplet.

Theta tips are nESI dual channel emitters that also function as micro-mixers prior to the ionization step [29]. They are pulled from theta capillaries made of borosilicate glass that contain a septum in the center dividing a capillary into two separate channels into which different solutions can be loaded. A platinum wire is placed in each channel to apply spraying and mixing voltages. By applying the same ESI voltage to both channels, the solutions are sprayed out simultaneously and subsequently mix in the Taylor cone as well as in the ensuing droplets on a sub-millisecond time scale [29, 33]. This method has been applied to study protein unfolding and folding by mixing protein solutions with acid or ammonium acetate in the theta tip Taylor cone and droplets [29, 30, 32]. Due to the short mixing time, short-lived unfolding intermediates have been observed [29]. A more recent study has shown that electro-osmotic flow can be induced between channels of a theta tip when applying differential voltages in the two channels [31]. The duration and extent of mixing can be controlled by tuning the applied voltage and time of electro-osmosis. The solution phase mixing overcomes the reagent volatility limitation in the vapor exposure strategy [25, 27] and does not require a special mass spectrometric interface set up. However, the mixing step can alter the protein solution pH and composition if the two sides are mixed with dissimilar solutions. This is unfavorable for reagent or pH-sensitive studies like covalent modification and HDX [34]. Here we demonstrate thermal denaturation of proteins in theta tips via Joule heating, which can be a useful way to manipulate protein conformation without altering solution composition.

Joule heating, also known as resistive or ohmic heating, arises from an electrical current passing through a conductor or semi-conductor. It is widely used in various research areas including, for example, melting point measurements [35], controlling thermosensitive polymer behavior [36], and facilitating chemical reactions [37]. Joule heating in electrophoretic separation has been well-studied as it has been shown to reduce separation efficiency [38]. The magnitude of the temperature change due to Joule heating in a solution is related *inter alia* to voltage, molar conductivity, and concentration via the following relationship:

$$\Delta T \sim V^2 \Lambda c \tag{1}$$

where ΔT is the temperature change (°C), V is the voltage (V), Λ is the molar conductivity ($S \cdot m^2 \cdot mol^{-1}$) of the electrolyte and c is the electrolyte concentration ($mol \cdot L^{-1}$). Other factors that affect the temperature change include geometric considerations, such as the radius at the tip, glass thickness, heat dissipation, etc. [38, 39]. The small size of the theta tip, and the associated large resistance, implies that Joule heating is expected to produce a substantial temperature rise near the apex of a theta tip (the upper limit of which may be roughly estimated as described in the SI). Herein, we demonstrate Joule heating in a theta tip resulting from electro-osmosis and take advantage of the effect to thermally denature proteins. The solution temperature was directly measured by Raman spectroscopy to establish a relationship between voltage and temperature. The influence of voltage and electrolyte concentration on the magnitude of Joule heating was investigated.

Experimental

Materials and Methods

Myoglobin from equine skeletal muscle, cytochrome *c* from bovine heart, cytochrome *c* from equine heart, ubiquitin from bovine erythrocytes, carbonic anhydrase II from bovine erythrocytes, and ammonium acetate were purchased from Sigma Aldrich (St. Louis, MO, USA). HPLC grade water was purchased from Fisher Scientific (Fair Lawn, NJ, USA). All proteins were dissolved in 0, 5, or 10 mM ammonium acetate solution at pH around 6 and the final protein concentration is 5–20 μM unless specifically noted. Proteins and chemical reagents were used without further purification.

Capillaries and Tip Holder

Dual channel borosilicate theta capillaries (1.5 mm o.d., 1.17 mm i.d., 0.165 mm septum thickness, 10 cm length) were purchased from Sutter Instrument Co. (Novato, CA, USA). Theta capillaries were pulled to theta tips (o.d. 10 μm) using a Flaming/Brown micropipette puller (P-87) from Sutter Instrument Co.

Solutions were loaded into both channels of a theta tip, which was held by a theta tip holder from Warner Instruments, LLC (Hamden, CT, USA), pictured in Supplemental Figure S-1. The original silver wires in the holder were replaced with Teflon coated platinum wires (A-M Systems, Sequim, WA, USA) to avoid discharge between the wires at the back of the theta capillary when voltages applied to the wires were different. The two wires were inserted into each channel of a theta tip to apply voltage to each side independently.

Mass Spectrometry

A quadrupole/time-of-flight (QqTOF) tandem mass spectrometer (QStar Pulsar XL; Sciex, Concord, ON, Canada) was used to perform all mass spectrometric experiments. The experimental procedure consists of four steps: electro-osmosis, ionization, dump spray, and mass analysis. In the electro-osmosis step the protein solution was electrically pumped back and forth between the two channels by grounding the wire in one theta tip channel while applying 100 ms of 10 Hz square wave voltage to the wire in the opposite channel. The square wave duty cycle

is 50% and the voltage is ±100 V to ±500 V, where "±" was used to indicate the switch between positive and negative voltages during an electro-osmotic cycle. Next, the ionization step was triggered (1500 V on both wires, 80 ms), during which the ions are accumulated in Q2. The dump spray step was then triggered to spray out any residual analyte that had been exposed to the electro-osmosis step. For this purpose, a dump spray step of 200 ms was found sufficient to return the mass spectrum to that of the pre-osmosis step. The ion path voltages were set such that no ions were accumulated in Q2 during the dump spray step. Finally, the mass spectrum was recorded during the 150 ms mass analysis step. The power supplies and detailed trigger system are summarized in Supplemental Figure S-2.

Raman Temperature Measurements

Temperature measurements within the theta tip were conducted off-line using a set-up to simulate the theta tip arrangement in front of the mass spectrometer. To measure the solution temperature via Raman spectroscopy, the timing of the voltages applied to the wires in the theta tip was designed to simulate the various steps described above for the mass spectrometry experiments. The detailed triggering method is shown in Supplemental Figure S-3.

The temperature of the fluid near the apex of the theta tip was obtained noninvasively using Raman spectroscopy. The micro-Raman spectra were measured using a custom-built instrument that includes a 532 nm laser excitation (Coherent Sapphire SF CDRH 532 nm) and a TE-cooled CCD (Princeton Instruments SP2300). A 100× objective (Olympus LM Plan Fl) with a working distance of 3.4 mm was used to both focus the laser and collect the backscattered Raman signal. Laser power at the sample was set to 24.5 mW. Fine positional control was accomplished with a motorized microscope stage (Prior H101A/C). For the Raman experiments, both channels of the theta tip were filled with 5 mM ammonium acetate. Consecutive spectra with 100 ms exposure time were acquired while continuously cycling through the process of electro-osmosis-spray-simulated mass analysis. To obtain the training spectra for temperature calibration, a Pyrex 9530-3 borosilicate glass capillary (1.5–1.8 mm o.d., 90 mm length) was filled with 18.2 MΩ cm ultrapure water and heated using a Physitemp TS-4MPER thermal stage to temperatures between 20 °C and 90 °C, measured using a needle thermocouple (Physitemp MT-26/4 with an Omega DP701 reader). The temperature training spectra were collected with an integration time of 5 min per spectrum. Two representative training spectra corresponding to 30.3 °C and 74.3 °C are shown in Figure 5 insert (b).

The shape and intensity of the OH stretching mode of water is highly temperature-dependent and has been used in the past for Raman thermometry. For example, D'Arrigo et al. calibrated temperatures based on a ratio of OH stretch areas with respect to measured temperature values from a thermocouple [40]. These areas were based on an approximate isosbestic point near 3400 cm^{-1}, and the calibrated value was the ratio

of the OH area to the left and to the right of that point. We employed an alternative hyperspectral procedure using self-modeling curve resolution (SMCR) to decompose the OH stretch into the two primary spectral components such that each spectrum is a linear combination of those two components. Each spectrum was first baseline-subtracted in the OH stretch region using a quadratic fit to user-defined points in the baseline on either side of the OH band. Next, using the baseline subtracted training spectra, a quadratic calibration curve relating measured temperature to a parameter representing the fractional spectral weight of the high temperature component in each measured spectrum was generated. Then for each experimental spectrum, a total least squares fit of the measured spectrum to the two SMCR components was used to quantify the fractional weight of the high temperature component, which was in turn converted to temperature using the training calibration curve. Two of these experimental spectra and their corresponding temperature values are shown in Figure 5 insert (b).

The Raman measurements were obtained asynchronously at a frame rate of about 6 fps, and subsequently synchronized with the applied voltage cycles to create plots similar to Figure 5 insert (a). Each curve of Figure 5 insert (a) includes 400 Raman measured temperature data points and approximately 110 cycles of electro-osmosis-spray-simulated mass analysis process.

Results and Discussion

Electro-osmosis Induced Protein Denaturation

Bovine carbonic anhydrase II, a 29 kDa protein reported to have a melting point of 64 °C [41], has been the subject of folding/denaturation studies under a variety of conditions, and several conformational states have been noted [42–44]. Mass spectrometry studies of conventional pH-induced unfolding of carbonic anhydrase II was also reported [29]. In its native state (i.e., the holo-carbonic anhydrase II (hCA II) form), a Zn^{2+} co-factor is present [45], although the presence of Zn^{2+} has not been observed to be key to folding of this protein. When hCA II dissolved in a 5 mM NH$_4$OAc aqueous solution was subjected to nESI from a theta tip without an electro-osmosis step, a narrow charge state distributions centered at +11 was observed containing the Zn^{2+} cofactor (Figure 1a). One hundred milli-seconds of a 10 Hz square wave at ±200 V resulted in the generation of higher charge states of hCA II (Figure 1b) with the +15 charge state being most abundant of the newly apparent charge states. The ±200 V square wave with 50% duty cycle induced a bidirectional electro-osmosis, which suppressed the bulk motion of the solutions from one channel to the other. Therefore, the small amount of denatured protein subjected to electro-osmosis can be cleared up by applying a dump spray voltage for 200 ms to regain the pre-osmosis spectrum. At ±230 V, a more extensive shift in charge states of hCA II was noted, along with low levels of apo-carbonic anhydrase II (aCA II) ions over a wide range of charge states (Figure 1c). In this case, the +18 charge state was most abundant of the higher
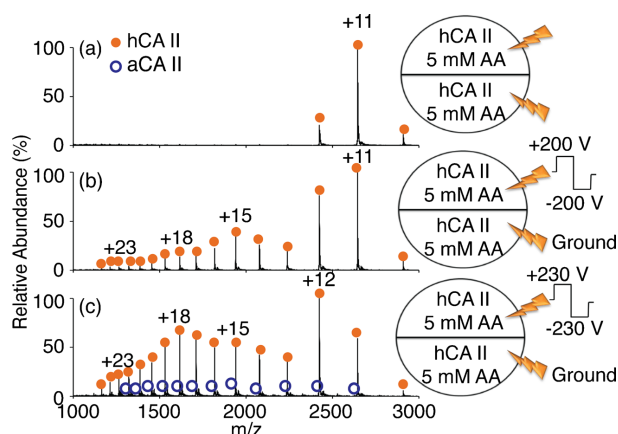
Figure 1. (**a**) Positive nESI of a solution of bovine CA II in 5 mM NH$_4$OAc (AA) solution, sprayed out of a theta tip with no electro-osmosis. Mass spectra of the same CA II solution after electro-osmosis via 100 ms of a 10 Hz square wave at (**b**) ±200 V and (**c**) ±230 V. The circles at the right of the spectra indicate the theta tip schematic; an aliquot of the same sample was loaded in each channel, and the lightning bolts depict the voltage applied to each side

charge states. The abundance pattern of the higher charge states is also suggestive of the presence of several charge state distributions. The data of Figure 1 clearly suggest that protein denaturation can take place upon electro-osmosis in the theta tip and that the extent of denaturation increases with the square wave voltage.

Myoglobin is another extensively studied globular protein and has a reported melting temperature of 76 °C at neutral pH [46]. In its native state, myoglobin contains a noncovalently-bound heme ligand. It is referred to as holo-myoglobin (hMb) when the heme group is present and apo-myoglobin (aMb) when it is absent. When exposed to heat, hMb undergoes stepwise unfolding through a series of intermediates [47]. The initial stage of unfolding involves a slight extension of the tertiary structure while preserving the heme ligand. In the following phase, a dramatic tertiary structure alteration occurs, resulting in the loss of the heme ligand and generation of unfolded aMb. Further heating of the protein may lead to polymerization of aMb before precipitation. Accumulated free heme ligand can also polymerize or nonspecifically attach to aMb and hMb [48]. The inserts of Figure 2 show a selection of nESI spectra obtained as a function of square wave voltage in a theta tip. Both channels of the theta tip contained a myoglobin solution in 5 mM NH$_4$OAc solution. Figure 2 shows the spectrum of myoglobin sprayed after applying 100 ms of square wave at a voltage of ±150 V. The spectrum as well as those obtained at lower square wave voltages are essentially identical to that obtained in the absence of electro-osmosis (not shown) and clearly suggests that the native hMb conformation is preserved because of the retention of the heme group and the low charge state distributions centered at +8. The insert of Figure 2b shows the spectrum obtained after 100 ms electro-osmosis induced by a

10 Hz ±230 V square wave. At this voltage, a portion of the hMb cation population lost the heme ligand to form aMb ions in two clearly apparent charge state distributions with maxima at +14 and +9, respectively, as shown by the open, green circles in Figure 2b. With the square wave voltage increased to ±300 V, the original hMb charge states were further depleted and the higher charge state aMb peaks grew in relative abundance (see the insert of Figure 2c). Some of the lost heme ligand was observed to attach to hMb to form a complex with two heme groups, as indicated by the blue triangles. The attachment of more than one heme group to denatured hMb has been noted in solution phase studies [49, 50]. The spectra of the inserts (b) and (c) show at least two distinct charge state distributions for aMb ions, which likely reflects distinct folding states of aMb. The plot of Figure 2 shows the percentage of aMb ion signal relative to total myoglobin ion signal (aMb+hMb ions) as a function of square wave voltage with the solid line representing a sigmoidal fit to the data. Although this plot does not reflect the evolution of different folding states of aMb, the percentage of aMb ions provides an overall reflection of the extent of denaturation of the protein. If the aMb ions are taken as representing any unfolded state while the hMb ions are taken as representative of the native state, the plot of Figure 2 treats myoglobin as a two-state system (i.e., folded versus unfolded). A sigmoidal shape for the percentage of the unfolded state as a function of denaturation condition (e.g., temperature, pH, concentration of denaturant, etc.) is expected for such a scenario [51].

Similar phenomena were noted with equine cytochrome *c* (eCyt *c*), which has a reported melting temperature of 85 °C [52]. This protein contains a covalently bound heme ligand, which remains bound to the protein upon denaturation [53]. Therefore, upon heating, eCyt *c* mainly undergoes tertiary
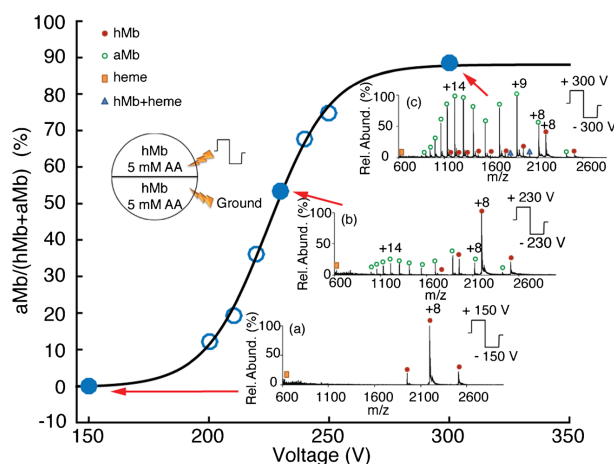
Figure 2. A plot of the percentage of aMb ions relative to all myoglobin ions (aMb+hMb) as a function of square wave voltage. Insert (**a**) positive nESI mass spectrum of a solution of hMb in 5 mM NH_4OAc (AA) solution, sprayed out of a theta tip with no electro-osmosis. Insert (**b**) mass spectrum of the same hMb solution after electro-osmosis via 100 ms of a 10 Hz square wave at ±230 V. Insert (**c**) mass spectrum obtained with a square wave voltage of ±300 V. Green open circles represent charge states of aMb, red closed circles represent charge states of hMb, blue triangles represent hMb with an additional heme group, filled gold square represents heme ion

structure extension, reflected by an increase in charge states in nESI mass spectra. In this case, we use the abundance weighted average charge state of the protein as a reflection of the extent of denaturation as a function of square wave voltage in the plot of Figure 3. These results were obtained from series of nESI mass spectra derived from eCyt c in an aqueous solution of 5 mM NH_4OAc as a function of square wave voltage. Inserts **(a)**–**(c)** show the mass spectra obtained using 100 ms of 10 Hz square wave at voltages of ± 290 V, ±310 V, and 340 V, respectively.

Collectively, the results for these proteins showed that protein denaturation under conditions of electro-osmosis in a theta tip at relatively high square wave voltages is a general phenomenon. Furthermore, the extent of denaturation was found to be both condition-dependent (e.g., the magnitude of the square wave voltage) and protein-dependent (e.g., higher square wave voltages were required to denature proteins with higher melting temperatures). The results are consistent with thermal denaturation as a result of Joule heating at the end of the theta tip during electro-osmosis.

Influence of Ammonium Acetate Concentration on Protein Denaturation

Ammonium acetate is a commonly used additive in native mass spectrometry [2]. High concentration of ammonium acetate displaces nonvolatile adducts and reduces the nonvolatile components influence [54]. It also stabilizes the native conformation of proteins in solution through ionic specific interaction, which is normally referred to as Hofmeister effects [55, 56]. The protein–ligand dissociation constant also decreases with higher ammonium acetate concentration when the protein's isoelectric point is higher than the pH of the solution [57]. The isoelectric point of myoglobin is 6.8–7.4, whereas the 5 mM ammonium acetate solution pH is around 6. At this pH, ammonium acetate enhances the retention of the heme in the myoglobin binding pocket. Since holo-myoglobin stability is determined by the heme ligand affinity [58], the high binding affinity of the heme in ammonium acetate solution can further stabilize myoglobin.

Based solely on the considerations mentioned above, an increase in ammonium acetate concentration in the theta tip under electro-osmosis conditions might be expected to inhibit the extent of denaturation. However, as demonstrated in Figure 4, the extent of denaturation increases with a doubling of ammonium acetate concentration. Figure 4a shows a mass spectrum of myoglobin obtained using deionized water (i.e., no added ammonium acetate) after 100 ms of electro-osmosis at ±230 V. The result is consistent with the native protein (i.e., low charge state distributions of hMb ions), suggesting that denaturation does not take place to a detectable extent under such solution conditions. Using the same square wave voltage, the addition of 5 mM NH_4OAc to the protein solution results in the spectrum in Figure 2b, which shows clear evidence for protein denaturation via the appearance of two aMb distributions. The hMb low charge state distributions remains highly abundant, however, which indicates that much of the protein in solution sampled by the mass spectrometer remains in the
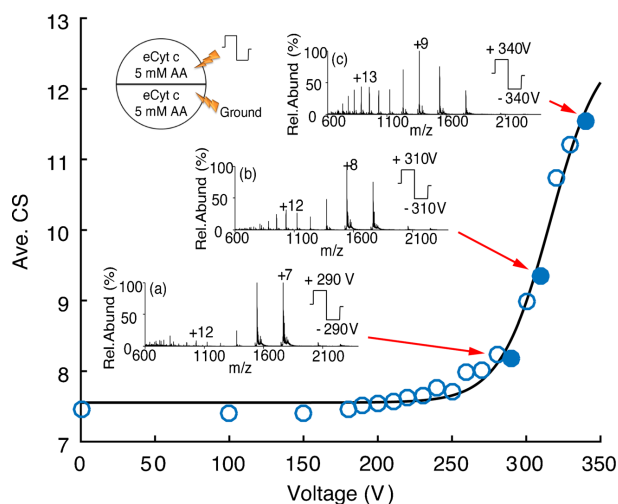
Figure 3. A plot of the abundance weighted average charge state of eCyt *c* ions as a function of square wave voltage after 100 ms of a 10 Hz square wave applied to a solution of eCyt *c* in 5 mM NH$_4$OAc (AA) solution. Insert (**a**) positive nESI mass spectrum obtained using ±290 V. Insert (**b**) mass spectrum obtained using ±310 V. Insert (**c**) mass spectrum obtained using ±340 V

native state. Figure 4b shows the spectrum obtained using 10 mM NH$_4$OAc where significant myoglobin denaturation during electro-osmosis was observed. The bimodal distribution of aMb peaks became dominant with only a small amount of hMb peaks remaining. The excess heme ligand formed via electro-osmosis is observed to form a nonspecific complex with hMb, indicating further denaturation. Electro-osmosis using ±200 V of bovine cytochrome *c* (bCyt *c*) in 5 mM and 10 mM NH$_4$OAc solution showed the same trend, where the 10 mM NH$_4$OAc solution gave rise to higher bCyt *c* denaturation (Supplemental Figure S-4). These results are consistent with an increase in Joule heating due to an increase in the conductivity of the solution with increasing electrolyte

concentration (see Equation 1), which overcomes any stabilization effects that might otherwise arise with increasing ammonium acetate concentration. The effect of electrolyte concentration, in addition to the voltage effect described above, provides another indirect piece of evidence for Joule heating.

Temperature Measurements Using Raman Spectroscopy

Protein denaturation can arise in a variety of ways and therefore provides only indirect evidence for Joule heating in a theta tip during electro-osmosis. We therefore examined the temperature of the solution very near to the end of the tip as a function
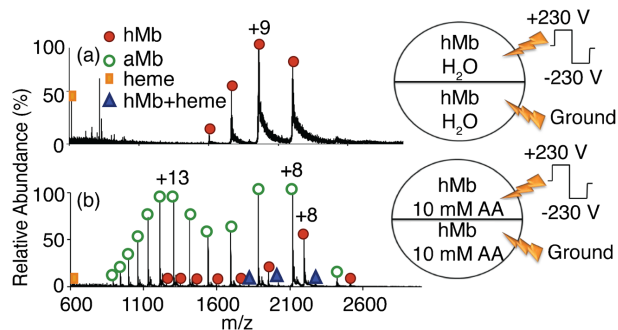

Figure 4. Electro-osmosis of myoglobin at ±230 V for 100 ms in (**a**) deionized water; (**b**) 10 mM NH$_4$OAc (AA) solution. The circles at the right of the spectra indicate the theta tip schematic; an aliquot of the same sample was loaded in each channel, and the lightning bolts depict the voltage applied to each side
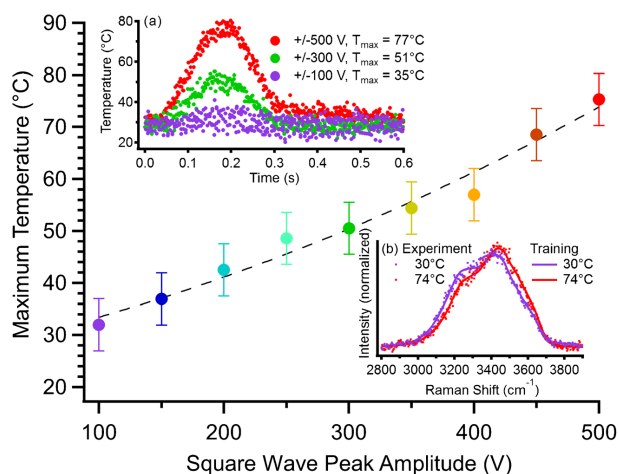
Figure 5. Raman thermometry measurements of 5 mM NH_4OAc solution in a theta tip. Maximum temperature reached during the electro-osmosis step is plotted with respect to the applied square wave peak amplitude. The dotted black line is included to guide the eye is a quadratic fit to the data points. Insert (**a**) shows the temperature profile during the electro-osmosis-spray-MS detection process with ±100 V (violet), ±300 V (green), and ±500 V (red). Insert (**b**) shows representative training spectra (lines) for two temperature values and shows experimental spectra taken during electro-osmosis (dots) to illustrate the sensitivity of the Raman measurements to temperature

of operating conditions. The highest resistance to current flow is expected to be at the narrowest point of the channel, which is at the end of the tip; thus the Joule heating effect is the strongest at the end of the tip. It was therefore desirable to be able to measure temperature in a small volume at or near the end of the tip to minimize error associated with the bulk solution elsewhere in the theta tip. The measurement of Raman scattering from a tightly focused laser spot, estimated to be 8–15 fL with our system, provides the needed spatial resolution. To measure the solution temperature during each step (electro-osmosis, spray, and mass analysis), a voltage supply and triggering system was established to mimic the procedure used in the mass spectrometry experiments, as described in Supplemental Figure S-3. A 5 mM NH_4OAc solution was loaded into both channels of the theta tip. The duration of electro-osmosis, spray, and mass analysis steps were set to 100 ms, 300 ms, and 200 ms, respectively, as in the MS experiment. A 10 Hz square wave was used to induce 100 ms of electro-osmosis with voltage values from ±100 V to ±500 V. The solution temperature was measured during this process and the resultant temperatures are shown in Figure 5. During the electro-osmosis step, the solution temperature increased from room temperature to maximum temperature. When the square wave was completed, the solution temperature cooled down and reached the starting room temperature, as shown in Figure 5 insert (a).

Figure 5 shows how the maximum solution temperature obtained during the electro-osmosis step is correlated to the applied square wave heating voltage. Based on the measured temperature, applying a ±200 V square wave to one channel

increased the solution temperature to about 44 °C, whereas ±300 V voltage increased the solution temperature to 51 °C. Increasing the voltage amplitude to 500 V led to a maximum temperature at 77 °C. The small size of the theta tip and the associated large resistance imply that Joule heating is expected to produce a substantial temperature rise near the apex of a theta tip (the magnitude of which may be roughly estimated as described in the Supplemental Information), although heat dissipation exists in the open system. The Raman laser measuring point is about 8 μm away from the end of the tip and the true maximum temperature at the tip apex may also be underestimated. Nevertheless, the Raman measurements directly show that the electro-osmosis process gives rise to an increase in the solvent temperature that is directly related to the square wave voltage applied to induce electro-osmosis.

Correlation Between Protein Melting Temperature and Denaturation Voltage

The melting temperature of a protein is a measure of its thermal stability towards denaturation, and several reports have employed heated ESI or nESI emitters to examine thermal denaturation of proteins and protein complexes [59–61]. Therefore, the onset and extent of protein denaturation might be expected to correlate with theta tip heating voltage. Indeed, the extents of denaturation observed for the three proteins discussed above (viz., bovine CA II, myoglobin, and eCyt *c*) are consistent with this expectation. That is, the protein with the lowest reported melting temperature (CA II) showed extensive

denaturation at the lowest square wave voltages and the protein with the highest reported melting temperature (eCyt c) required the greatest square wave voltages to lead to extensive denaturation. A more reliable comparison, however, can be made with a mixture of proteins such that all experiments are conducted with the same theta tip and solution conditions, thereby ensuring that each protein is exposed to the same extent of Joule heating. To study the correlation between protein melting temperature and heating voltage, a 5 mM NH_4OAc solution containing myoglobin (melting temperature of 76 °C [46]), bovine cytochrome c (melting temperature of 80 °C [62]), and ubiquitin (melting temperature of 100 °C [63]) was subjected to electro-osmosis in a theta tip. Since the ionization efficiencies of these three proteins are different, the concentrations of myoglobin, cytochrome c, and ubiquitin in the mixture were adjusted to 0.11, 0.07, and 0.02 mg/mL, respectively. Figure 6a shows the spectrum obtained when the protein mixture was subjected to 100 ms of electro-osmosis using a 10 Hz

±200 V square wave. No change in the mass spectrum was noted relative to the spectrum obtained without electro-osmosis (not shown), suggesting that none of the proteins underwent measurable denaturation. Myoglobin showed signs of denaturation (viz., the appearance of aMb ions of relatively high charge states) using a ±230 V square wave for heating (Figure 6b), whereas the bCyt c and ubiquitin ions remained unchanged at this voltage. The first sign of the denaturation of bCyt c, as reflected by the appearance of a higher charge state distribution, is observed at ±250 V (Figure 6c). The abundances of the higher charge state distributions of myoglobin and bCyt c were observed to increase further at ±300 V (Figure 6d) and ±500 V (Figure 6e). Ubiquitin, which has the highest melting temperature in the mixture, showed no charge state distribution change until ±500 V square wave voltage was applied. Figure 6e shows a modest charge state shift from +5 to +6 at ±500 V heating, which suggests that the ubiquitin tertiary structure might be perturbed under these conditions. Overall,
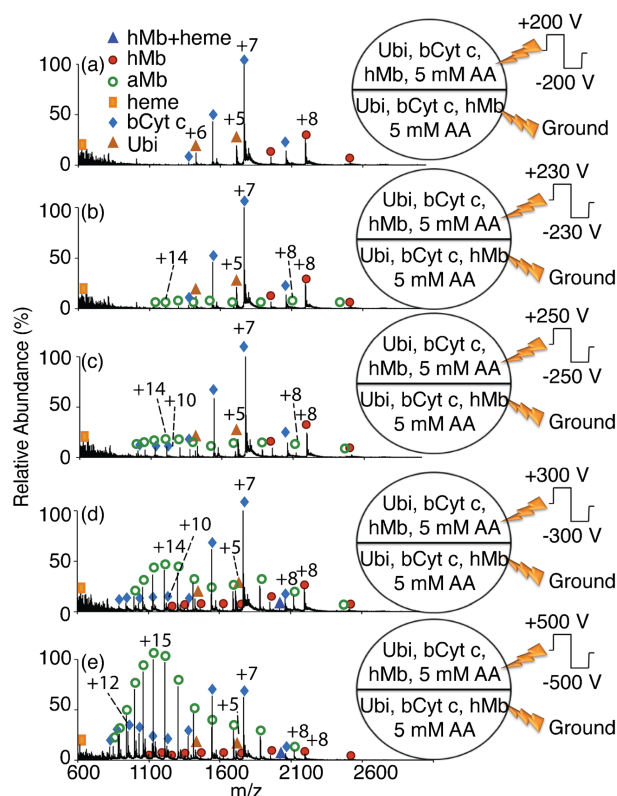
**Figure 6.** Electro-osmosis of a solution mixture of ubiquitin, bCyt c, and myoglobin in 5 mM NH_4OAc solution in a theta tip at (**a**) ±200 V; (**b**) ±230 V; (**c**) ±250 V; (**d**) ±300 V, and (**e**) ±500 V. The circles at the right of the spectra indicate the theta tip schematic; an aliquot of the same sample was loaded in each channel, and the lightning bolts depict the voltage applied to each side

these results are fully consistent with an increase in solution temperature with increasing square wave heating voltage.

Conclusions

In this report, we demonstrate protein denaturation resulting from electro-osmosis in a theta tip nano-ESI capillary. The effect is shown to arise from Joule heating via both direct and indirect evidence. Indirect evidence included an increase in the extent of protein denaturation with the magnitude of the voltage of a square wave used to effect electro-osmosis. This effect was demonstrated for myoglobin, equine cytochrome *c*, and carbonic anhydrase II solutions. Joule heating is expected to increase with field strength. An increase in the extent of denaturation for myoglobin was also observed with an increase in the ammonium acetate concentration. Joule heating is expected to increase with solution conductivity. Using Raman spectroscopy temperature measurements near to the capillary tip, an increase in solution temperature, direct evidence for Joule heating, was found to correlate with the amplitude of the square wave voltage. Electro-osmosis-induced Joule heating was observed to be positively correlated to protein melting temperature when a solution of a mixture of proteins of known melting temperature was subjected to a series of experiments with increasing square wave heating voltage. This work points to the development of a convenient and efficient way to modulate solution temperature in a nano-ESI theta tip prior to spraying into a mass spectrometer. It represents a flexible approach for controlled protein denaturation that does not depend on changes in solution additives or solvent composition. With further development, this effect may serve as the basis for a method to study protein thermal stabilities on small quantities of materials and with mixtures of proteins. Given the ability to alter temperatures in a pulsed fashion on the time-scales of tenths of seconds, this effect may also prove to be useful in studying protein unfolding and refolding dynamics on such a time-scale.

Acknowledgements

References

1. Fenn, J.B., Mann, M., Meng, C.K., Wong, S.F., Whitehouse, C.M.: Electrospray ionization for mass spectrometry of large biomolecules. Science **246**, 64–71 (1989)

2. Heck, A.J.R.: Native mass spectrometry: a bridge between interactomics and structural biology. Nat. Methods **5**, 927–933 (2008)

3. Kaltashov, I.A., Eyles, S.J.: Studies of biomolecular conformations and conformational dynamics by mass spectrometry. Mass Spectrom. Rev. **21**, 37–71 (2002)

4. Liu, J., Konermann, L.: Irreversible thermal denaturation of cytochrome *c* studied by electrospray mass spectrometry. J. Am. Soc. Mass Spectrom. **20**, 819–828 (2009)

5. Kaltashov, I.A., Abzalimov, R.R.: Do ionic charges in ESI MS provide useful information on macromolecular structure? J. Am. Soc. Mass Spectrom. **19**, 1239–1246 (2008)

6. Cassou, C.A., Williams, E.R.: Anions in electrothermal supercharging of proteins with electrospray ionization follow a reverse Hofmeister series. Anal. Chem. **86**, 1640–1647 (2014)

7. Reid, G.E., Wu, J., Chrisman, P.A., Wells, J.M., McLuckey, S.A.: Charge-state-dependent sequence analysis of protonated ubiquitin ions via ion trap tandem mass spectrometry. Anal. Chem. **73**, 3274–3281 (2001)

8. Jockusch, R.A., Schnier, P.D., Price, W.D., Strittmatter, E.F., Demirev, P.A., Williams, E.R.: Effects of charge state on fragmentation pathways, dynamics, and activation energies of ubiquitin ions measured by Blackbody infrared radiative dissociation. Anal. Chem. **69**, 1119–1126 (1997)

9. Breuker, K., Oh, H.B., Horn, D.M., Cerda, B.A., McLafferty, F.W.: Detailed unfolding and folding of gaseous ubiquitin ions characterized by electron capture dissociation. J. Am. Chem. Soc. **124**, 6407–6420 (2002)

10. Zubarev, R.A., Kelleher, N.L., McLafferty, F.W.: Electron capture dissociation of multiply charged protein cations. A nonergodic process. J. Am. Chem. Soc. **120**, 3265–3266 (1998)

11. Xu, D., Tsai, C.J., Nussinov, R.: Hydrogen bonds and salt bridges across protein-protein interfaces. Protein Eng. **10**, 999–1012 (1997)

12. Kumar, S., Nussinov, R.: Close-range electrostatic interactions in proteins. ChemBioChem **3**, 604–617 (2002)

13. Mirza, U.A., Cohen, S.L., Chait, B.T.: Heat-induced conformational changes in proteins studied by electrospray ionization mass spectrometry. Anal. Chem. **65**, 1–6 (1993)

14. Sterling, H.J., Williams, E.R.: Origin of supercharging in electrospray ionization of noncovalent complexes from aqueous solution. J. Am. Soc. Mass Spectrom. **20**, 1933–1943 (2009)

15. Gratacós-Cubarsí, M., Lametsch, R.: Determination of changes in protein conformation caused by pH and temperature. Meat Sci. **80**, 545–549 (2008)

16. Russo, N., Estrin, D., Martí, M., Roitberg, A.: pH-dependent conformational changes in proteins and their effect on experimental pKas: the case of nitrophorin 4. PLoS Comput. Biol. **8**, e1002761 (2012)

17. Park, Y., Kim, K., Lim, D., Lee, E.K.: Effects of pH and protein conformation on in-solution complexation between bovine α-lactalbumin and oleic acid: binding trend analysis by using SPR and ITC. Process Biochem. **50**, 1379–1387 (2015)

18. Thakur, G., Jiang, K., Lee, D., Prashanthi, K., Kim, S., Thundat, T.: Investigation of pH-induced protein conformation changes by nanomechanical deflection. Langmuir **30**, 2109–2116 (2014)

19. Ohyashiki, T., Taka, M., Mohri, T.: The effects of ionic strength on the protein conformation and the fluidity of porcine intestinal brush border membranes. J. Biol. Chem. **260**, 6857–6861 (1985)

20. Iavarone, A.T., Jurchen, J.C., Williams, E.R.: Effects of solvent on the maximum charge state and charge state distribution of protein ions produced by electrospray ionization. J. Am. Soc. Mass Spectrom. **11**, 976–985 (2000)

21. Nemethy, G., Peer, W.J., Scheraga, H.A.: Effect of protein–solvent interactions on protein conformation. Annu. Rev. Biophys. Bioeng. **10**, 459–497 (1981)

22. Yu, Y., Wang, J., Shao, Q., Shi, J., Zhu, W.: The effects of organic solvents on the folding pathway and associated thermodynamics of proteins: a microscopic view. Sci. Rep. **6**, 19500 (2016)

23. Mortensen, D.N., Williams, E.R.: Surface-induced protein unfolding in submicron electrospray emitters. Anal. Chem. **88**, 9662–9668 (2016)

24. Sterling, H.J., Cassou, C.A., Susa, A.C., Williams, E.R.: Electrothermal supercharging of proteins in native electrospray ionization. Anal. Chem. **84**, 3795–3801 (2012)

25. Kharlamova, A., Prentice, B.M., Huang, T., McLuckey, S.A.: Electrospray droplet exposure to gaseous acids for the manipulation of protein charge state distributions. Anal. Chem. **82**, 7422–7429 (2010)

26. Kharlamova, A., DeMuth, J.C., McLuckey, S.A.: Vapor treatment of electrospray droplets: evidence for the folding of initially denatured proteins on the sub-millisecond time-scale. J. Am. Soc. Mass Spectrom. **23**, 88–101 (2012)

27. Girod, M., Antoine, R., Dugourd, P., Love, C., Mordehai, A., Stafford, G.: Basic vapor exposure for tuning the charge state distribution of proteins in negative electrospray ionization: elucidation of mechanisms by fluorescence spectroscopy. J. Am. Soc. Mass Spectrom. **23**, 1221–1231 (2012)

28. Mortensen, D.N., Williams, E.R.: Electrothermal supercharging of proteins in native ms: effects of protein isoelectric point, buffer, and nanoESI-emitter tip size. Analyst **141**, 5598–5606 (2016)

29. Fisher, C.M., Kharlamova, A., McLuckey, S.A.: Affecting protein charge state distributions in nano-electrospray ionization via in-spray solution mixing using theta capillaries. Anal. Chem. **86**, 4581–4588 (2014)

30. Mortensen, D.N., Williams, E.R.: Investigating protein folding and unfolding in electrospray nanodrops upon rapid mixing using theta-glass emitters. Anal. Chem. **87**, 1281–1287 (2015)

31. Fisher, C.M., Hilger, R.T., Zhao, F., McLuckey, S.A.: Electro-osmotically driven solution mixing in borosilicate theta glass nESI emitters. J. Mass Spectrom. **50**, 1063–1070 (2015)

32. Mortensen, D.N., Williams, E.R.: Ultrafast (1 μs) mixing and fast protein folding in nanodrops monitored by mass spectrometry. J. Am. Chem. Soc. **138**, 3453–3460 (2016)

33. Mortensen, D.N., Williams, E.R.: Theta-glass capillaries in electrospray ionization: rapid mixing and short droplet lifetimes. Anal. Chem. **86**, 9315–9321 (2014)

34. Englander, S.W.: Hydrogen exchange and mass spectrometry: a historical perspective. J. Am. Soc. Mass Spectrom. **17**, 1481–1489 (2006)

35. Blanco, E., Ruso, J.M., Sabín, J., Prieto, G., Sarmiento, F.: Thermal stability of lysozyme and myoglobin in the presence of anionic surfactants. J. Therm. Anal. Calorim. **87**, 211–215 (2007)

36. Aseyev, V., Hietala, S., Laukkanen, A., Nuopponen, M., Confortini, O., Prez, F.E.D., Tenhu, H.: Mesoglobules of thermoresponsive polymers in dilute aqueous solutions above the LCST. Polymer **46**, 7118–7131 (2005)

37. Upadhyay, S.K.: Chemical Kinetics and Reaction Dynamics. Springer: New York City, NY; Anamaya Publishers: New Delhi, India (2006)

38. Grossman, P.D., Colburn, J.C.: Capillary Electrophoresis: Theory and Practice. Academic Press, Inc., Cambridge, MA (1992)

39. Whatley, H.: Basic principles and modes of capillary electrophoresis. In: Petersen, J.R., Mohammad, A.A. (eds.) Clinical and Forensic Applications of Capillary Electrophoresis, p. 37. Humana Press Inc, Totowa, NJ (2001)

40. D'Arrigo, G., Maisano, G., Mallamace, F., Migliardo, P., Wanderlingh, F.: Raman scattering and structure of normal and supercooled water. J. Chem. Phys. **75**, 4264–4270 (1981)

41. Sarraf, N., Saboury, A., Ranjbar, B., Moosavi-Movahedi, A.: Structural and functional changes of bovine carbonic anhydrase as a consequence of temperature. Acta Biochim. Pol. **51**, 665–671 (2004)

42. Gudiksen, K.L., Urbach, A.R., Gitlin, I., Yang, J., Vazquez, J.A., Costello, C.E., Whitesides, G.M.: Influence of the Zn(II) cofactor on the refolding of bovine carbonic anhydrase after denaturation with sodium dodecyl sulfate. Anal. Chem. **76**, 7151–7161 (2004)

43. Bushmarina, N.A., Kuznetsova, I.M., Biktashev, A.G., Turoverov, K.T., Uversky, V.N.: Partially folded conformations in the folding pathway of bovine carbonic anhydrase II: a fluorescence spectroscopic analysis. ChemBioChem **2**, 813–821 (2001)

44. Semisotnov, G.V., Rodionova, N.A., Kutyshenko, V.P., Ebert, B., Blanck, J., Ptitsyn, O.B.: Sequential mechanism of refolding of carbonic anhydrase B. FEBS Lett. **224**, 9–13 (1987)

45. Saito, R., Sato, T., Ikai, A., Tanaka, N.: Structure of bovine carbonic anhydrase II at 1.95 A resolution. Acta Crystallogr. **D60**, 792–795 (2004)

46. Wan, L., Twitchett, M., Eltis, L., Mauk, G., Smith, M.: In vitro evolution of horse heart myoglobin to increase peroxidase activity. Proc. Natl. Acad. Sci. **95**, 12825–12831 (1998)

47. Awad, E.S., Deranleau, D.A.: Thermal denaturation of myoglobin. I. Kinetic resolution of reaction mechanism. Biochemistry **7**, 1791–1795 (1968)

48. Hargrove, M., Barrick, D., Olson, J.S.: The association rate constant for heme binding to globin is independent of protein structure. Biochemistry **35**, 11293–11299 (1996)

49. Lee, V.W.S., Chen, Y.-L., Konermann, L.: Reconstitution of acid-denatured holomyoglobin studied by time-resolved electrospray ionization mass spectrometry. Anal. Chem. **71**, 4154–4159 (1999)

50. Simmons, D.A., Konermann, L.: Characterization of transient protein folding intermediates during myoglobin reconstitution by time-resolved electrospray mass spectrometry with on-line isotopic pulse labeling. Biochemistry **41**, 1906–1914 (2002)

51. Gillespie, B., Plaxco, K.W.: Nonglassy kinetics in the folding of a simple single-domain protein. Proc. Natl. Acad. Sci. U. S. A. **97**, 12014–12019 (2000)

52. Bágel'ová, J., Antalík, M., Tomori, Z.: Effect of polyglutamate on the thermal stability of ferricytochrome *c*. Biochem. Mol. Biol. Int. **43**, 891–900 (1997)

53. Milne, J., Xu, Y., Mayne, L., Englander, S.W.: Experimental study of the protein folding landscape: unfolding reactions in cytochrome *c*. J. Mol. Biol. **290**, 811–822 (1999)

54. Hernández, H., Robinson, C.V.: Determining the stoichiometry and interactions of macromolecular assemblies from mass spectrometry. Nat. Protoc. **2**, 715–726 (2007)

55. Cacace, M.G., Landau, E.M., Ramsden, J.J.: The Hofmeister series: salt and solvent effects on interfacial phenomena. Q. Rev. Biophys. **30**, 241–277 (1997)

56. Salis, A., Ninham, B.W.: Models and mechanisms of Hofmeister effects in electrolyte solutions, and colloid and protein systems revisited. Chem. Soc. Rev. **43**, 7358–7377 (2014)

57. Gavriilidou, A.F.M., Gülbakan, B., Zenobi, R.: Influence of ammonium acetate concentration on receptor-ligand binding affinities measured by native nano ESI-MS: a systematic study. Anal. Chem. **87**, 10378–10384 (2015)

58. Hargrove, M.S., Olson, J.S.: The stability of holomyoglobin is determined by heme affinity. Biochemistry **35**, 11310–11318 (1996)

59. Benesch, J.L., Sobott, F., Robinson, C.V.: Thermal dissociation of multimeric protein complexes by using nanoelectrospray mass spectrometry. Anal. Chem. **75**, 2208–2214 (2003)

60. Geels, R.B.J., Calmat, S., Heck, A.J.R., van der Vies, S.M., Heeren, R.M.A.: Thermal activation of the cochaperonins GroES and gp31 probed by mass spectrometry. Rapid Commun. Mass Spectrom. **22**, 3633–3641 (2008)

61. Wang, G., Abzalimov, R.R., Kaltashov, I.: Direct monitoring of heat-stressed biopolymers with temperature-controlled electrospray ionization mass spectrometry. Anal. Chem. **83**, 2870–2876 (2011)

62. Yang, F., Zhou, B., Zhang, P., Zhao, Y., Chen, J., Liang, Y.: Binding of ferulic acid to cytochrome *c* enhances stability of the protein at physiological pH and inhibits cytochrome *c*-induced apoptosis. Chem.-Biol. Interact. **170**, 231–243 (2007)

63. Makhatadze, G., Lopez, M., Richardson, J., Thmos, S.: Anion binding to the ubiquitin molecule. Protein Sci. **7**, 689–697 (1998)